NOTICE

AVIS

The quality of this microform is heavily dependent upon the quality of the original thesis submitted for microfilming. Every effort has been made to ensure the highest quality of reproduction possible.

La qualité de cette microforme dépend grandement de la qualité de la thèse soumise au microfilmage. Nous avons tout fait pour assurer une qualité supérieure de reproduction.

If pages are missing, contact the university which granted the degree.

S'il manque des pages, veuillez communiquer avec l'université qui a conféré le grade.

Some pages may have indistinct print especially if the original pages were typed with a poor typewriter ribbon or if the university sent us an inferior photocopy.

La qualité d'impression de certaines pages peut laisser à désirer, surtout si les pages originales ont été dactylographiées à l'aide d'un ruban usé ou si l'université nous a fait parvenir une photocopie de qualité inférieure.

Canadä

UNIVERSITY OF ALBERTA

VOLTAGE-ACTIVATED CURRENTS IN IDENTIFIED MOTOR NEURONS
FROM THE HYDROMEDUSA *POLYORCHIS PENICILLATUS*.

by

Jan Przysiezniak

.

A thesis submitted to the Faculty of Graduate Studies and Research in
partial fulfillment of the requirements for the degree of **Doctor of**
Philosophy.

DEPARTMENT OF ZOOLOGY

Edmonton, Alberta
SPRING 1993

UNIVERSITY OF ALBERTA

FACULTY OF GRADUATE STUDIES AND RESEARCH
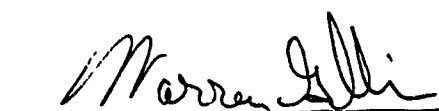
The undersigned certify that they have read, and recommend to the Faculty of Graduate Studies and Research for acceptance, a thesis entitled <u>Voltage-activated currents in identified motor neurons from the hydromedusa</u> <u>*Polyorchis penicillatus*</u> submitted by **Jan Przysiezniak** in partial fulfillment of the requirements for the degree of **Doctor of Philosophy**.

Dr. Andrew N. Spencer, supervisor

Dr. Andrew S. French, examiner

Dr. Sudarshan K. Malhotra, examiner

Dr. Robert J. French, external examiner

Dr. Warren J. Gallin, examination committee chairman

Date of supervisor's signature: 22 April 1993

Jan Przysiezniak, Dept. of Zoology, University of Alberta, Edmonton, Alberta, Canada, T6G 2E9.
Ph. (403) 492-5494 or 3309   Fax : (403) 492-7033   Email: jany@ualtamts.bitnet

I, the undersigned, permit Jan Przysiezniak to include in his thesis a
copy of the article "Presynaptic spike broadening reduces junctional
potential amplitude" (Spencer, Przysiezniak, Acosta-Urquidi & Basarsky,
1989; Nature, 340: 636-638), of which I am a co author. I understand
that my permission is required for said thesis to be microfilmed.

4/8/93

Date

Dr. Juan Acosta-Urquidi

Jan Przysiezniak, Dept. of Zoology, University of Alberta, Edmonton, Alberta, Canada, T6G 2E9.
Ph. (403) 492-5494 or 3309   Fax : (403) 492-7033   Email: jany@ualtamts.bitnet

I, the undersigned, permit Jan Przysiezniak to include in his thesis a copy of the article "Presynaptic spike broadening reduces junctional potential amplitude" (Spencer, Przysiezniak, Acosta-Urquidi & Basarsky, 1989; Nature, 340: 636-638), of which I am a co-author. I understand that my permission is required for said thesis to be microfilmed.

4/7/93
Date

Trent A. Basarsky

I, the undersigned, permit Jan Frzysiezniak to include in his thesis copies of the three articles listed below, of which I am co-author. I understand that my permission is required for said thesis to be microfilmed.

Przysiezniak J, Spencer AN (1989) Primary culture of identified neurones from a cnidarian. J Exp Biol 142: 97-113.

Spencer AN, Przysiezniak J, Acosta-Urquidi J, Basarsky TA (1989) Presynaptic spike broadening reduces junctional potential amplitude. Nature 340: 636-638

Przysiezniak J, Spencer AN (1992) Voltage-activated calcium currents in identified neurons from a hydrozoan jellyfish, *Polyorchis penicillatus*. J of Neurosci 12(6):2065-2078.

April 6 '93
Date

A.N. Spencer
Dr. Andrew N. Spencer

Jan Przysiezniak, Dept. of Zoology, University of Alberta, Edmonton, Alberta, Canada, T6G 2E9.
Ph. (403) 492-5494 or 3309   Fax : (403) 492-7033   Email: jany@ualtamts.bitnet

Dr. R.J. Skaer, Company Secretary
The Company of Biologists Limited
Department of Zoology
Downing Street
Cambridge CB2 3EJ
England

Edmonton, December 10th, 1991

Dear Sir/Madam,

This letter is to kindly request your permission to reproduce the text and figures of the article entitled "Primary culture of identified neurones from a cnidarian", appearing in the Journal of Experimental Biology, 142:97-113 (1989), written by myself and Dr. Andrew N. Spencer. The substance of the article would appear with additions as a chapter in the thesis that I am presently completing. For my thesis to be microfilmed, I require a letter of permission from the person(s) or publishing company holding the copyright to the article mentioned above. I would greatly appreciate you sending me such a letter as soon as possible. Thank you in advance.

Respectfully,

Jan Przysiezniak

Jan Przysiezniak, Dept. of Zoology, University of Alberta, Edmonton, Alberta, Canada, T6G 2E9.
Ph. (403) 492-5494 or 3309   Fax : (403) 492-7033   Email: jany@ualtamts.bitnet

Edmonton, Feb. 18th, 1993

Dr. William D. Willis, Jr.
Journal of Neuroscience
Department of Anatomy and Neuroscience
Marine Biomedical Institute
200 University Boulevard, Suite 608
Galveston, Texas, 77550-2772
USA

Dear Dr. Willis,

This letter is to kindly request permission to reproduce the text and figures of the article entitled "Voltage-activated calcium currents in identified neurons from a hydrozoan jellyfish, *Polyorchis penicillatus*", written by myself and Dr. Andrew N. Spencer and appearing in the Journal of Neuroscience, 12(6):2065-2078 (1992). Also, in case it is accepted for publication, I request permission to reproduce, in its present form, the recently submitted article entitled "Voltage-activated potassium currents in isolated motor neurons from the jellyfish, *Polyorchis penicillatus*" (MS #JN0086-93), by the same authors. Both of these articles would appear as chapters in the thesis that I am presently completing. For my thesis to be microfilmed, I require a letter of permission from the person(s) or publishing company holding the copyright to these articles. I would greatly appreciate you sending me such a letter as soon as possible, since I must submit my thesis for microfilming before April 23rd, 1993. Thank you in advance.

Respectfully,

Jan Przysiezniak

Reprinted by permission of the Journal of Neuroscience.

Wm. D. Willis, Jr.   Date
Editor-in-Chief

Jan Przysiezniak, Dept. of Zoology, University of Alberta, Edmonton, Alberta, Canada, T6G 2E9.
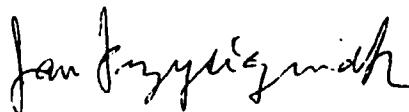Ph. (403) 492-5494 or 3309   Fax : (403) 492-9234   Email: jany@ualtamis.bitnet

Nature:
1234 National Press Building
Washington, DC 20045
USA
fax. (202) 628-1609

Edmonton, March 25th, 1993
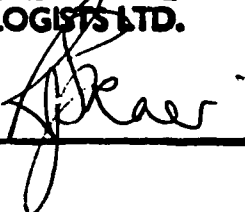
Dear Sir/Madam,

This letter is to kindly request your permission to reproduce the text and figures of the article entitled "Presynaptic spike broadening reduces junctional potential amplitude", appearing in Nature, 340: 636-638 (1989), written by A. N. Spencer, J. Przysiezniak, J. Acosta-Urquidi & T. A. Basarsky. The article would appear with minor changes (to hyphenated words, figure references, literature references) as a small part (13 out of 221 pages) of the thesis that I am presently completing. The figures have been re-lettered and reconstructed from originals. For my thesis to be accepted by the Faculty of Graduate Studies and Research at the University of Alberta, and for it to be microfilmed, I require a letter of permission from the person(s) or publishing company holding the copyright to the article mentioned above. I would greatly appreciate you sending me such a letter as soon as possible. Thank you in advance.

Respectfully,

Jan Przysiezniak

UNIVERSITY OF ALBERTA

LIBRARY RELEASE FORM

NAME OF AUTHOR: Jan Przysiezniak

TITLE OF THESIS: Voltage-activated currents in identified motor neurons from the hydromedusa *Polyorchis penicillatus*.

DEGREE: Doctor of Philosophy

YEAR THIS DEGREE GRANTED: 1993

Jan Przysiezniak
8790 André-Grasset
Montréal, PQ
Canada
H2M 2L4

Date: 13- IV-22

ABSTRACT

Nervous systems probably first evolved in close ancestors of the Cnidaria, when certain cells became specialized for electrical excitation and rapid chemical neurotransmission. The evolutionary adaptations of ion channels to these specialized functions can be studied using tight-seal voltage clamp of whole-cell membrane ionic currents. This work focuses on voltage-activated ionic currents shaping the action potentials of the "swimming motor neurons" (SMNs) in the jellyfish *Polyorchis penicillatus*. Five calcium, sodium, and potassium currents were described in isolated SMNs, at room temperature (19–22°C).

A transient, high-voltage-activated, inward, calcium current, HVA–t, arose within 10 ms, inactivated rapidly ($\tau \approx 26$ ms, 187 ms) and was selective for Ca^{2+} over Ba^{2+}. Submillimolar Cd^{2+} blocked HVA–t completely and removed the action-potential plateau. A sustained calcium current, HVA–s, was an order of magnitude smaller than HVA–t and did not distinguish between Ca^{2+} and Ba^{2+}.

The inward sodium current, I_{Na}, rose to peak and decayed within about 2 ms. It also activated at high voltages. The voltages of half-inactivation of I_{Na} and HVA–t were almost identical (~–25 mV). Tetrodotoxin had no effect at concentrations up to 140 μM, but cadmium at 1–10 mM inhibited I_{Na} without affecting the outward currents. The above evidence suggests that the channels underlying I_{Na} and HVA–t were similar at the molecular level.

A rapidly-arising potassium current, I_{K-fast}, reached peak in ~10 ms, and decayed bi-exponentially but incompletely in 1 s. It activated at more negative voltages than the other currents. It was half-inactivated by prepulses to –53 mV, which allowed it to regulate the duration of spikes elicited from baselines around this voltage. Other evidence suggests I_{K-fast} probably modulates neurotransmitter release and synchronizes muscle contractions around the swimming bell. A sustained potassium current, I_{K-slow}, rose to peak in about 200 ms and activated at more positive voltages than the other currents.

The variety of ionic currents in *Polyorchis* suggests that much of the evolution of voltage-activated ion channels occurred in a phylum more primitive than the Cnidaria.

ACKNOWLEDGEMENTS

I would like to thank the following people for their help:

Dr. Andrew N. Spencer, for patience that seems inextinguishable; for well-dosed reminders of the work to do, encouragement for the work being done, and praise for work well done; for pleasantly choreographed paper- and chapter-editing sessions; for being a cool guide through my oft-frazzled thoughts.

My housemates and work colleagues in Edmonton and in Bamfield, for accepting and sometimes tolerating me in their midst, specially before deadlines or after broken deadlines; Dr. Nikita Grigoriev for discussions on real and hypothetical subjects, his sense of humor and some pharmacological results; Dr. Jun-Mo Chung, for his friendship and tolerance and our long discussions, technical or otherwise; Dr. Juan Acosta-Urquidi for his encouragements in my first, successful, tight-seal, whole-cell recordings and for help in analyzing the early potassium current data; Mr. Trent A. Basarsky for data from short-spike neurons and for his enthusiasm (Chapter 5); Dr. C. J. P. Grimmelikhuijzen for providing antiserum 146II and Ms. Nancy McFadden for help with the RFamide immunocytochemistry (Chapter 2); Dr. Lisa Stockbridge, for introducing me to patch electrode making; Dr. Norman L. Stockbridge for patient discussions on space clamping, help in computer programming, his close participation in the Arsenazo attempts, and his laugh; Dr. Ebenezer Yamoah for helpful discussions, generous sharing of modeling programs, and his friendship; Drs. Andrew French, Lisa Stockbridge and Marek Duszyk for discussions on ion permeation; Ms. Lan Diep for valuable help with ion chromatography and atomic absorption spectroscopy (Chapter 3); Ms. Dianne Formanski for carrying out the inductively coupled plasma spectroscopy (Chapter 3); Mr. George Braybrook for carrying out the scanning electron microscopy of electrodes (Chapter 3); Dr. William Dryden, for having been briefly on my committee; Drs. William Mackay, John Addicott and Richard Palmer, for their help with a tricky point of statistics; Dr. Larry Guilbert for a brief but fruitful discussion on neuronal labelling; my family and friends, for being there or here; Pipo the pitbull parrot, for his company.

TABLE OF CONTENTS

Chapter 5 - Voltage-activated potassium currents in isolated motor neurons from the jellyfish *Polyorchis penicillatus*. 124

LIST OF TABLES

LIST OF FIGURES

Chapter 5

Appendix

LIST OF SYMBOLS, NOMENCLATURE AND ABBREVIATIONS

$[Ca^{2+}]_{in}$, $[K^+]_{in}$, $[Na^+]_{in}$ - Intracellular ion concentrations.

$[Ca^{2+}]_{out}$, $[K^+]_{out}$, $[Na^+]_{out}$ - Extracellular ion concentrations.

4-AP - 4-aminopyridine.

ASW - Artifical seawater.

"B" neurons - Neurons showing bursts of action potentials, located in the outer nerve ring of *Polyorchis*.

BS, BSD, BSD2 - Types of recording solutions used in the bath (see Table 5.1).

Choline-Cl - Choline chloride.

C_m - Membrane capacitance.

d - Day.

DMSO - Dimethyl sulfoxide.

e - The mathematical constant, 2.718281...

E_k, E_{Na}, E_{Ca}, E_{Cl} - Theoretical reversal potential, from the Nernst equation.

EGTA - Ethyleneglycol-bis-(β-aminoethyl ether) N,N,N',N'-tetraacetic acid.

EJP - Excitatory junctional potential.

epsp - Excitatory postsynaptic potential.

E_{rev} - Reversal potential of a current.

ES, ESA, ESD, ESE, ESE2, ESE3 - Types of recording electrode solutions (see Table 5.1).

FM - Frequency modulation.

G_{Na}, G_K - Conductances, expressed in siemens.

GFNN - Giant fiber nerve net.

GHK - Goldman-Hodgkin-Katz.

$G\Omega$ - Gigaohm (10^9 Ω).

h - Hour.

HEPES - N-2-Hydroxyethylpiperazine-N'-2-ethanesulfonic acid.

HVA - High-voltage-activated.

HVA-t - High-voltage-activated, transient calcium current

HVA-s - High-voltage-activated, sustained calcium current

Hz - Hertz.

I - Current.

I_{Ba} - Barium current.

I_{Ca} - Calcium current

I_{fitted} - Current calculated from an equation and fitted to data.

I_{in} - Inward current.

I_{K-fast} - Rapidly activating potassium current

I_{K-slow} - Slowly activating potassium current

I_{leak} - Leakage current.

I_{max} - Maximum current.

I_{min} - Minimum current.

I_{Na} - Sodium current

I_{out} - Outward current.

$I_{overall\ mean}$ - Average of currents measured for an entire data set.

I_{peak} - Peak current.

I_{trans} - Transient, outward current seen in potassium current recordings.

I-V - Current-voltage relationship.

K_a - Voltage interval across which the conductance or permeability increase
   e-fold; also referred to as slope or steepness factor.

$K_{a,HV}$ - Slope factor for the high-voltage-activated calcium current.

kHz - Kilohertz.

K_i - Voltage interval across which the availability of the current decreases

e-fold; also referred to as slope or steepness factor.

LVA - Low-voltage-activated.

min - Minute.

mM - Millimolar.

ms - Millisecond.

mV - Millivolt.

$M\Omega$ - Megaohm ($10^6 \ \Omega$).

μm - Micrometer.

μM - Micromolar.

μs - Microsecond.

N - Numer of measurements averaged.

nA - Nanoampere (10^{-9} A).

NMG - N-methyl-D-glucamine.

Nomarski-DIC - Differential interference contrast optics, developed by Nomarski.

nS - Nanosiemen, a unit of electrical conductance.

"O" neurons - Neurons showing a slowly oscillating membrane potential, identified in the outer nerve ring of *Polyorchis*.

P - Statistical probability that a difference is not significant.

P_{Na}, P_{Ca}, P_K, P_{Ba} - Permeabilities, expressed in 1/s, calculated using the Goldman-Hodgkin-Katz constant-field equation.

pA - Picoampere (10^{-12} A).

PBS - Phosphate-buffered saline.

$P_{D,HV}$ and $P_{max,HV}$ - Permeability, and maximally-activated permeability of the high-voltage-activated, divalent cation channels.

$P_{D,VHV}$ - Permeability of the very-high-voltage-activated, divalent cation channels.

pF - Picofarad.

r^2 - Coefficient of correlation, indicating the closeness of a relationship between two variables.

RFamide - Peptide containing an amidated carboxy-ending with the sequence Arg-Phe.

R_{fit} - Index of fitting quality.

R_{leak} - Leakage resistance.

R_{ser} - Series resistance.

s - Second.

SAL1 - Type of saline used in the bath.

SEM - Standard error of the mean.

SMN - Swimming motor neuron

S_{repol} - Repolarization rate or repolarization slope, in V/s.

SSN - Short-spike neuron, found in cultures of *Polyorchis* nerve ring.

STX - Saxitoxin.

TEA - Tetraethylammonium.

T_{peak} - Time to peak, measured from the voltage transition to peak current.

TTX - Tetrodotoxin.

τ - Time constant

τ_{off} - Time constant of exponential decay or inactivation.

τ_{onset} - Time constant of current onset.

U/ml - Units of enzyme activity per ml of solution.

V/s - Volts per second.

$V_{1st\ act}$ - Voltage of first activation.

V_a - Voltage of half-activation.

$V_{a,HV}$ - Voltage of half-activation of the high-voltage-activated calcium current.

V_c - Command voltage, or voltage reached by a voltage-clamp step.

V_{corr} - Voltage corrected for series resistance error.

V_h - Holding potential, at which the cell is held between the application of voltage steps.

VHVA - Very-high-voltage-activated calcium current

V_i - Voltage of half-inactivation.

V_m - Transmembrane voltage.

V_{max} - Voltage at which current is maximal.

V_{pp} - Prepulse voltage, at which the cell membrane is momentarily conditioned before applying a test pulse.

V_{Rser} - Voltage drop across the series resistance.

Chapter 1

GENERAL INTRODUCTION

THE PLACE OF THE CNIDARIA IN NERVOUS SYSTEM EVOLUTION

The Cnidaria (jellyfish, anemones, hydra and kin) constitute the most primitive group of animals with a tissue level of organization. In these animals, cells of a given type (neuron, epithelial, muscular) not only can coexist with different cell types, as in the Porifera (sponges), but they also associate with their kind to produce recognizable layers and structures. With this level of organization appeared, what are believed to be the most primitive nervous systems, with functionally specialized neurons, defined signal conduction pathways, and rapid, chemical and electrical synapses.

Numerous, if not all, protozoans are excitable (Kung and Saimi, 1982, on *Paramecium*; Deitmer, 1984, on *Stylonychia*; Febvre-Chevalier et al., 1986, on *Actinocoryne*; Krüppel and Lueken, 1988, on *Euplotes*) and some forms even show what appear to be conduction pathways along vacuolar membranes (Wood, 1982, on *Stentor*). The molecular bases of excitability and electrical conduction in the multicellular animals may have evolved directly from those in excitable protozoans, by the restriction of functions to certain cell types (neurons). Alternately, these mechanisms may have evolved independently in the protists and multicellular animals. Recent molecular evidence (T. Jegla, unpublished) indicates that there may be important differences between amino-acid sequences of channel proteins in protozoa and in metazoans. Thus the second hypothesis may be more likely.

Electrical recordings from cells of the Porifera (sponges) have not yet been achieved, so it is not known whether they are electrically excitable. However ciliary arrest in the hexactinellid sponge, *Rhabdocalyptus dawsoni*, is all-or-none and is triggered by electrical stimuli with a definite threshold (Mackie et al., 1983). While the conduction speed of this response (~0.2 cm/s) is slower than that of electrical conduction in hydrozoan epithelia (Anderson, 1980) and is at the lower range of values measured in the sensitive plant, *Mimosa* (Sibaoka, 1966), it is several orders of magnitude too rapid to reflect mechanically propagated events (Pavans de

1

Ceccatty, 1969; Mackie et al., 1983). Finally, the syncytium contacting all ciliated cells throughout the animal (Mackie and Singla, 1983) is a likely substrate for electrical conduction. Thus, Mackie et al. (1983) conclude that the ciliary arrest response of *Rhabdocalyptus* is probably coordinated by a propagated action potential.

Because sponges are sessile filter-feeders, the structures and mechanisms underlying their behavior have likely evolved away from those of more active metazoans, so these animals may not be suitable representatives of the first metazoans. It seems more probable that excitable cells and proto-nerves appeared in a more motile animal. For example, Grell (1981) believes that the multicellular, ciliated *Trichoplax adhaerens*, the only representative of the phylum Placozoa, represents the most primitive metazoan group. This ciliated animal resembles the planula larval stage common in most cnidarians and possesses two epithelial cell layers protecting a layer of contractile, mesenchymal cells. However, Nielsen (1985) believes that *Trichoplax* represents a secondarily degenerate form of flatworm, rather than the primordial metzoan.

Whatever the initial, metazoan ancestor, it probably gave rise to the radially symmetrical Cnidaria, with an appropriately circular nervous system (nerve net, nerve ring), and all the bilaterally symmetrical animals, starting with the flatworms, which exhibit an equally appropriate, two-sided and cephalized nervous system. Because of the architectural differences between the nervous systems of the Radiata and Bilateria, there may also be differences in how nerve cells conduct signals electrically, and in how they transmit them to other cells. Membrane excitability is involved in both conduction and neurotransmission, but it isn't clear to what extent it may adapt to such a large-scale feature as the type of nervous system symmetry. This work focusses on the biophysical description of cnidarian neuronal excitability.

CNIDARIAN NEUROANATOMY

These diploblastic animals are composed of an ectoderm on the outside and an endoderm lining the gastrovascular cavity, separated by an extracellular matrix, the mesoglea, which may contain cells. The muscles are contractile processes of the epithelial cells ("myoepithelial cells"), to which they are connected by narrow, cytoplasmic bridges, and are attached to the mesoglea. Nerve cells develop from pluripotent interstitial cells in

2

either epithelial layer, and remain protected beneath the epithelial surface, although some may extend sensory processes to the surface.

The organization of nervous systems in the three classes of the Cnidaria will be summarized here. The Anthozoa (anemones and corals) exhibit the most diffuse nervous system, which forms several nets around the column, the tentacles, and within the mesenteries, and sometimes becomes denser around the mouth (Barnes, 1987). The neurons are generally small and communicate with each other through chemical synapses (Mackie et al., 1984). Electrical synapses are unknown.

The Scyphozoa, or true jellyfish, also contain several nets, spread diffusely throughout the swimming bell (Anderson and Schwab, 1981). One, the Motor Nerve Net or Giant Fiber Nerve Net (GFNN), radiates from sensory-motor integrative centers, the rhopalia, located around the margin, and innervates the swimming muscle. The neurons are generally large and communicate via chemical synapses. Once again electrical communication is unknown.

The Hydrozoa exist in either the hydroid stage or the medusa stage of their life cycle. Hydromedusae exhibit nerve nets, which are often condensed into a nerve ring located around the margin of the swimming bell, or into radial nerves connecting the nerve ring to the centrally located mouth, or manubrium. A subset of large motor neurons is present in these nerves which drives swimming contractions (Satterlie and Spencer, 1983). The Hydrozoa are the only cnidarians in which intercellular communication can occur through electrically conducting gap junctions (King and Spencer, 1979; Spencer and Satterlie, 1980; Mackie et al., 1984), always between neurons of the same kind, and through chemical synapses (Roberts and Mackie, 1980; Spencer and Arkett, 1984), between networks of cells. The epithelia of hydrozoans are usually able to propagate action potentials (Mackie and Passano, 1968), which reduces the need for diffuse nerve nets to ensure the spatial recruitment of muscle cells, for example.

Since the work presented here focuses on the hydromedusan *Polyorchis penicillatus*, its neuroanatomy will be described in some detail. The nerve ring of *Polyorchis* is composed of the inner and outer nerve rings, which are located on either side of the base of the velum (an annulus of tissue attached at its circumference to the bell margin and serving to constrict the bell opening during a swimming contraction). The outer nerve ring, on the exumbrellar side of the velum, contains many small neurons (Spencer, 1979) composing at least two ("B" and "O" neurons) distinct networks of electrically-coupled neurons (Spencer and Arkett, 1984). The inner nerve ring, on the subumbrellar side of the velum, contains small neurons and

3

the large, electrically-coupled "swimming motor neurons" (SMNs; Spencer, 1979, 1981). All of these neurons are ensheathed by epithelial cells sending processes from the surface. The SMNs synapse onto the overlying epithelium which is electrically coupled to the circular swimming muscle on the subumbrellar surfaces of the bell and of the velum (Spencer, 1982).

CNIDARIAN ELECTROPHYSIOLOGY

All of the early cnidarian electrophysiology involved extracellular recording. Through the 1960s and 1970s, the functional organization of the nervous systems in numerous anthozoans (reviewed by McFarlane, 1982), scyphozoans (Horridge, 1954; reviewed by Passano, 1965, 1973, 1982) and hydrozoans (Spencer, 1974, 1975, 1978; King and Spencer, 1981) were studied most often using this approach, which allows the identification of different networks involved in producing a specific behavior, and the description of inhibitory or excitatory interactions in or between these networks. It could be inferred that signal propagation depended on all-or-none events in these primitive animals, because the extracellular action potentials had a consistent shape in a given recording and were often conducted without decrement.

The first intracellular, current-clamp recordings (Spencer, 1971) were made from hydrozoan myoepithelial cells. These recordings supported the hypothesis that myoid conduction was widespread in the hydromedusae (Mackie, 1965; Mackie and Passano, 1968) and showed that there was a discrete threshold for events that propagated through the myo-epithelium. However, the first neuronal intracellular recordings (Patton and Passano, 1972), from the GFNN cells of the schyphomedusan, Cyanea capillata, showed a variable resting potential and impulses of variable amplitude, although the pulse shape was consistent for any given cell. This was interpreted as the presence of "conduction elements without conducted action potentials", momentarily casting doubt on the all-or-none nature of neuronal signalling in the Cnidaria. This followed the popular impression that the cnidarian nervous system should behave in a "primitive" or unconventional manner even at the cellular level. However, as more intracellular recordings were made, it was found that signalling in neurons of the hydromedusae (Mackie, 1973, on Nanomia cara; Anderson and Mackie, 1977, on Polyorchis penicillatus; Roberts and Mackie, 1980, on Aglantha digitale; Satterlie and Spencer, 1983) and scyphomedusae

4

(Satterlie, 1979, on *Carybdea rastonii*; Anderson and Schwab, 1983, on *Cyanea*) was clearly all-or-none. Interesting variations were discovered, such as the presence of discrete, sodium and calcium action potentials in the same motor giant neurons of *Aglantha* (Mackie and Meech, 1985), or variable action-potential durations in swimming motor neurons (SMNs) of many hydromedusae (Anderson and Mackie, 1977; Satterlie and Spencer, 1983).

Intracellular, current-clamp recordings permitted more careful descriptions of the ionic bases of the action potentials in neurons (Anderson, 1979; Anderson and Schwab, 1983, 1984; Mackie and Meech, 1985) and in muscle cells (Spencer and Satterlie, 1981), and allowed direct recordings of electrical coupling between hydrozoan cells (Spencer and Satterlie, 1980; Spencer, 1981) and of chemical synaptic interactions between different cells (Spencer, 1982; Spencer and Arkett, 1984; Roberts and Mackie, 1980; Kerfoot et al., 1985).

The earliest reported voltage-clamp study of membrane ionic currents in the Cnidaria was carried out by Hagiwara et al. (1981), who analyzed the time course and voltage dependence of potassium currents in the egg cell of the sea pansy *Renilla*. Anderson (1987, extended in 1989) first described cnidarian neuronal currents using the tight-seal, whole-cell voltage clamp of GFNN cells from *Cyanea*. He provided descriptions of the voltage dependence and pharmacology of the sodium current and outlined the voltage dependencies, time courses, and pharmacologies of the calcium and potassium currents in these cells. Other studies have since described currents in neurons (Mackie and Meech, 1989, using single-channel recording), epithelial cells (Dunlap et al., 1987; Holman and Anderson, 1991) and cnidocytes (Anderson and McKay, 1987), but only to a limited degree. Most studies provide a sample of the time course, the current-voltage relationship, and some pharmacology of the current. However, few provide data on the voltage dependence of steady-state inactivation, the time course of recovery from inactivation, or the ionic selectivity of the current (but see Anderson, 1987, on sodium current; Holman and Anderson, 1991, on calcium current), and none give most of this information for all the observable currents. The work presented in this thesis is the most extensive and detailed description yet available of membrane ionic currents in a given neuronal type of a cnidarian.

5

CHOICE OF PREPARATION

The preparations that have provided the most complete description of cnidarian physiology from behavior to cellular excitability and synaptic function are the hydromedusae *Aglantha* (Singla, 1978; Mackie, 1980; Roberts and Mackie, 1980; Mackie and Meech, 1985; Kerfoot et al., 1985; Mackie and Meech, 1989) and *Polyorchis*. *Polyorchis* has received much attention, being the subject of anatomical studies (Spencer, 1979; King and Spencer, 1979; Singla and Weber, 1982; Grimmelikhuijzen and Spencer, 1984; Satterlie, 1985); behavioral studies (Arkett, 1984, 1985); extracellular electrophysiological studies (Spencer, 1978; King and Spencer, 1981); and current-clamp studies of the SMNs (Anderson and Mackie, 1977; Anderson, 1979; Spencer and Satterlie, 1980; Spencer, 1981), swimming muscle (Spencer and Satterlie, 1981), two other neuronal types in the nerve ring and the synaptic interactions of SMNs with these (Spencer and Arkett, 1984; Arkett and Spencer, 1986) and the muscle cells (Spencer, 1982). Thus, the existing work on the swimming motor neurons of *Polyorchis* provides a background to which the biophysical data presented here can be related to uncover its biological relevance. The availability of electrophysiological data on several cell types from this animal allows a functional interpretation of the data obtained on the ionic channel populations of each cell type.

ABOUT THE THESIS

This project began as a continuation of work on the effects of RFamide neuropeptides on the electrical activity of SMNs (Grimmelikhuijzen and Spencer, 1984; Grimmelikhuijzen et al., 1988; Spencer, 1988). The semi-dissected preparation used by Spencer proved limiting in that the epithelium ensheathing the SMNs slowed or prevented the access of applied peptide to putative membrane receptors. Also, the presence of neurons known to impinge on the SMNs (Spencer and Arkett, 1984) made it difficult to distinguish direct peptide effects from those mediated by presynaptic neurons. Even after the removal of the epithelium to improve diffusion, some synaptic contacts remained. To alleviate these problems, a procedure was developed to isolate the SMNs in primary cultures (Chapter 2).

Intracellular recordings, used in Chapter 2, proved difficult to achieve and somewhat damaging to the cells, so the tight-seal, whole-cell recording

technique was used instead, since the isolated cell membranes were relatively free from debris. Since nothing was known of the voltage-dependent currents that produce the SMN action potentials, and the neuropeptides appeared to be altering some features of SMN excitability (Spencer, 1988), it was decided that this work should focus on establishing the baseline properties of the voltage-dependent currents in the SMNs. The isolated neurons presented relatively simple and compact shapes so that voltage clamping from a point current source (the electrode tip) was expected to offer adequate spatial control of the membrane voltage.

Calcium, sodium or potassium currents were isolated from the total current with substitutions of impermeant ions for the complementary cations in the external solution or the electrode/internal solution. The calcium current, described in Chapter 3, yielded the most detailed results and is described first, with a technical discussion of the problems of series resistance and space clamping. This is followed in Chapter 4 by a description of the sodium, inward current in these cells. This chapter also elaborates on a mathematical procedure to correct for series resistance error. Finally, the potassium currents are described in Chapter 5. The work relating to synaptic function was included as an appendix.

REFERENCES

Anderson PAV (1979) Ionic basis of action potentials and bursting activity in the hydromedusan jellyfish *Polyorchis penicillatus*. J Exp Biol 78: 299-302.

Anderson PAV (1980) Epithelial conduction: its properties and functions. Prog Neurobiol 15: 161-203.

Anderson PAV (1985) Physiology of a bidirectional, excitatory, chemical synapse. J Neurophysiol 53: 821-835.

Anderson PAV (1987) Properties and pharmacology of a TTX-insensitive Na^+ current in neurons of the jellyfish, *Cyanea capillata*. J Exp Biol 133: 231-248.

Anderson PAV (1989) Ionic currents of the Scyphozoa. In: Evolution of the first nervous systems (Anderson PAV, ed), pp 267-280. New York: Plenum.

Anderson PAV, Mackie GO (1977) Electrically coupled, photosensitive neurons control swimming in a jellyfish. Science 197: 186-188.

Anderson PAV, McKay MC (1987) The electrophysiology of cnidocytes. J Exp Biol 133: 215-230.

Anderson PAV, Schwab WE (1981) The organization and structure of nerve and muscle in the jellyfish *Cyanea capillata* (Coelenterata: Scyphozoa). J Morphol 170: 383-399.

Anderson PAV, Schwab WE (1983) Action potential in neurons of the motor nerve net of *Cyanea* (Coelenterata). J Neurophysiol 50: 671-683.

Anderson PAV, Schwab, WE (1984) An epithelial cell-free preparation of the motor nerve net of *Cyanea* (Coelenterata; Scyphozoa). Biol Bull Mar Biol Lab, Woods Hole 166: 396-408.

Arkett SA (1984) Diel vertical migration and feeding behavior of a demersal hydromedusan *Polyorchis penicillatus*. Can J Fish Aquat Sci

8

41: 1837-1843.

Arkett SA (1985) The shadow response of a hydromedusan (*Polyorchis penicillatus*): behavioral mechanisms controlling diel and ontogenic vertical migration. Biol Bull 169: 297-312.

Arkett SA, Spencer AN (1986) Neuronal mechanisms of a hydromedusan shadow reflex. I- Identified reflex components, and sequence of events. J comp Physiol A 159: 201-213.

Barnes RD (1987) Invertebrate zoology. 5th edition. New York, NY: Saunders College Publishing.

Deitmer JW (1984) Evidence for two voltage-dependent calcium currents in the membrane of the ciliate *Stylonychia*. J Physiol (Lond) 355: 137-159.

Dunlap K, Takeda K, Brehm P (1987) Activation of a calcium-dependent photoprotein by chemical signalling through gap junctions. Nature 325: 60-62.

Febvre-Chevalier C, Bilbaut A, Bone Q, Febvre J (1986) Sodium-calcium action potential associated with contraction in the heliozoan *Actinocoryne contractilis*. J Exp Biol 122: 177-192.

Grell KG (1981) *Trichoplax adhaerens* and the origin of Metazoa. International congress on the origin of the large phyla of metazoans. Accademia Nazionale Lincei. Atti Conv Lincei 49: 107-121.

Grimmelikhuijzen CJP, Hahn M, Rinehart KL, Spencer AN (1988) Isolation of <Glu-Leu-Leu-Gly-Gly-Arg-Phe-NH$_2$ (Pol RFamide), a novel neuropeptide from hydromedusae. Brain Res 475: 198-203.

Grimmelikhuijzen CJP, Spencer AN (1984) FMRFamide immunoreactivity in the nervous system of the medusa *Polyorchis penicillatus*. J Comp Neurol 230: 361-371.

Hagiwara S, Yoshida S, Yoshii M (1981) Transient and delayed potassium curents in the egg cell membrane of the coelenterate, *Renilla koelikeri*. J Physiol (Lond) 318: 123-141.

Holman MA, Anderson PAV (1991) Voltage-activated ionic currents in myoepithelial cells isolated from the sea anemone *Calliactis tricolor*. J Exp Biol 161: 333-346.

Horridge GA (1954) The nerves and muscles of medusae. I. Conduction in the nervous system of *Aurelia aurita* Lamarck. J Exp Biol 31: 594-600.

Kerfoot PAH, Mackie GO, Meech RW, Roberts A, Singla CL (1985) Neuromuscular transmission in the jellyfish *Aglantha digitale*. J Exp Biol 116: 1-25.

King MG, Spencer AN (1979) Gap and septate junctions in the excitable endoderm of *Polyorchis penicillatus* (Hydrozoa, Anthomedusae). J Cell Sci 36: 391-400.

King MG, Spencer AN (1981) The involvement of nerves in the epithelial control of crumpling behavior in a hydrozoan jellyfish. J Exp Biol 94: 203-218.

Krüppel T, Lueken W (1988) Membrane excitability and membrane currents in the marine ciliate *Euplotes vannus*. Eur J Protistol 24: 11-21.

Kung C, Saimi Y (1982) The physiological basis of taxes in *Paramecium*. Ann Rev Physiol 44: 519-534.

Mackie GO (1965) Conduction in the nerve-free epithelia of siphonophores. Amer Zool 5: 439-453.

Mackie GO (1973) Report on giant nerve fibers in *Nanomia*. Publ Seto Mar Biol Lab 20: 745-756.

Mackie GO (1980) Slow swimming and cyclical "fishing" behavior in *Aglantha digitale* (Hydromedusae: Trachylina). Can J Fish Aquat Sci 37: 1550-1556.

Mackie GO, Anderson PAV, Singla CL (1984) Apparent absence of gap junctions in two classes of Cnidaria. Biol Bull 167: 120-123.

Mackie GO, Lawn ID, Pavans de Ceccatty M (1983) Studies on hexactinellid

sponges. II. Excitability, conduction and coordination of responses in *Rhabdocalyptus dawsoni* (Lambe, 1873). Phil Trans R Soc Lond B 301: 401-418.

Mackie GO, Meech RW (1985) Separate sodium and calcium spikes in the same axon. Nature 313: 791-793.

Mackie GO, Meech RW (1989) Potassium channel family in axons of the jellyfish *Aglantha digitale*. J Physiol (Lond) 418: 14P.

Mackie GO, Passano LM (1968) Epithelial conduction in Hydromedusae. J Gen Physiol 52: 600-621.

Mackie GO, Singla CL (1983) Studies on hexactinellid sponges. I. Histology of *Rhabdocalyptus dawsoni* (Lambe, 1873). Phil Trans R Soc Lond B 301: 365-400.

McFarlane ID (1982) *Calliactis parasitica*. In: Electrical conduction and behavior in "simple" invertebrates (Shelton GAB, ed), pp 243-265. Oxford: Clarendon.

Nielsen C (1985) Animal phylogeny in the light of the trochaea theory. Biol Jour Linn Soc 25: 243-299.

Passano LM (1965) Pacemakers and activity patterns in medusae: homage to Romanes. Amer Zool 5: 465-481.

Passano LM (1973) Behavioral control systems in medusae; a comparison between hydro- and scyphomedusae. Publ Seto Mar Biol Lab 20: 615-645.

Passano LM (1982) Scyphozoa and Cubozoa. In: Electrical conduction and behavior in "simple" invertebrates (Shelton GAB, ed), pp 149-202. Oxford: Clarendon.

Patton ML, Passano LM (1972) Intracellular recording from the giant fiber nerve-net of a scyphozoan jellyfish. Amer Zool 12: XXXV.

Pavans de Ceccatty M (1969) Les systèmes des activités motrices, spontanées et provoquées des Éponges. C R Hebd Séanc Acad Sci Paris 269: 596-599.

Roberts A, Mackie GO (1980) The giant axon escape system of a hydrozoan medusa, *Aglantha digitale*. J Exp Biol 84: 303-318.

Satterlie RA (1979) Central control of swimming in the cubomedusan jellyfish *Carybdea rastonii*. J Comp Physiol 133: 357-367.

Satterlie RA (1985) Putative extraocellar photoreceptors in the outer nerve ring of *Polyorchis penicillatus*. J Exp Zool 233: 133-137.

Satterlie RA, Spencer AN (1983) Neuronal control of locomotion in hydrozoan medusae. A comparative study. J Comp Physiol A 150: 195-206.

Sibaoka T (1966) Action potentials in plant organs. Symp Soc Exp Biol 20: 49-74.

Singla CL (1978) Locomotion and neuromuscular system of *Aglantha digitale*. Cell Tiss Res 188: 317-327.

Singla CL, Weber C (1982) Fine structure studies of the ocelli of *Polyorcis penicillatus* (Hydrozoa, Anthomedusae) and their connection with the nerve ring. Zoomorph 99: 117-129.

Spencer AN (1971) Myoid conduction in the siphonophore *Nanomia bijuga*. Nature 233: 490-491.

Spencer AN (1974) Behavior and electrical activity in the hydrozoan *Proboscidactyla flavicirrata* (Brandt). I. The hydroid colony. Biol Bull 145: 100-115.

Spencer AN (1975) Behavior and electrical activity in the hydrozoan *Proboscidactyla flavicirrata* (Brandt). II. The medusa. Biol Bull 148: 236-250.

Spencer AN (1978) Neurobiology of Polyorchis. I. Function of effector systems. J Neurobiol 9: 143-157.

Spencer AN (1979) Neurobiology of *Polyorchis*. II. Structure of effector systems. J Neurobiol 10: 95-117.

12

Spencer AN (1981) The parameters and properties of a group of electrically coupled neurons in the central nervous system of a hydrozoan jellyfish. J Exp Biol 93: 33-50.

Spencer AN (1982) The physiology of a coelenterate neuromuscular synapse. J Comp Physiol A 148: 353-363.

Spencer AN (1988) Effects of Arg-Phe-amide peptides on identified motor neurons in the hydromedusa Polyorchis penicillatus. Can J Zool 66: 639-645.

Spencer AN, Arkett SA (1984) Radial symmetry and the organization of central neurons in a hydrozoan jellyfish. J Exp Biol 110: 69-90.

Spencer AN, Satterlie RA (1980) Electrical and dye coupling in an identified group of neurons in a coelenterate. J Neurobiol 11: 13-19.

Spencer AN, Satterlie RA (1981) The action potential and contraction in subumbrellar swimming muscle of Polyorchis penicillatus (Hydromedusae). J Comp Physiol 144: 401-407.

Wood DC (1982) Membrane permeabilities determining resting, action and mechanoreceptor potentials in Stentor coeruleus. J Comp Physiol 146: 537-540.

Chapter 2

PRIMARY CULTURE OF IDENTIFIED NEURONS FROM A CNIDARIAN.[1]

INTRODUCTION

Despite strong evidence, both morphological and physiological, that chemically mediated synaptic transmission occurs in all the cnidarian ("coelenterate") classes (see Martin and Spencer, 1983 and Satterlie and Spencer, 1988 for reviews), there is insufficient information to identify the transmitter substances. There are, however, several preparations, in which it is possible to record intracellularly both pre- and postsynaptically in the Hydrozoa and Scyphozoa [*Aglantha* neuromuscular junction (Kerfoot et al. 1985); *Polyorchis* neuromuscular and neuroneuronal synapses (Spencer, 1982 and Spencer and Arkett, 1984); *Cyanea* neuroneuronal synapse (Anderson, 1985)]. The opportunities afforded by these preparations have not been fully exploited. A major reason for this appears to be that the epithelium covering the synaptic sites forms an effective diffusion barrier (King and Spencer, 1979) to substances applied to the bathing medium. Some success at removing these diffusional barriers has been achieved by partial dissociation of the covering epithelium following treatment with collagenase and hyaluronidase (Spencer, 1988). Using the scyphozoan medusa *Cyanea* (Anderson, 1985, 1987), it has been possible to expose the subumbrellar motor nerve-net by destroying most of the overlying epithelial cells by brief oxidation of the perirhopalial tissue with sodium hypochlorite. This has enabled the study of bidirectional synaptic transmission and a voltage-sensitive sodium current. However, using this isolation technique, it has not been possible to demonstrate postsynaptic effects of applied putative transmitters that mimic natural release (Anderson, personal communcation).

A technique has been developed that produces primary cultures of identifiable neurons from *Polyorchis penicillatus* that will survive for

many days and has important experimental advantages over *in vivo* studies; for example, no diffusion barrier surrounds the neurons. Also, using cultured neurons it is possible to test whether a particular agent is having a direct effect (and not via intervening cells) since a visual check can be made for possible contact with presynaptic neurons. It has been established that all the identified neurons in *Polyorchis*, and probably in all hydrozoans, belong to electrically coupled networks (Spencer, 1981; Spencer and Arkett, 1984). Therefore any attempts to use such networks, either *in vivo* or partially isolated, to examine their biophysical properties using voltage-clamp methods will be complicated by neighbouring, coupled cells acting as current sinks and thus preventing the experimenter achieving an effective clamp at the command voltage.

Polyorchis penicillatus was used to develop this culture technique as it is the cnidarian species for which there is most information concerning the distributions, properties, and synaptic interactions of identified neuronal networks. Four discrete neuronal networks have been described: a) the giant swimming motor neuron network (SMN) which innervates the striated muscle of the bell (Spencer, 1981); b) the burster or "B" network whose neurons are excitatory presynaptic neurons to the SMNs and the tentacle longitudinal muscle (Spencer and Arkett, 1984); c) the oscillator or "O" network whose neurons are photosensitive and are probably presynaptic to both the SMNs and the "B" neurons (Arkett and Spencer, 1986a,b); d) the network of neurons that are immunoreactive to antisera raised against peptides containing Arg-Phe-amide (Grimmelikhuijzen and Spencer, 1984). Three neuronal types have now been identified in culture (SMN, B-like, and RFamide-containing). These provide the essential cellular elements for examining chemical transmission: namely a target neuron (SMN) suspected of being responsive to the neuromodulatory effects of Arg-Phe-amide carboxy-terminal peptides (Spencer, 1988), a neuronal type that may release Arg-Phe-amides, and a neuron that resembles a type ("B") which is known to produce epsps in SMNs.

This study describes a technique for culturing hydrozoan neurons and gives preliminary evidence that such neurons show properties of electrical excitability *in vitro* that are very similar to those seen *in vivo*. It can be expected that such cultures could be used not only to study the neuropharmacology of chemical transmission but also to give essential, basic data on the membrane currents that are present in each of these neuronal types. Data such as this is lacking for the Hydrozoa and is essential to enable the reconstruction of the early evolution of excitable systems in the Metazoa.

MATERIALS AND METHODS

Specimens of *Polyorchis penicillatus* were collected from Bamfield Inlet, on the West coast of Vancouver Island, and kept in running seawater (10–12°C) at Bamfield Marine Station or in cooled, recirculated artificial seawater (8–13°C) in Edmonton, for about 1 week.

The procedure used for dissociation is summarized in Fig. 2.1. All steps were carried out at room temperature (20–25°C), unless stated otherwise. Jellyfish with a bell diameter of 1.5–2 cm were used. Vela were removed, in an anaesthetic solution of 1:1 isotonic $MgCl_2$ and seawater, by cutting as close to the ring canal as possible. Strips of velum containing the nerve-rings, were cut out, divided into 1–2 mm segments, and placed for 10 min in a silicon-coated test tube (Siliclad, Clay-Adams; used at 0.01% v/v in distilled water) containing artificial seawater (ASW) of the following ionic concentrations (in mM) NaCl, 376; $MgCl_2$, 41.4; Na_2SO_4, 26; KCl, 8.5; $CaCl_2$, 10; HEPES, 10; and gentamycin-sulfate, 50 mg/l (Sigma G-3632; ~ 65 μM). pH was adjusted to 7.5 using 1 M NaOH. Gentamycin is a bacterial protein synthesis inhibitor with several components (MW 451–477), and has no effect on mammalian cells at bactericidal concentrations (Sigma, Calbiochem). The tissue was rinsed again for 5 min in ASW, and then exposed to ASW free of divalent cations ($CaCl_2$ and $MgCl_2$ were replaced with 76.5 mM choline chloride and 1 mM EGTA) for 10–15 min. A brief rinse in ASW was followed by digestion in collagenase (Type I or Type XI, Sigma) at 1000 units/ml (cf. Schmid and Alder, 1984) in ASW, for 3–5 h at 20–25°C. The time required for satisfactory digestion varied from animal to animal. If cells tended to slough off easily during dissection, the digestion was stopped after 3 h. Tissue from freshly captured animals tended to be less fragile and digestion was prolonged.

The enzyme solution was then replaced with 8.0 ml of ASW, some of which was pipetted off to leave a volume of 0.5–2.0 ml. The tissue was immediately triturated through the fire-polished tip (inner diameter 0.5–0.8 mm) of a silicon-coated (see above, for test tube) Pasteur pipette. Approximately 10 gentle strokes against the end of the tube were usually sufficient to cause dissociation, leaving only a few pieces of mesoglea. Excessive trituration tended to reduce the yield of large neurons. In later experiments, a 10 min rinse in ASW free of divalent cations immediately followed digestion, and preceded trituration in normal ASW, to reduce

16

aggregation (Fig. 2.1).

The cell suspension obtained from one animal was divided among 2–8 culture dishes coated with a layer of mesogleal substratum (see below). Generally, a large drop (0.2–0.3 ml) of suspension was deposited in the middle 1–1.5 cm^2 area of the dish to make the cells more accessible for electrophysiology. After cultures had settled for at least 1 h at 10–15°C, about 2 ml of medium (unsupplemented ASW with gentamycin) was added. Cultures were held at 10–15°C and the medium replaced daily. Healthy cultures could be kept in this way for 4–10 d and, on occasion, for up to 2 weeks. In more recent experiments, the culture medium was changed only once after plating; this seemed to allow longer survival.

Substrata

Several potential substrata were examined (tissue-culture plastic, slide glass, poly-lysine, gelatin). Of these, only mesoglea gave reliable attachment of cells and reasonable longevity. To prepare a mesogleal substratum, swimming bells were dissected into halves or quarters and the peduncle removed. Gently stirring the bell sections from one animal in 50 ml of distilled water for 1 h removed all cells from the mesoglea. The mesogleal lamella on the subumbrellar side was then peeled off and discarded The remaining exumbrellar jelly was rinsed briefly (30 s) several times until the supernatant was no longer cloudy. Salts were diluted out by soaking the mesoglea in distilled water for at least 3 h, with water changes every hour. Cleaned mesoglea was placed with the exumbrellar surface upward, on plastic Petri dishes (Falcon 3001 or 1008) or on glass slides and was dried flat at 25–30°C, for 1–2 d, in a dust-free environment.

Homogenized mesoglea was also used as a substratum. In this case cleaned mesoglea from one animal was minced coarsely, placed in 50 ml of distilled water, and blended at top speed for 30 s (VirTis 23 blender). Two ml of the resulting suspension was plated in each culture dish and left to settle at room temperature. After 1–3 h, excess suspension was discarded, and the dishes were dried overnight at 25–30°C. This method produced about 20 coated dishes with mesoglea from one animal. Homogenized substrata gave optically superior images to whole mesoglea; however, cultures survived a day or two longer on whole mesoglea. Cultureware containing homogenized or whole mesoglea substratum was kept at room temperature, in dust-free conditions until used (within a week), or at 0–4°C if kept longer.

17

Identification of swimming motor neurons with intracellular tracer

The velum was dissected from the bell margin as described above, and pinned onto a Sylgard-coated Petri dish with cactus spines (from *Opuntia* sp.). Microelectrodes were filled either with 5% Lucifer Yellow CH (Sigma L-0259) in distilled water and backfilled with 1 M LiCl, or with 200 mM 5(6)–carboxyfluorescein (Sigma C-7153) in 10 mM HEPES buffer at pH 7–8 (Sigma H-3375) and backfilled with 1 M KCl. Electrode resistances were 30–100 MΩ. A neuron was penetrated with a dye-filled electrode for 10–25 min. Hyperpolarizing current pulses of 2–8 nA lasting 10–30 s were alternated with brief checks of the resting potential and presence of plateau spikes (characteristic of the SMNs; see Fig. 2.5) on depolarization. To limit the region through which the dye spread, two incisions were made through the nerve-ring, 2–3 mm apart. Several (up to seven) fills were made in this segment of the SMN network, until all cells (some 200 neurons) were fluorescent.

The labelled section of nerve-ring was dissected out and dissociated as described above, to give 0.2–0.3 ml of suspension. This was plated on dry mesoglea on a glass slide, and allowed to settle and attach for 3–5 h, in a moist chamber at 10–15°C. The slide was then briefly rinsed with ASW to remove unattached cells. For observations, a coverslip was placed on the suspension, with supporting coverslips forming a cavity. Labelled cells were photographed both under ultraviolet illumination and with Nomarski-DIC optics (see Fig. 2.4). In most cases, these slide cultures were kept coverslipped for one to several days in moist, cool conditions. Carboxyfluorescein remained visible for at least 3 d, but Lucifer Yellow lost much of its brightness within 1 day.

RFamide immunocytochemistry

All treatments were carried out at 4°C. Two-day-old cultures were fixed for 1 day with 4% paraformaldehyde in ASW (pH 7.5), rinsed in ASW free of divalent cations for 1 h (to prevent phosphate salt precipitation), and fixed for 5 more days with 4% paraformaldehyde in phosphate-buffered saline (PBS; 440 mM NaCl, 35 mM sodium phosphate, pH 7.0). After a 15 min wash in PBS, cultures were incubated for 4 h in 0.2 M glycine in distilled water, and for 1 h in PBS-Triton (0.25% Triton-X). Rabbit antiserum 146II (1/200 in PBS-Triton + 0.25% human serum albumin; Grimmelikhujizen, 1985) against RFamide was applied overnight (18–24 h). Cultures were then washed for 1 h in PBS-Triton. FITC-labelled goat-anti-rabbit IgG (1/200) was applied for 18–24 h. After a 10 min wash in PBS,

18

cultures were mounted in glycerol and photographed under ultraviolet epi-illumination.

Electrophysiology

One- to five-day-old cultures were used for intracellular recording. Dissociated neurons were observed through a Nikon Diaphot inverted microscope and, in some cases, photographed with phase-contrast and/or Nomarski optics. Electrophysiology was carried out at room temperature, using 30–150 MΩ electrodes filled with 2 M potassium acetate. Grounding was through a chloridized silver wire across an agar-ASW bridge (5% agar in ASW), or with an Ag-AgCl pellet. The membrane potential was monitored across a bridge circuit (Getting Model 5), amplified and stored on FM tape. For current-passing, the bridge was balanced in the bath. Penetrations were achieved by ringing the capacity-compensation circuit, or by very gently tapping the manipulator. Recordings could be maintained for several minutes to more than an hour.

For averages of spike parameters, one action potential per cell penetrated was measured from tape recordings. The amplitude of an action potential was measured from the beginning of the steeply rising phase to the peak. The duration was measured from the same starting point, to the point where the repolarizing phase reached the resting membrane potential present 50 ms before the spike. The amplitude of the after-hyperpolarization was measured from the latter point to the maximum level of the hyperpolarization. The duration of this hyperpolarization was measured from the end of the spike to where the membrane potential reached the resting level again. Rising and falling slopes were calculated from tape-recorded action potentials; the most linear part of a trace was used. The rising slopes of swimming motor neuron spikes were calculated for 1–2 ms; plateau and rapidly repolarizing slopes were calculated for 8–30 ms and 3–10 ms, respectively. Rising and falling slopes of short-duration spikes were calculated over periods of 1–2.4 ms. All values are expressed as mean ± standard deviation.

RESULTS

Isolated cells and clusters (50–400 µm in diameter) of cells settled within an hour of plating, attached to the mesoglea, and began extending processes. Epithelial cells were abundant during the first 2 d in culture and often

19

formed monolayers of varying sizes (50 μm to >2 mm in diameter). After 1 day, processes bearing growth cones were seen radiating from the clusters. Over several days, many of the cells forming the monolayers and clusters floated away, leaving isolated, process-bearing cells. Several neuronal types could be recognized morphologically, electrophysiologically or immunocytochemically. These included the swimming motor neurons (SMNs), and small neurons (Fig. 2.2).

Swimming motor neuron morphology

One to five percent of neurons counted in 2- to 4-day-old cultures were distinguishable by their large size (soma 30–50 μm long, with processes up to 200 μm) and clear cytoplasm. The nucleus was usually surrounded by membranous structures (Fig. 2.3A, 2.4B) which appeared as concentric sheaths or as vacuoles, and often extended into the processes, where they appeared as longitudinal bands or folds. Similar bands were sometimes also seen scattered along the neurites. These structures may represent the reflexive membrane infoldings observed in an ultrastructural study of the swimming motor neurons (Spencer, 1979).

Initially these large cells were fusiform or multipolar with short, wide processes, bearing lamellipodial growth cones (Fig. 2.3A). As cultures aged, the processes became elongated and often tapered, while growth cones became smaller. Fig. 2.3B shows an SMN with a long non-tapered process. Neurites could be straight, apparently with no other attachment to the substratum besides their growth cones, or flat and spread at additional contact points, becoming quite irregular.

Fluorescent labelling of the dye-coupled SMN network after physiological identification, followed by dissociation, was carried out in 7 preparations (Fig. 2.4). Results confirmed that the large cells described above were SMNs. The fluorescent cells in culture were usually large (30–50 μm long), presented a clear cytoplasm and membranous inclusions around the nucleus (Fig. 2.4B). Since cultures were photographed only 1 or 2 d after plating, neurites were not always present, and if present, were usually short. Some small fluorescent cells (soma 10–15 μm long) were also observed, suggesting the cultured SMNs have a range of sizes.

Swimming motor neuron electrophysiology

The mean resting potential of isolated SMNs was -53 ± 20 mV (N = 16), and ranged from -33 mV to -95 mV, for different cells. Spencer (1981) measured an average in vivo resting potential for SMNs of -57 mV, and Anderson and Mackie (1977) measured a mean of -60 ± 5 mV.

Approximately half the cells penetrated were excitable to depolarizing current pulses of 0.5–4.0 nA, or produced spikes after being released from prolonged hyperpolarization with 1.0–4.0 nA of current ("rebound" or "anode-break stimulated" spikes). Of these excitable neurons, 13% were spontaneously active.

Amplitudes of spontaneous and rebound spikes in isolated SMNs (50 ± 11 mV, N = 18; Fig. 2.5A) were lower than those recorded from neurons *in vivo* (Fig. 2.5B) using the method of Spencer (1981). For example, Anderson and Mackie (1977) and Satterlie and Spencer (1983) measured spike amplitudes of 80–100 mV for neurons *in vivo*. Action-potential time courses *in vitro* were characteristic of action potentials in intact SMNs (Fig. 2.5A,B and Anderson and Mackie, 1977; Spencer, 1981; Satterlie and Spencer, 1983). *In vitro* spikes depolarized at a mean maximum rate of 20 ± 13 V/s (N = 15), overshot on occasion, and then slowly repolarized along a plateau at a mean rate of –1.1 ± 0.3 V/s (N = 11). The final repolarizing phase was more rapid, at –4.4 ± 3.3 V/s (N = 15). Mean spike duration, from the beginning of the steeply rising phase to the time when the repolarizing phase reached resting potential, was 37 ± 11ms (N = 18) and ranged from 25 to 50 ms. Satterlie and Spencer (1983) found a range of 8–50 ms for neurons *in vivo*. The spikes were followed by after-hyperpolarizations with a mean amplitude of –13 ± 6 mV and a mean duration of 260 ± 140 ms (N = 17).

The action-potential peak and the shoulder at the end of the plateau were seen to vary in shape from sharp to rounded, particularly when depolarizing stimuli served to elicit the spike. Action-potential duration varied during a recording, and appeared to be related to the degree of hyperpolarization when the cell was excited. This was most evident in the rebound action-potential trains elicited upon anode-break stimulation (Fig. 2.5C): spikes generated during the depolarizing return to resting potential were invariably of short duration (10–20 ms), and lacked plateaux, whereas spikes occurring later (after 20 ms) in the train showed more distinct plateaux. There was no detectable change in spike shape related to the age of cultures.

Small neurons

Most of the cells with neuron-like morphology were small (somata <20 μm long). Cells with somatal lengths of 10–20 μm could be separated into two fairly distinct morphological classes: neurons with spindle-shaped, indistinct somata (Fig. 2.6A), and bipolar or multipolar neurons with more

distinct, convex somata and narrow, sometimes beaded, processes (Fig. 2.7). Cells from these two classes could be identified by electrophysiology and immunocytochemistry against RFamide, respectively. Very small cells, with somata 5–10 μm long were also observed but will not be described further, as no attempt was made to record from them, and they did not stain immunocytochemically.

Short-spike neurons

One population of small neurons present in cultures was characterized by narrow, indistinct, spindle-shaped somata (10–20 μm in length) and processes which could be tapered and straight, or flat and irregular (Fig. 2.6A). As for the SMNs, the cytoplasm was clear, but the nucleus was less obvious than in the SMNs. Few, if any, membranous inclusions were seen around the nucleus. However, these cells often showed single, phase-yellow spots near the bases of their processes.

These neurons had a mean resting potential of –55 ± 9 mV, ranging from –45 to –80 mV (N = 6). Injection of small (approx. 0.1 nA), depolarizing current pulses or release from strong hyperpolarization elicited spikes (Fig. 2.6B) that were of short duration (5.4 ± 1.4 ms; N = 7), had a mean amplitude of 25 ± 7 mV and were followed by a large after-hyperpolarization of –18 ± 7 mV which lasted 52 ± 27 ms. Both the depolarizing and repolarizing slopes of the spikes were of similar magnitude, measuring 12 ± 2 V/s and –11 ± 2 V/s, respectively (N = 6).

Action potentials recorded from these short-spike neurons (SSNs) closely resembled those that can be recorded from neurons of an identified outer nerve-ring network, the "B" system (Fig. 2.6C), but spike amplitudes were smaller *in vitro* than *in vivo* (75–80 mV, from Spencer and Arkett, 1984). Resting potentials were lower in "B" neurons (mean –40 mV, from Spencer and Arkett, 1984) than in isolated SSNs. Occasionally, recordings from small cells without processes gave action potentials with the characteristics described above. Fig. 2.6D shows a recording of a spontaneous train of spikes from one such neuron. It can be seen how similar the firing pattern is to that observed in "B" system neurons (Fig. 2.6E).

RFamide neurons

A second class of small neurons, with somatal diameters of 10–20 μm, could be characterized by their immunoreactivity using anti-RFamide serum (Fig. 2.7). Such cells had one to three narrow (approx. 1 μm in diameter), often long processes which could extend for more than 100 μm and usually showed many small (2–3 μm) varicosities. Other neurons

22

having a very similar morphology, such as long narrow processes and small somata, did not stain for the RFamide peptide. No electrophysiological recordings were obtained from neurons with these morphologies.

Neuronal complexes

Various combinations of SMNs and small neurons could be observed in cultures one to several days after plating. Neuronal complexes of anastomosing SMNs, overlapping small neurons, or of both neuronal size classes could be observed. The presence of chemical synapses in these "networks" has not yet been examined electrophysiologically. However, simultaneous intracellular recording from two closely apposed SMNs revealed the presence of electrical coupling.

Clusters of cells which settled initially (see beginning of Results section), could be followed for several days. They were often seen to give rise to neuronal complexes once the overlying epithelial cells sloughed off, suggesting the complexes were "preformed" in the settling clusters. In other cases, neurons which settled far apart (3–5 soma lengths) were seen to extend processes which overlapped with those of distant neighbours and in some cases, neurites were seen approaching nearby cells, appearing to have turned at some point in their extension.

DISCUSSION

A technique is described for isolating different identifiable neuronal types from a cnidarian in order to study individual features of each type, such as their morphology, passive and active electrical properties, and sensitivity to putative neurotransmitters or neuromodulators. Among the different neurons isolated from the jellyfish *Polyorchis penicillatus*, the swimming motor neurons have proven to be the most easily identified, and the most accessible for electrophysiological recording. Their distinctive morphology is similar *in vitro* and *in vivo*: membrane inclusions and clear cytoplasm were seen in an ultrastructural study by Spencer (1979), and their large size and wide processes were also visible in Lucifer Yellow-filled preparations (Spencer and Satterlie, 1980; Spencer, 1981). Fluorescent labelling before dissociation (Fig. 2.4) has shown that these morphological features can be used to identify SMNs reliably. Swimming motor neurons were electrophysiologically identified by their characteristic action potentials with plateaux showing similar time courses in culture (Fig. 2.5A) and in the

23

intact network (Fig. 2.5B; see also Anderson and Mackie, 1977; Spencer, 1981). That this spike shape occurs in isolated, cultured neurons shows that the plateau phase does not result from the temporal summation of several short-duration action potentials from adjacent neurons in the network but is due to summed membrane currents which are intrinsic to each neuron (see discussion by Spencer, 1981). In culture, these action potentials show a variability in duration (25–50 ms; Fig. 2.5C) which is similar, though not identical, to that observed in the semi-intact preparation (8–50 ms; Anderson and Mackie, 1977; Spencer, 1981; Satterlie and Spencer, 1983). The variability *in vivo* may result from changes in activation states of channel proteins, with spike duration varying with the value of the resting potential when a spike is initiated (Anderson, 1979; Spencer, 1981). Such an explanation is also suggested by the occurrence, *in vitro*, of short-duration SMN spikes immediately following sudden release from hyperpolarization (Fig. 2.5C, spike no. 1). It is possible that a rapid repolarizing current, presumably carried by potassium ions and having characteristics similar to I_A (Hille, 1984), is released from inactivation during the hyperpolarizing prepulse. Dissociated SMNs prepared by the present method will be used for a more detailed description of this phenomenon using voltage-clamp techniques.

The small neurons which were identified will offer the possibility of studying synaptic interactions in culture, as they represent networks which are thought to be presynaptic to the SMNs *in vivo*. The cultured short-spike neurons (SSNs) generate rapid action potentials (Fig. 2.6B) that can appear in spontaneous bursts (Fig. 2.6D) and which resemble recordings from the "B" system neurons (Fig. 2.6C,E, respectively). These are the only neurons in semi-intact preparations known to produce such short-duration spikes (Spencer and Arkett, 1984). This is strong evidence that SSNs are "B" system neurons which are presynaptic to the SMNs. This can be confirmed, in the future, by fluorescent labelling and dissociation of the "B" network, followed by electrophysiological recording from isolated, labelled "B" neurons.

RFamide-containing neurons were identified immunocytochemically in 2-day-old cultures, and may play a role in modulating SMN excitability (Spencer, 1988). Their origin in culture has recently been questioned by Alder and Schmid (1987) who have shown that free-floating myoepithelial cells isolated from the medusa *Podocoryne carnea* (Hydrozoa, Anthomedusae) can transdifferentiate and divide, producing FMRFamide-containing cells 4 days, at the earliest, after an intense and prolonged collagenase treatment (1400 units/ml, 25–28°C, for 3 h) which removes the

mesoglea. This could also occur in *Polyorchis* (Hydrozoa, Anthomedusae). However, since the presence of a mesogleal substratum in the experiments described here probably prevents this trandifferentiation (Schmid, 1978), and since the cultures stained with anti-RFamide were too young to have transdifferentiated (2 days old; cf. Alder and Schmid, 1987), it is unlikely that many, if any, of the dissociated RFamide neurons arose by transdifferentiation.

RFamide-containing neurons and short-spike neurons may constitute two distinct cell populations, as suggested by their morphological differences. Unfortunately these differences may be a result of the fixation procedure since cells with wide, tapered processes (similar to SSNs) have been seen to become cells with narrow, beaded processes (similar to RFamide neurons), when the medium was agitated or replaced with hypotonic artificial seawater. The relationship between SSNs and RFamide neurons must be determined by recording from isolated neurons to identify SSNs, followed by staining with antiserum against RFamide.

Spike amplitudes observed for SMNs (Fig. 2.5*A*,*B*) were lower than those observed *in vivo* (Anderson and Mackie, 1977; Spencer, 1981; Satterlie and Spencer, 1983) and a similar reduction was seen for SSNs (Fig. 2.6*B*,*C*) relative to their *in vivo* counterparts (Spencer and Arkett, 1984). This may have resulted from the intense and prolonged treatment with collagenase, as most preparations of this enzyme contain trace activities of trypsin (1.5 units per 1000 units collagenase I, from Sigma), that may be sufficient to damage the ionic channels which carry the action-potential currents. However, since the shapes of spikes *in vivo* and *in vitro* are so similar this seems unlikely. A more attractive possibility is that the ensheathing epithelial cells of *in vivo* preparations could either regulate the extracellular ionic environment or act as high-resistance barriers preventing shunting of any leakage currents due to damage by the microelectrode. It is not clear what effect isolation of neurons, which are normally members of an electrically coupled network, should have on spike amplitude. On one hand one might expect some degree of summation of action potentials in an electrically coupled population but, on the other, decreased input resistance due to coupling should reduce the amplitude of action potentials. Finally, the decreased excitability of SMNs and the reduced amplitude of action potentials *in vitro* may be due to the ionic composition of the bathing medium. Anderson and Schwab (1984) found that motor neurons of *Cyanea* were difficult to excite when bathed in ASW but that when a bathing medium containing less Mg^{2+} and more K^+ was

used then the neurons became far more excitable. It is possible that the ionic composition of the ASW used in these experiments is different from the extracellular fluid *in vivo*. Voltage-clamp recordings of peak currents from neurons dissociated with different enzymatic treatment, or from neurons in the presence or absence of apposed epithelial cells, could help clarify the relative contribution of these factors in altering action-potential amplitude.

This culture system will be used to describe the electrophysiological properties of each neuronal type *in vitro* using voltage- and current-clamp recording and to give qualitative and quantitative descriptions of the effects of putative neurotransmitters or neuromodulators on neuronal function *in vitro*. This information on target cells in culture, combined with experimental data on presynaptic release in cultured neuronal complexes and in semi-intact preparations, will allow the determination of the nature of chemical transmitters in this primitive nervous system.

Dissected nerve-ring tissue

↓

ASW, twice:
10 and 5 min

↓

Divalent cation-free ASW (1 mM EGTA),
15 min, room temperature

↓

ASW, 30-60 s

↓

1 ml collagenase I
(1000 units/ml in ASW)
3-5 hours, 22-25°C

→ **Divalent cation-free**
ASW, 10 min

↓

8 ml ASW

↓

Remove ASW to leave 0.5-2 ml

↓

Triturate 10 strokes with siliconized,
smooth-tipped Pasteur pipette

↓
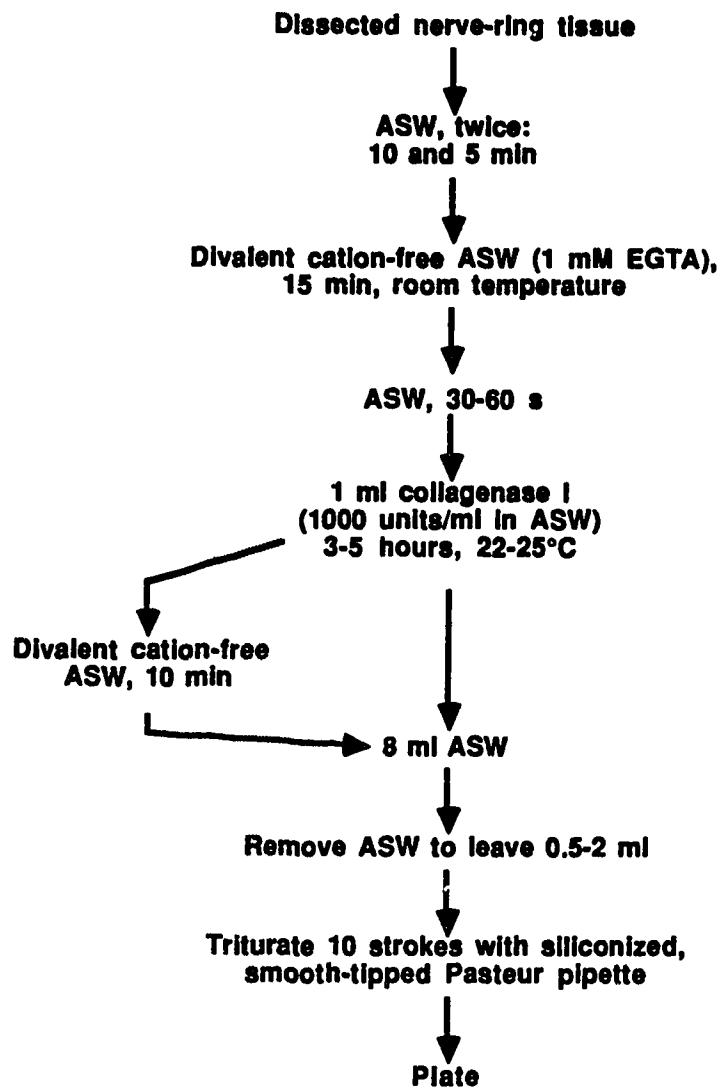
Plate

Figure 2.1 - A flow chart of the procedure used for dissociating the nerve-rich bell margin of *Polyorchis penicillatus*. ASW, artificial seawater.

27

Figure 2.2 - Cell types found in a 1-day-old primary culture of nerve-rich tissue. Cells were plated on homogenized mesogleal substratum (*ep*, epithelial cells; *fb*, mesogleal fibers; SMN, swimming motor neuron; *sn*, small neurons).
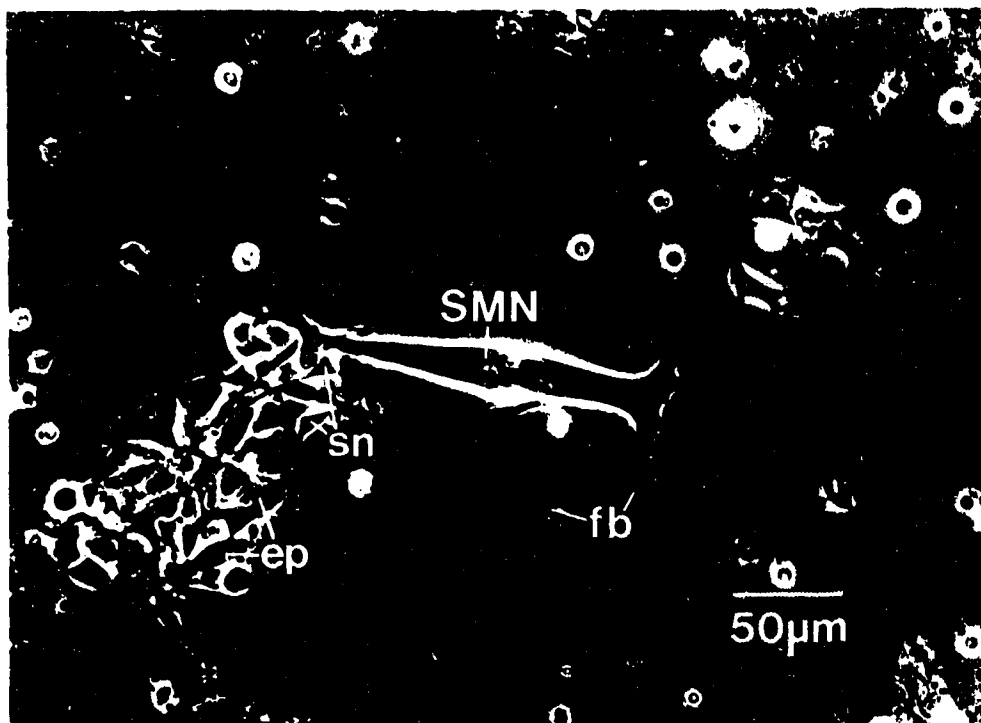
Figure 2.3 - Swimming motor neurons (SMNs) in culture viewed with Nomarski optics. *A*. Membranous inclusions (*mi*) were apparent around the nucleus of an SMN, 1 day after plating. The remainder of the soma had clear cytoplasm. Extensive growth cones (*gc*) were typical at this stage. *B*. A different SMN in a 3-day-old culture extending a long process, bearing a reduced growth cone.
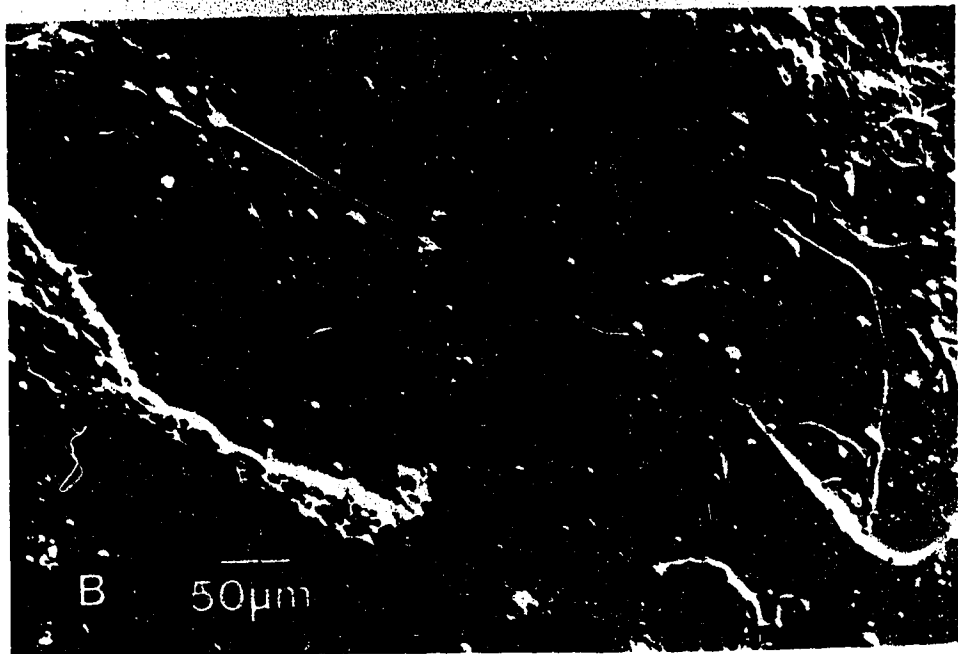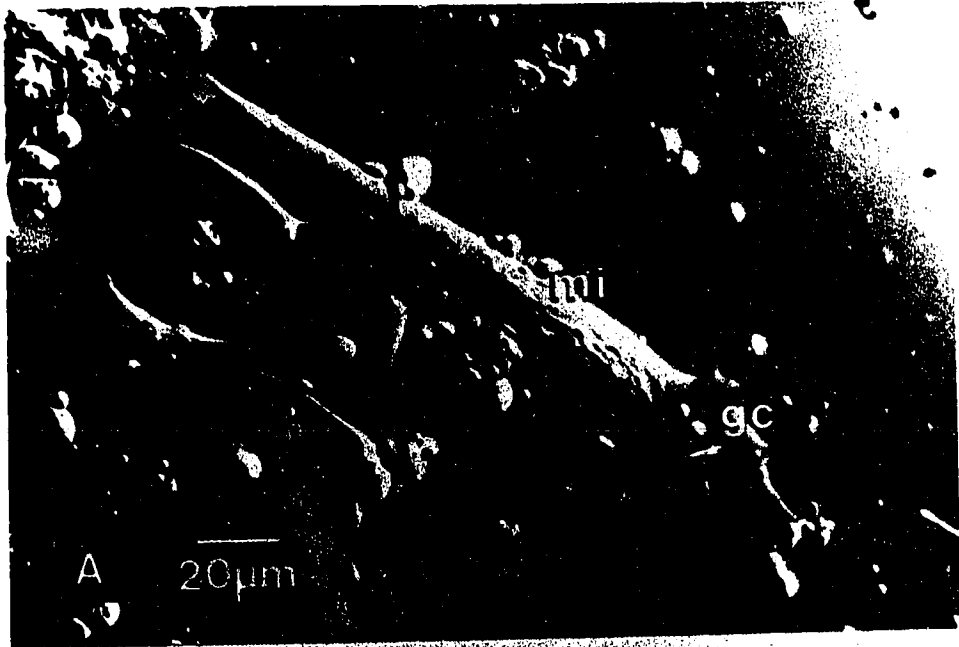
Figure 2.4 - Identification of SMNs using a fluorescent marker. *A*. Two large, fluorescent cells found in a 1-day-old culture after dissociating a nerve-ring containing carboxyfluorescein-labelled swimming motor neurons and viewing under ultraviolet illumination. Note that two smaller SMNs are also present in the field but they are in a slightly different focal plane. Scale bar applies to both panels. *B*. The same cells seen using Nomarski optics showed the clear cytoplasm and perinuclear membranous structures typical of SMNs.
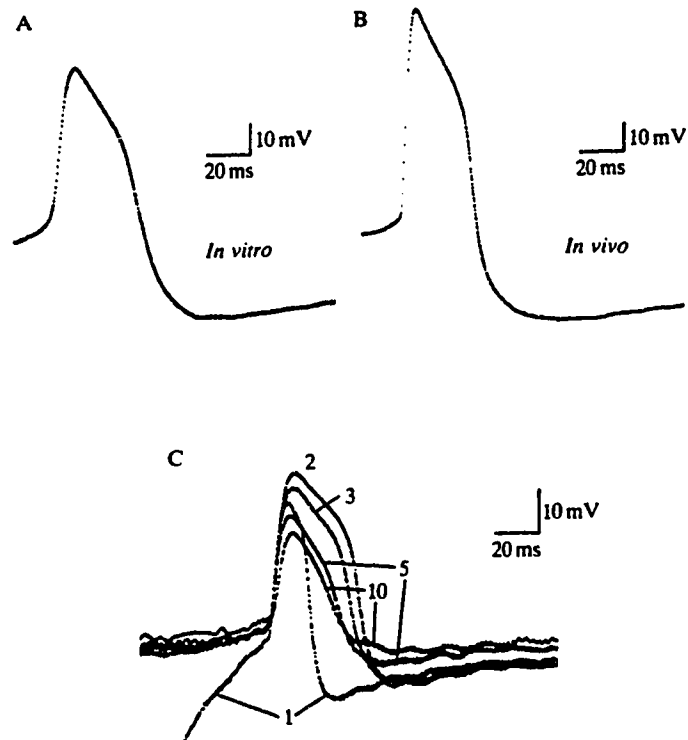
Figure 2.5 - Action potentials recorded from swimming motor neurons (SMNs) both *in vitro* and *in vivo*. *A.* Anode-break stimulated action potential recorded from a SMN *in vitro* for 2 d, shows that spike parameters are similar to those recorded from swimming motor neurons *in vivo*. *B.* Spontaneous action potential recorded *in vivo* using the method of Spencer (1981). *C.* A train of spikes elicited by a single anode-break stimulation of an SMN, in culture for 3 d. The position of each spike in the train is indicated by a number. The initial spike was of short duration while the second had a pronounced plateau. The third to tenth spikes decreased progressively in amplitude, duration and in expression of the after-hyperpolarization.

34

Figure 2.6 - Morphology and physiology of short-spike neurons. *A.* Short-spike neuron after 4 d in culture showing small fusiform soma and processes only slightly narrower than the soma. The extremity of one process is covered by a spherical epithelial cell. *B.* Action potential elicited by a small, slowly depolarizing stimulation of the neuron in *A.* *C.* Spontaneous action potential recorded from a "B" system neuron *in vivo. D. and E.* Firing pattern of a short-spike neuron compared with the pattern seen in "B" system neurons. *D.* A train of spontaneous action potentials recorded from a short-spike neuron after 1 day in culture. *E.* A train of "B" system action potentials recorded *in vivo*, in response to a shadow stimulus (*arrow*). *C* and *E* reproduced with permission from Spencer and Arkett (1984).

A 20μm

B 10 mV 10 ms

C 25 mV 10 ms

D 40 mV 1 s

E 50 mV 1 s
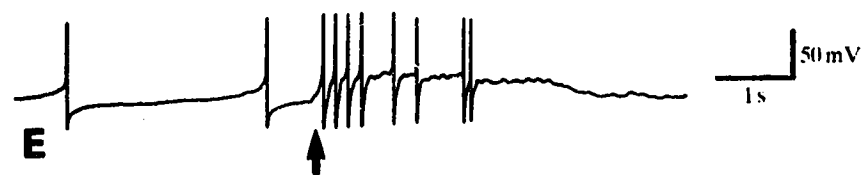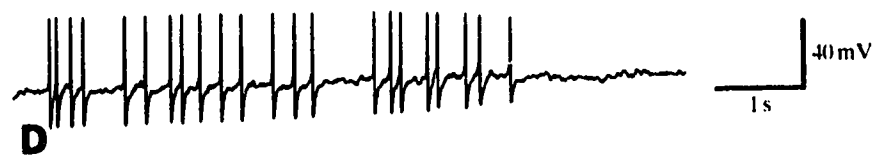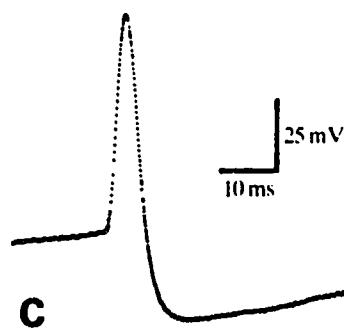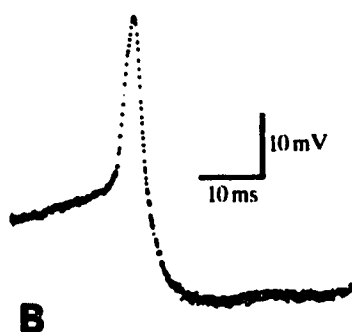
Figure 2.7 - Morphology of small neurons showing immunoreactivity to anti-RFamide serum. Note the convex somata, and the narrow process bearing several small varicosities.

20µm

REFERENCES

Alder H, Schmid V (1987) Cell cycles and *in vitro* transdifferentiation and regeneration of isolated, striated muscle of jellyfish. Devel Biol 124: 358-369.

Anderson PAV (1979) Ionic basis of action potentials and bursting activity in the hydromedusan jellyfish *Polyorchis penicillatus*. J Exp Biol 78: 299-302.

Anderson PAV (1985) Physiology of a bidirectional, excitatory, chemical synapse. J Neurophysiol 53: 821-835.

Anderson PAV (1987) Properties and pharmacology of a TTX-insensitive Na^+ current in neurons of the jellyfish, *Cyanea capillata*. J Exp Biol 133: 231-248.

Anderson PAV, Mackie GO (1977) Electrically coupled, photosensitive neurons control swimming in a jellyfish. Science 197: 186-188.

Anderson PAV, Schwab, WE (1984) An epithelial cell-free preparation of the motor nerve net of *Cyanea* (Coelenterata; Scyphozoa). Biol Bull Mar Biol Lab, Woods Hole 166: 396-408.

Arkett SA, Spencer AN (1986a) Neuronal mechanisms of a hydromedusan shadow reflex. I- Identified reflex components, and sequence of events. J Comp Physiol A 159: 201-213.

Arkett SA, Spencer AN (1986b) Neuronal mechanisms of a hydromedusan shadow reflex. II- Graded response of reflex components, possible mechanisms of photic integration, and functional significance. J Comp Physiol A 159: 215-225.

Grimmelikhuijzen CJP (1985) Antisera to the sequence Arg-Phe-amide visualize neuronal centralizaton in hydroid polyps. Cell Tissue Res 241: 171-182.

Grimmelikhuijzen CJP, Spencer AN (1984) FMRFamide immunoreactivity in the nervous system of the medusa *Polyorchis penicillatus*. J Comp

Neurol 230: 361-371.

Hille B (1984) Ionic channels of excitable membranes. Sunderland, MA: Sinauer.

Kerfoot PAH, Mackie GO, Meech RW, Roberts A, Singla CL (1985) Neuromuscular transmission in the jellyfish *Aglantha digitale*. J Exp Biol 116: 1-25.

King MG, Spencer AN (1979) Gap and septate junctions in the excitable endoderm of *Polyorchis penicillatus* (Hydrozoa, Anthomedusae). J Cell Sci 36: 391-400.

Martin SM, Spencer AN (1983) Neurotransmitters in coelenterates. Comp Biochem Physiol 74C: 1-14.

Satterlie RA, Spencer AN (1983) Neuronal control of locomotion in hydrozoan medusae. A comparative study. J Comp Physiol A 150: 195-206.

Satterlie RA, Spencer AN (1988) Organization of conducting systems in "simple" invertebrates: Porifera, Cnidaria and Ctenophora. In: Nervous systems in invertebrates (Ali MA, ed), pp 213-264. New York: Plenum.

Schmid V (1978) Striated muscle: influence of an acellular layer on the maintenance of muscle differentiation in anthomedusae. Dev Biol 64: 48-59.

Schmid V, Alder H (1984) Isolated, mononucleated, striated muscle can undergo pluripotent transdifferentiation and form a complex regenerate. Cell 38: 801-809.

Spencer AN (1979) Neurobiology of *Polyorchis*. II. Structure of effector systems. J Neurobiol 10: 95-117.

Spencer AN (1981) The parameters and properties of a group of electrically coupled neurons in the central nervous system of a hydrozoan jellyfish. J Exp Biol 93: 33-50.

Spencer AN (1982) The physiology of a coelenterate neuromuscular synapse. J Comp Physiol A 148: 353-363.

Spencer AN (1988) Effects of Arg-Phe-amide peptides on identified motor neurons in the hydromedusa *Polyorchis penicillatus*. Can J Zool 66: 639-645.

Spencer AN, Arkett, SA (1984) Radial symmetry and the organization of central neurons in a hydrozoan jellyfish. J Exp Biol 110: 69-90.

Spencer AN, Satterlie RA (1980) Electrical and dye coupling in an identified group of neurons in a coelenterate. J Neurobiol 11: 13-19.

Chapter 3

VOLTAGE-ACTIVATED CALCIUM CURRENTS IN IDENTIFIED NEURONS FROM A HYDROZOAN JELLYFISH, *POLYORCHIS PENICILLATUS*.[2]

INTRODUCTION

Nervous systems probably first evolved in close ancestors of the Cnidaria, when certain cells became specialized for electrical excitation and rapid chemical neurotransmission. The voltage-clamp study of membrane ionic currents from these primitive animals is significant to comparative physiology since it can provide information on the molecular evolution of ion channel populations that paralleled the functional emergence of neurons. Calcium currents were studied in "swimming motor neurons" (SMNs) isolated from the hydrozoan jellyfish *Polyorchis penicillatus* to identify characteristics that will help in describing the roles of these currents in excitability and synaptic function.

The SMNs of *Polyorchis penicillatus* have been described *in situ* both morphologically (Spencer, 1979) and electrophysiologically (Anderson and Mackie, 1977; Spencer, 1981), and their role in the control of swimming is established (Spencer, 1978, 1982; Satterlie and Spencer, 1983). These cells form an electrically coupled network around the bell margin (Spencer and Satterlie, 1980) which synapses onto the swimming muscle sheets (Spencer, 1979, 1982) and drives swimming. To circumvent the voltage-clamp problems associated with electrical coupling, a primary culture technique was recently developed for the isolation of the SMNs (Przysiezniak and Spencer, 1989 [Chapter 2]).

In these SMNs, firing patterns and synaptic transmission probably depend on the influx of calcium ions, as demonstrated, respectively, by Anderson (1979) using ionic substitutions and by Spencer (1982) using Mg^{2+} blockade. However, more direct interventions are needed to understand the mechanisms of calcium influx in these cells. Tight-seal, whole-cell voltage

---

clamp has recently been used to describe calcium currents in various cnidarians (Anderson, 1987, in *Cyanea*; Dunlap et al., 1987, in *Obelia*; Meech, 1989, in *Aglantha*; Holman and Anderson, 1991, in *Calliactis*). A brief description has been presented of the transient calcium current from isolated SMNs of *Polyorchis* and its relevance to neuromuscular synaptic physiology has been discussed (Spencer et al., 1989 [Appendix A]). Following the latter study, the composition of both electrode and bath solutions has been improved, allowing better identification of a very slowly inactivating component that was originally contaminated by residual outward current. An extensive description is given of the time courses, voltage dependencies and ionic selectivities of the calcium currents, some pharmacological characterization of these currents is included. Possible mechanisms of ionic selectivity and inactivation, and the number of calcium channel populations present in these neurons are discussed.

MATERIALS AND METHODS

Animals

Animals were collected in Bamfield Inlet (Vancouver Island, British Columbia) from the surface by dip netting, or at depth by scuba divers using plastic bags. The jellyfish were maintained in a recirculating, refrigerated (10°C) aquarium containing a mixture of Rila Marine Mix and seawater from Bamfield Inlet, on a cycle of 12 h of light, 12 h of dark. The animals were fed newly-hatched brine shrimp larvae once or twice a week.

Dissociation

The culture techniques are described more fully in Przysiezniak and Spencer (1989 [Chapter 2]), but have been slightly modified and will be summarized here. The nerve-rings were dissected from the bell margin as previously described and placed in artificial seawater (ASW; see below) in a borosilicate test tube for 5 min. The solution was then replaced with 10% ASW for 5 min and with divalent cation-free ASW (Ca^{2+} and Mg^{2+} replaced with choline and 1 mM EGTA) for 15 min. Digestion was carried out in collagenase type I (Sigma), 1000 units/ml ASW, at room temperature (20–25°C), for 3–7 h depending on the integrity of the tissue (decreases with time since capture) observed during dissection. The enzyme solution was then replaced with an excess of ASW, with minimal disturbance to the tissue. The solution was pipetted off until the volume was appropriate for effective trituration and plating (usually 0.5 ml for 5 dishes). Up to 10

strokes of trituration against the bottom of the test tube were given with a fire-polished Pasteur pipette. Three or four drops of the suspension were plated in the centers of Falcon 1008 culture dishes coated with dried homogenate of desalted, cleaned, bell mesoglea (Przysiezniak and Spencer, 1989). After being left to settle for 30 min to 4 h at room temperature, cultures were rinsed twice with ASW and incubated at 10°C until used. No nutrients were added to the cultures, which survived at least 1 week. Recordings were made on cells plated for 0–5 d. Major features of the calcium and barium currents, namely time to peak, peak current, voltage dependence of activation, time course of inactivation and voltage dependence of inactivation, did not change with the age of the culture.

Solutions

Artificial seawater contained (in mM) NaCl, 378; CaCl$_2$, 9.5; MgCl$_2$, 29; Na$_2$SO$_4$, 5.7; KCl, 13.4; choline–Cl, 42; HEPES buffer, 10; NaOH, 5. The antibiotic gentamycin sulfate was added at 50 mg/l (Sigma, G-3632; ~65 μM). The pH of all solutions was adjusted to 7.5 ± 0.05. All culture and recording solutions were filtered through cellulose acetate or nylon membrane cartridges with 0.2 μm pore size before use.

In early recordings, caesium was used to replace internal potassium and sodium while choline replaced external sodium ions. However it was found that caesium ions carried a slow, outward current, possibly through potassium or calcium channels, which caused the apparent reversal of I$_{Ca}$ at positive voltages (cf. Spencer et al., 1989 [Appendix A]) and when long depolarizations were given. In the experiments presented in this article, N-methyl-D-glucamine (NMG) replaced potassium and sodium inside as well as outside the cell, which eliminated the contaminating outward current.

All recordings were carried out with the following two solutions, unless otherwise specified. The bath solution for recording contained (in mM) CaCl$_2$, 10; MgCl$_2$, 40; NMG, 433; HEPES, 10; and HCl, 421. This composition was based on the results of analyses of ions in natural seawater and mesoglea using ion chromatography (Cl$^-$ and SO$_4^{2-}$), atomic absorption spectroscopy (K$^+$) and inductively coupled plasma spectroscopy (Na$^+$, Mg^{2+}, Ca^{2+}). Magnesium and calcium in the bath were at concentrations close to their concentrations in seawater (44.1 mM and 9.0 mM, respectively). Barium replaced calcium mole for mole, where appropriate. Before recording from a culture, the medium was exchanged for recording bath solution by the slow addition of one bath volume followed by at least two

44

complete bath exchanges.

The electrode solution contained (in mM) $CaCl_2$, 1; EGTA, 11; $MgCl_2$, 2; NMG, 508; HEPES, 10; HCl, 477. The calcium concentration in this solution was estimated to be ~1 nM, using a computer program (Stockbridge, 1987). To improve sealing, the electrode solution in some recent experiments was made hypotonic (90–98%) by adding the appropriate amount of distilled water. Electrode solutions were allowed to dialyze into the cells, until current responses to voltage-clamp pulses were stable for more than 1 min; this took 3–10 min, as estimated by maximal test responses elicited every minute.

Pharmacological agents

Cadmium chloride was made up as a 100 mM solution in distilled water. Nifedipine (Sigma, N–7634) stock solution was made up to 10 mM in 5% dimethyl sulfoxide (DMSO) and 66.5% ethanol. Verapamil HCl (Sigma, V–4629) stock solution was 20 mM in 70% ethanol. Chemicals were diluted further in the recording bath solution, ad were either applied to the bath through a fine polyethylene tube to within 8 mm of the electrode tip or superfused into the bath 8–12 mm from the cell while suction was applied at the solution surface from the edge of the dish.

Electrodes and equipment

Electrodes were pulled on a Narishighe PP–83 puller, from non-heparinized hematocrit tubing (Fisher, thin-walled soda glass, cat.#02-668-68). Before polishing, the electrode tips were dipped in a siliconizing agent, Sigmacote (Sigma), diluted to between 1/10 and 1/20 with n-heptane; this treatment significantly increased the rate and tightness of seal formation and greatly improved the quality of the phase-contrast optics when the electrode was in the bath. Electrodes were stored at room temperature, in a loosely covered jar for up to a few days. Day-old, siliconized electrodes seemed to attach better than did freshly siliconized electrodes, although both fresh and old electrodes were used in these experiments. The pipettes had an average resistance of 0.9 MΩ (range, 0.6 to 1.3 MΩ; N = 47).

The cultures were viewed under phase-contrast with a Nikon Diaphot inverted microscope. Electrodes were positioned with a "Huxley-Goodfellow"-type micromanipulator (Campden Instruments, London, UK). Grounding was through a silver chloride-coated silver wire inserted into an agar bridge (4% agar in electrode solution described above). An L/M-EPC7 amplifier (List Medical, Darmstadt, Germany) was used for tight-seal, whole-cell voltage clamping. Stimulus control and data acquisition and

processing were carried out with an IBM-PC computer, an XT clone, or a 386-SX clone, fitted with a Labmaster TL-1 interface, using pCLAMP 5.5 software (Axon Instruments interface and software).

Recordings

The swimming motor neurons (SMNs) were identified by their characteristically large size (usually about 70 μm x 25 μm), compact shape, and clear cytoplasm (Przysiezniak and Spencer, 1989 [Chapter 2]). Recordings were made at 20–22°C. Long processes were absent or removed by cutting with a pipette tip. Seal resistances before access ranged between 0.5 and 5 GΩ.

Liquid junctional potentials between electrode and bath solutions were cancelled electronically when the electrode was in the bath. Offset compensation was occasionally checked after recordings and was found to vary by less than 3 mV. In all experiments except that in Fig. 3.2, the ionic composition of the bath solution was fixed, so it is unlikely that changes in the junctional potential affected the results. However, assuming large, anionic proteins with poor mobility were present in the cytoplasm, it is possible that a junctional potential was present that made the bulk of the cytoplasm more negative than the electrode tip (Marty and Neher, 1983). Thus, most of the voltages in the Results may be more positive than the true values by a fixed amount (5–10 mV).

Leakage and capacitive current subtraction protocols were composed of 4 or 5 hyperpolarizing pulses one-fourth or one-fifth the size of the test pulse, respectively, and were applied from a holding potential of –60 mV. The holding potential was then set to –80 mV for 500 ms, and a test pulse was applied to elicit an active response. The passive responses to the leakage pulses were summated and added online to the active response. This protocol assumes that leakage resistance is linear throughout the range of leakage and test pulse voltages used. Passive test responses to depolarizing or hyperpolarizing pulses of 40 mV amplitude lasting 5 or 10 ms were recorded repeatedly during an experiment, usually before and after protocols eliciting active currents, to monitor series resistance (R_{ser}) and leakage resistance (R_{leak}). Test pulses were applied from a holding potential of –80 mV if depolarizing, and from –40 mV if hyperpolarizing. Passive responses were low-pass filtered at 10 kHz, while active responses were filtered at 3 kHz before acquisition, using a three-pole Bessel filter.

R_{leak} was calculated from the current at the end of the passive responses. R_{ser} was estimated from the amplitude of the capacitive transient, obtained

by back-extrapolation of a single-exponential fit to the beginning of the passive test pulse. The voltage error caused by active currents flowing through R_{ser} was calculated as follows: leakage current was calculated from R_{leak} and the amplitude of the command pulse and was added to the active current amplitude; the voltage error was obtained as the product of R_{ser} by this "reconstituted" current. No R_{ser} compensation was used since active currents were small. In addition, the rising phase of active currents was masked by an initial, transient, outward current, and could not have been resolved further by R_{ser} compensation.

Data analysis

Data for all experiments were selected on the basis of the following criteria. 1) The neuron must be clearly identified as a "swimming motor neuron" by its large size, compact shape, and clear cytoplasm (Przysiezniak and Spencer, 1989 [Chapter 2]). While characteristic plateau action potentials were produced by these cells in normal ionic conditions (Spencer, 1981; Przysiezniak and Spencer, 1989), no spikes were generated in calcium current recording conditions; thus spike shape could not be used for cell identification. 2) Leakage resistance must be larger than or equal to 0.5 GΩ. 3) Series resistance must not exceed 10 MΩ. 4) Active currents must show no sign of major instability such as the large, random fluctuations caused by seal disruption.

Unless specified, data for calcium and barium currents were collected from different cells, in static conditions, that is, without solution changes, because superfusions tended to disrupt recordings. Comparisons between calcium and barium currents are thus between populations of cells.

All traces were digitally filtered at 1 kHz (Gaussian filter) before measurements were taken. Peak currents were measured using the automatic peak detection function in the Clampan section of the pCLAMP software. Late currents measured isochronally were taken slightly before the end of the pulse (e.g., at 78.2 ms on an 80 ms pulse) to avoid capacitive transients spread out by digital filtering.

An attempt was made to normalize absolute current amplitudes to current densities, using capacitance an as estimate of cell surface. Cell capacitance was obtained by calculation from R_{ser} and τ values measured from the passive test responses, and by integration of the capacitive transients. However, the variability in the data did not seem to be diminished by this approach, suggesting that capacitance is not a reliable indicator of cell surface, or that channel number is independent of cell

47

surface area. Consequently, this type of normalization was not used.

Statistical significance was determined as a probability of 0.05 or less, obtained from a two-tailed Student's t test (Sokal and Rohlf, 1981).

Equations and curve fitting

Exponentials were fitted to current traces using the Clampfit section of the pCLAMP 5.5 software (Axon Instruments). Exponentials in the experiments on recovery from inactivation were fitted with a C-language (Turbo-C version 2, Borland International) program using a least-squares procedure.

Initial transient current activation curves were fitted with the modified Boltzmann distribution:

$$I_{init} = I_{min} + (I_{max} - I_{min})/\{1 + exp[(V_a - V)/K_a]\} \tag{1}$$

where V is the command voltage, I_{min} is an offset component, I_{max} is the current at saturation, V_a is the voltage at half-activation, and K_a is the slope factor, expressed as mV/e-fold change. This and other equations were fitted by iterating parameters to the nearest single-decimal value (0.1 mV or 0.1 pA) using a least-squares procedure adapted to a spreadsheet (Microsoft Excel, version 2.2, Microsoft Corporation).

Other equations fitted are described in the appropriate table notes.

RESULTS

The following evidence will show that the most prominent calcium current in SMNs of *Polyorchis*, the high-voltage-activated (HVA) current, exhibits a transient, ion-selective component (HVA-t) and a sustained, non-selective component (HVA-s). These will be distinguished and described in sections on time course, voltage dependence of activation and steady-state inactivation. A third, "very-high-voltage-activated" (VHVA) current, exhibits a more positive I-V relationship and a slower onset, and will be distinguished from the HVA currents in the section on voltage dependence of activation. First, however, the passive cell properties are described, and I_{Ca} is distinguished from sodium currents and a possible gating current.

Passive properties

The passive membrane properties of SMNs were measured from

48

responses to ±40 mV pulses applied from -80 mV (if depolarizing) or -40 mV (if hyperpolarizing). Leakage resistances (R_{leak}) had a mean of 1.2 GΩ (range, 0.5 to 3.7 GΩ; N = 123 measurements). The series resistance (R_{ser}) averaged 3.8 MΩ, ranging from 1.4 to 9.1 MΩ. Single-exponential fits to the transients decayed e-fold in 121 μs (range, 36–246 μs), indicating a cell capacitance around 30 pF. As calculated from these fits, voltage-clamp pulses reached 95% of the command step after an average of 362 μs (range, 108–737 μs). In data collected with a single electrode, double exponentials fitted the capacitive transients slightly better than did single exponentials, yielding a rapidly decaying component (τ = 88 μs) and a slower component (τ = 542 μs) which represented about 1.8% (range, 0.2–9.1%) of the total transient amplitude, indicating the presence of an electrically remote part of the cell membrane even in cells that were almost spherical. The average voltage error due to active currents flowing through R_{ser} was calculated to be -0.4 mV at maximal calcium current (range, -1.5 to $+0.3$ mV).

Distinguishing I_{Ca} from other currents

In conditions where calcium was the only cation in the bathing solution expected to be permeant (9.5 mM), an inward, inactivating current was observed in response to 50-ms-long depolarizing pulses to $+20$ mV (Fig. 3.1) from a holding potential of -40 mV. This current was eliminated by the replacement of external calcium with cobalt (N = 9). It was not carried by magnesium, since a 10-fold reduction of $[Mg^{2+}]_{out}$ (to 4 mM) did not change the amplitude of the current (N = 3; data not shown). I_{Ca} showed very little "rundown" after more than 60 min. When the cell was suddenly released from voltage clamp to current clamp, the membrane potential rose slowly, then rapidly to a resting level around $+15$ mV.

Calcium current is known to flow through sodium channels in the squid giant axon when the bath solution contains no sodium and a large concentration of calcium (Meves and Vogel, 1973). To show that channels specific for calcium, and not sodium, mediated the calcium current, recordings were made in conditions where both I_{Na} and I_{Ca} could occur simultaneously while no other permeant ion was present. Under these conditions, two currents with distinctly different time courses could be recorded. Figure 3.2 shows that a net inward current was observed in saline containing 100 mM Na$^+$ and 10 mM Ca^{2+}, and with an internal solution containing 50 mM Na$^+$ and low calcium. When the sodium gradient was reversed by a brief superfusion with Na$^+$-free saline, a rapid, transient outward current carried by sodium and a slower, inactivating, inward

current carried by calcium, occurred simultaneously. Further superfusion increased the outward I_{Na}, which almost obscured I_{Ca}.

In separate recordings of I_{Na} and I_{Ca}, cadmium specifically blocked the calcium current (see Fig. 3.9A) but did not affect the sodium current substantially (J. Przysiezniak and A. N. Spencer, in preparation), once more indicating that distinct channel populations mediated these two currents.

The selectivity of the calcium channels for divalent cations, such as calcium or barium, may not be absolute. For example, in the absence of calcium or barium (replaced with cobalt) and in the presence of sodium, the SMNs were seen to generate plateau action potentials (data not shown), which are typically produced by calcium currents (e.g., see Fig. 3.9B). This suggests the calcium channels in SMNs pass sodium ions in the absence of divalent cations, a common occurrence in other preparations (e.g., Hess and Tsien, 1984; Almers and McLeskey, 1984; Lux et al., 1990).

When either Ca^{2+} or Ba^{2+} was the only permeant ion inside and outside the cell, a transient, outward current usually preceded the inward current (Fig. 3.3A). This outward current was not a capacitive artifact, because R_{ser} compensation did not remove it. This current was not visible in the experiment shown in Figure 3.2A because the rapid, outward, sodium current masked it. The transient, outward current appeared to be larger in barium than in calcium (Fig. 3.3A; see below), probably because the inward current was smaller in barium and masked less of the transient current. In response to graded depolarizations, the transient current measured at 600 µs from the beginning of averaged traces (nine cells in each ion) showed a sigmoid voltage dependence. This transient outward current may have reflected the movement of channel gating charges in sodium, potassium or calcium channels.

Time course of maximal responses

Most of the experiments described in this and the following sections were carried out on both calcium and barium currents, with external Ca^{2+} or Ba^{2+} at a concentration of 10 mM. Usually, only one of the two ionic species was used in a given cell so that calcium and barium current data were collected from sets of different cells. All data are expressed as mean ± SEM.

In all cells with SMN morphology, maximal, rapidly activating divalent cation currents could be elicited by voltage-clamp commands (V_c) to +10 mV from a holding potential (V_h) of −80 mV. The early activation phase of I_{Ca} and I_{Ba} was contaminated by capacitive transients, which saturated the analog-to-digital converter for the first ~0.5 ms, and by the transient, initial, outward current (see above section), which occupied the next ~0.5 ms.

50

Consequently, exponential fitting to the rising phase was not done and time to peak (T_{peak}) was used to estimate activation rate.

Table 3.1 summarizes and compares the different features of maximal calcium and barium current responses. Both I_{Ca} and I_{Ba} activated rapidly at similar rates, each reaching a peak in about 4 ms, at which point I_{Ba} was 40% smaller than I_{Ca} (Fig. 3.3A, Table 3.1). The inactivation phase of the responses during 400 ms pulses to +10 mV followed a double-exponential time course that reached a non-zero steady state. The back-extrapolated amplitudes of both rapidly and slowly inactivating components were significantly larger in calcium than barium (Table 3.1). I_{Ba} and I_{Ca} exhibited only slight, statistically insignificant differences between the time constants fitted. The amplitude of I_{Ba} was significantly smaller than that of I_{Ca} for the first several hundred milliseconds, while the amplitudes of the currents carried by both ionic species reached an identical, sustained level at the end of 1-second-long pulses (Fig. 3.3C; Table 3.1). These results indicate the presence of a transient, selective current with complex inactivation, and a sustained, non-selective current. Because the transient current was much larger than the sustained current, the behavior of the "peak" current will be assumed to adequately represent that of the "transient" current.

Tail currents were visible upon repolarization to –80 mV (Fig. 3.3B), in calcium and barium. A large, rapid (~200 pA, $\tau \approx$ 150–290 μs), exponential component occurred within the voltage-clamp transition time (~360 μs; see above), and was too rapid to measure accurately. A smaller, slower relaxation component (~20 pA, $\tau \approx$ 2 ms) and a small, sustained tail current could be seen upon repolarization to –80 mV from test pulses eliciting I_{Ca} or I_{Ba}. The sustained I_{Ca} tail current was absent after return to a holding potential of –40 mV, suggesting it was not a chloride current ($E_{Cl} \approx$ 0 mV, in these conditions). The sustained tail current was larger in calcium than barium, like the selective, transient current seen above. It was not an artifact of leakage subtraction because it was also observed without subtraction. Neither was it an artifact of bad space clamping, because it was observed in multiple-channel patches (preliminary data), which should have been well clamped. It likely represented current through calcium-selective channels.

Voltage dependence of activation of divalent cation currents
Current-voltage relationships

The transient and sustained currents differed little in their current-voltage (I–V) relationships (Fig. 3.4A,B). The peak current on 80 ms

51

pulses and the current at the end of 1 s pulses first activated around -30 mV, rose sigmoidally with voltage, and reached a maximum around +10 mV. Because of their voltage range of activation and their time courses, these currents will be referred to as the HVA-t (HVA, transient) current HVA-s (HVA, sustained) current, respectively.

The maxima of I_{Ca} and I_{Ba} occurred at the same voltage (+10 mV), suggesting barium and calcium exerted the same effect on the membrane surface potential. It is unlikely that surface charges were altogether absent because a ten-fold decrease of external magnesium concentration caused a -10 mV shift of the voltage of maximal I_{Ca} (N = 3; data not shown). The HVA-t component was significantly larger in Ca^{2+} than Ba^{2+} from -10 mV to +60 mV (Fig. 3.4A), while no such selectivity was apparent for the HVA-s current (Fig. 3.4B).

Current responses to commands ranging up to +70 mV behaved in a manner that suggested the presence of another current, which seemed to activate at higher voltages but with a slower time course than did the HVA components. This VHVA current (very-high-voltage-activated) was most evident using averaged barium current responses. Figure 3.5A shows I_{Ca} and I_{Ba} responses to an incrementing series of 80 ms depolarizations applied from a V_h of -80 mV. At voltages beyond +40 mV, the population-averaged I_{Ca} activated fairly rapidly and inactivated partially during the pulse, while I_{Ba} arose slowly ($\tau \approx$ 10 ms) and showed little inactivation for the duration of the stimulus. Apparently, at very high voltages, the HVA-t current was small when barium was the charge carrier, but the more slowly activating, VHVA component was carried equally well by barium or by calcium.

A plot of I_{Ba} at 78 ms versus voltage shows a distinct shoulder at about +50 mV (Fig. 3.5B). Seven of the 9 data sets averaged exhibited a secondary increase in barium current between +30 mV and +60 mV. Such a shoulder could occur if the large, hyperpolarizing, leakage pulses preceding very positive test pulses (see Materials and Methods) elicited non-linear, inward current responses that were then summated to the test responses. However, plots of late I_{Ba} responses recorded without any digital leakage subtraction also exhibited an inward shoulder at very positive test-pulse voltages (data not shown), indicating that the VHVA current was not an artifact of subtraction. It remains possible that the VHVA current resulted from a voltage-dependent current elicited at a site that was electrotonically distant from the electrode tip, where the voltage commands would be rounded and attenuated (see Discussion).

The sustained tail current showed a non-saturating I-V relationship (data not shown), reflecting contamination by an additional, decaying tail current

52

apparent after large depolarizations (Fig. 3.5A, traces at +60, +70 mV). This is likely associated with the VHVA current.

Simulated I-V curves and activation curves

Steady-state activation of the HVA-t current was determined assuming that the amplitude of the peak current represented the steady-state current that would have been measured in the absence of inactivation. Single-exponential fits to the inactivation phase of 80 ms responses were back-extrapolated to the voltage transition, and these initial current amplitudes, equivalent to steady-state I_{Ca} or I_{Ba}, were found not to be significantly different from peak amplitudes.

Simulated curves (equations in Table 3.2 notes) were fitted to the I-V data in Fig. 3.4A. Curves fitted assuming a single current component (Fig. 3.4A, broken curves) corresponded well with the HVA-t maximum but were smaller than the data at very positive voltages. This difference was statistically significant from +50 mV to +70 mV for I_{Ca}, and at +50 mV for I_{Ba}, and probably reflected the appearance of the VHVA component at those voltages. Curves fitted assuming two components (Fig. 3.4A, solid curves) showed no statistical difference from the data at any voltage, for both ions.

Table 3.2 shows the average parameters used to fit simulated I-V curves to data from individual cells. The only parameter that showed any significant difference between ionic conditions was the maximal permeability of the HVA-t component, which was smaller for I_{Ba} than for I_{Ca}. The voltages at half-activation ($V_{a,HV}$) and the slope factors ($K_{a,HV}$) of the HVA-t current did not appear significantly sensitive to ionic species. The parameters fitted to the VHVA current data showed relatively larger standard errors than did the HVA-t parameters, indicating that this current did not behave consistently in different cells.

The sigmoid, voltage-dependent activation of HVA-t was calculated as described in the Figure 3.6 caption. The resulting activation curves were averaged and plotted in that figure. The curves for normalized permeabilities P_{Ca} and P_{Ba} showed significant differences only at -30 mV and -10 mV (standard errors were very small). The HVA-t permeability first activated just above -30 mV, reached half-activation just above 0 mV, and saturated around +40 mV. The activation curve of the VHVA component that was extracted from the averaged data first activated around +20 mV and saturated beyond the voltage range studied (not shown). Similar results were obtained regarding VHVA activation when measurements were taken at the end of 80 ms I_{Ba} responses, where VHVA

53

was most prominent (Fig. 3.5*B*).

Time to peak

Time to peak current (Fig. 3.7) followed a U-shaped function of voltage, reflecting the appearance of the slowly rising, VHVA current in addition to the HVA–t current. If a single population of HVA channels were present, T_{peak} would decline as the channels activate, without increasing again, assuming these channels exhibit classical activation kinetics.

Times to peak were statistically indistinguishable between I_{Ca} and I_{Ba} at all voltages but –10 mV, although T_{peak} was consistently longer for I_{Ba} than I_{Ca}, at voltages where the VHVA current did not contaminate the HVA–t responses (–10 mV to +20 mV). Two repeated "autopeak" measurements (cf. caption to Fig. 3.4) using search regions of varying sizes gave differences in the same direction, although in no case was there statistical significance of the average difference calculated across four voltages. The speed of voltage clamping did not appear to depend on ionic conditions, because the time constants of passive, capacitive current decay did not differ significantly between the I_{Ca} and I_{Ba} conditions.

Steady-state inactivation of HVA currents

The availability of peak I_{Ca} or I_{Ba} was measured immediately after 1 s prepulses during which inactivation had reached a steady state. Prepulse/test pulse pairs were applied every 10 s Both ascending and descending voltage series gave similar results, indicating there was little cumulative inactivation at this stimulation rate. Only data from the ascending series were used.

The steady-state inactivation data (Fig. 3.8*A*) suggested the presence of distinct components of the calcium current, one showing selectivity for calcium over barium and inactivation with depolarizing prepulses (HVA–t), and another showing no selectivity and incomplete inactivation at the positive prepulses applied (HVA–s). Peak I_{Ca} and I_{Ba} differed in amplitude following negative prepulses. The difference was significant from –90 mV to –20 mV. Up to –50 mV, I_{Ca} seemed to show a slight, progressive decrease, while I_{Ba} did not appear to change. Above –50 mV, increasingly positive prepulses inactivated the peak current. Following prepulses above 0 mV, a significant current (~–31 pA; $P < 0.001$ for I_{Ca} and I_{Ba} being different from zero) persisted which had the same amplitude in calcium and barium. These data mirror the results of Figure 3.3*C*, which shows the prepulse responses exhibiting inactivating (HVA–t) and

sustained (HVA-s) components with different ionic selectivities. Figure 3.8A confirms that HVA-t and HVA-s have different voltage dependencies of inactivation. The slight recovery from inactivation at positive voltages was not significant, even after prepulses to +50 mV (data not shown).

Data from Figure 3.8A were fitted with a modified Boltzmann distribution. Table 3.3 gives the equation fitted and the fitting parameters for steady-state calcium and barium current inactivation, which were averaged from fits to individual data sets. Normalized, steady-state inactivation curves for the transient I_{Ca} and I_{Ba} are presented in Figure 3.8B. The voltage dependencies of inactivation were identical in calcium and barium.

Preliminary experiments using barium currents to measure the time course of recovery from inactivation of the peak, HVA-t component gave an average time constant of 50 ms at -80 mV.

Pharmacology

Experiments were carried out to test the sensitivity of divalent cation currents to pharmacological agents, namely cadmium, verapamil, and nifedipine.

Cadmium, applied at concentrations of 0.08-1.3 mM, greatly reduced I_{Ca} responses to maximal depolarizations (Fig. 3.9A), although a small residual, sustained current was present in 5 out of 8 experiments. Cadmium insensitivity is usually associated with low-voltage-activated (LVA) currents (Durroux et al., 1988; Hernández-Cruz and Pape, 1989).

The slow and sustained tail currents seemed unaffected by cadmium, possibly because of release of Cd^{2+} block by hyperpolarization (Lansman et al., 1986). When current-clamp recordings were made in total-current conditions, application of Cd^{2+} removed the plateau phase of the action potential, indicating that some component of I_{Ca} underlies this phase of the spike (Fig. 3.9B). The slower rising phase in Cd^{2+} also shows that HVA-t contributed to the rising phase of the spike.

Verapamil, dissolved in ethanol, did not produce any obvious effect when it was applied at 50-100 µM, although only two such experiments were attempted.

Nifedipine, superfused at a concentration of 100 µM, consistently blocked the sustained component of I_{Ca} (Fig. 3.9C) in a completely reversible manner. Blockade of the sustained current was more complete and more rapid than that of the peak, transient component. This differential blockade was seen in 5 out of 6 experiments, with only 1 case out of 6 showing little

55

blockade. Application of the vehicle to one cell had no effect (Fig. 3.9C). When a double exponential was fitted to the current traces, it appeared that the sustained current (N = 5, 80% block) was inhibited more effectively than the slowly inactivating exponential (N = 3, 57% block), while the amplitude of the rapidly inactivating exponential was increased by ~60%. Neither the slow nor the fast time constant of inactivation seemed to change.

DISCUSSION

Quality of the voltage clamp

The quality of the voltage clamp was assessed from passive and active responses. Capacitive transients on passive test pulses indicated the presence of a rapidly charging region of the cell clamped through a low-series-resistance pathway, and a slowly charging area of the cell membrane separated from the electrode tip by a high series resistance (see Results on passive properties). For areas of the membrane nearest the electrode, the speed of clamping was satisfactory for peak current measurements, but it did not allow reliable measurement of events that occurred less than 0.5 ms after the application of a voltage command step, that is, current activation time course and fast tail currents. The calculated series resistance error at peak current was negligible near the electrode (-1.5 mV, maximum), so the voltages applied were very close to the desired command voltages. At more remote membrane sites, voltage pulses were probably rounded and attenuated by passive propagation.

The possible morphological basis for a region with high access resistance is interesting. Swimming motor neurons *in vitro* presented a compact morphology with processes that, when present, were usually wide. The cytoplasm in these cells contains membranous inclusions (Spencer, 1979; Przysiezniak and Spencer, 1989 [Chapter 2]) and deep infoldings of the plasmalemma. These membranes often show reflexive gap junctions (Spencer, 1979) and may create considerable access resistance, either internally by compartmentalizing the cell cytoplasm, or externally by restricting current flow from the bath to the membrane inside the infoldings (Keynes et al., 1973).

The VHVA current

The VHVA current behaved in a way that suggested it was being elicited

at an electrotonically remote area of membrane, although no single piece of evidence directly demonstrates this. The slow onset of the VHVA current (Fig. 3.5A, I_{Ba} trace at +70 mV) may have reflected an underlying voltage pulse rounded by conduction through a region of high resistance and membrane capacitance (see above discussion). While a calcium current with a slow onset is found in vertebrate skeletal muscle (Beaty et al., 1987; Bean, 1989), it is maximal at a much lower voltage (0 mV). Maximal currents at very positive potentials are usually seen when the space clamp is non-uniform (Keynes et al., 1973; Stanley, 1989). Thus, at a large electrotonic distance from the electrode, where a voltage step would be attenuated by passive propagation, a calcium current maximal at +10 mV could be elicited by command voltages that appear more positive (e.g., +40 mV) at the current injection site.

It is unlikely that screening of the membrane surface charge by high concentrations of external divalent cations could account for the very positive voltage dependence of the VHVA current (Fig. 3.5B, Table 3.2) since screening would have caused a positive shift in the voltage dependence of all HVA channels, not just of a subset of channels. Furthermore, the onset of VHVA current was almost an order of magnitude slower than the slowest HVA current onset (Fig. 3.5A, compare I_{Ba} trace at +70 mV to trace at −20 mV) so it is unlikely that the VHVA current represents an HVA current with a very-positively shifted voltage dependence.

Taken together, this evidence suggests that the VHVA current was carried through HVA channels located on an electrotonically remote area of the cell membrane, possibly membrane infoldings.

The HVA currents
Ionic selectivity

The calcium current was significantly larger than barium current at peak but not at the sustained level reached after 1 s of depolarization (Fig. 3.3C). The peaks of the inactivating I_{Ca} and I_{Ba} showed no significant differences in voltage dependencies of activation, time to peak, or inactivation (Figs. 3.6, 3.7, 3.8B, respectively), and there was no obvious difference in the time course of the tail currents (Fig. 3.3B). The functions fitted to the peak I–V data (Table 3.2) suggest that only macroscopic permeabilities differed between ionic species. These results indicate that the difference in peak I_{Ba} and I_{Ca} amplitudes does not reflect an ion-selective effect on membrane surface charge, but may indicate selective permeability. A more subtle ion-dependence of channel gating or flickering cannot be excluded, because

there is a consistent, though insignificant, lengthening of T_{peak} for I_{Ba} relative to I_{Ca}.

Reports describing the effects of barium on calcium channel gating show many-fold shortenings of single-channel open or closed times (Nelson et al., 1984, in rat channels; Chesnoy-Marchais, 1985 in Aplysia patches) or dramatic lengthening of whole-cell current onset or tail-current (Saimi and Kung, 1982, in Paramecium). Such dramatic effects were not observed, so the ionic selectivity measured in the HVA calcium currents of Polyorchis neurons likely arises not from differential channel gating, but from differential ion permeation.

The selective permeability of calcium channels to divalent cations is believed to depend on the binding affinities of different ions for certain sites on the channels (Almers and McCleskey, 1984; Hess and Tsien, 1984; Tsien et al., 1987; cf. Kostyuk et al., 1983). Blocking ions also bind to the same sites on the channels as do permeant ions, and a permeant ion with a strong binding affinity may act a a blocker when competing against another permeant ion of weaker binding affinity (Lansman et al., 1986). The permeability of a calcium channel to a certain ion depends therefore on the relative affinity of the channel binding sites for different cations present, on the concentrations of these ions around the channel, and on the interactions between these ions.

The ionic selectivity observed could arise if impermeant magnesium ions, which occur at a high concentration in the bath (40 mM), were more effective in competing against barium than calcium for channel occupancy. The preferential inhibition by magnesium of I_{Ba} relative to I_{Ca} has been reported to occur (Ganitkevich et al., 1988). The existence of such a mechanism would be confirmed if selectivity were seen to reverse in the absence of external magnesium. The blockade of a channel by magnesium ions can appear at the single-channel level as a flickering of the unitary current (Lansman et al., 1986). Because the kinetics of blocking and unblocking are usually more rapid than the closed and open gating kinetics, respectively, modulation of blockade may have only subtle effects on the time course of macroscopic current activation and deactivation, but may affect the mean amplitude of whole-cell current dramatically. The results presented here exhibit a dramatic, ion-dependent difference in current amplitude (Fig. 3.3A) accompanied by a subtle difference in the kinetics of activation (Fig. 3.7).

Another possible mechanism is that residual calcium, leached from the electrode glass into the bath (Furman and Tanaka, 1988; Copello et al., 1991),

may have inhibited I_{Ba} because of its higher affinity for calcium channels, compared to that of barium. This mechanism does not preclude the action of the magnesium blockade described above. Alternately, the binding affinity of calcium might have been weaker than that of barium, allowing a faster transit time and a larger current of calcium than of barium. However, most other works report a greater affinity of calcium than barium (cf. Almers and McCleskey, 1984; Hess and Tsien, 1984; Lansman et al., 1986; Ganitkevich et al., 1988). In summary, it is likely that the ionic selectivity observed is due to magnesium competing differentially with calcium and barium, although calcium leaching from the electrode glass could also have a similar effect.

The absence of ionic selectivity of the sustained current may have resulted from the reduction of apparent I_{Ca} by contamination with a slow, outward current that was blocked in barium. However, such an effect is unlikely to have occurred because it would have had to compensate exactly for the differences between sustained I_{Ca} and I_{Ba} throughout the voltage range studied (Fig. 3.4B). Similarly, relief from calcium-dependent inactivation may have caused sustained I_{Ba} to be larger and more similar to I_{Ca} than expected, but this effect would likely not occur with such exactness throughout the voltage range studied. Thus, the difference in ionic selectivity between the HVA-t and HVA-s currents probably reflected the selectivities of the underlying calcium channels.

The non-selective, sustained current might flow through a single population of inactivating channels, which inactivate incompletely and change their selectivity in the process. Incomplete inactivation of a single channel population has been reported frequently (Chad et al., 1984; Hennessey and Kung, 1985; Swandulla and Armstrong, 1988; Jones and Marks, 1989; Plummer et al., 1989; Plummer and Hess, 1991; Slesinger and Lansman, 1991a,b). However, in no case has a change in ionic selectivity with inactivation been studied or observed. It is more likely that HVA-s current flows through a non-inactivating, non-selective channel population distinct from that mediating the HVA-t current. The coexistence of separate channel populations with distinct inactivation kinetics and/or ionic selectivities occurs frequently (McCleskey et al., 1986; Yaari et al., 1987; Durroux et al., 1988; Hernández-Cruz et al., 1989; Carbone et al., 1990; Regan, 1991), although in no case has the particular combination described here been observed. Usually, sustained current is selective for barium over calcium (L-type channels), and the transient component is non-selective (HVA or "N") or selective for calcium over barium (LVA or "T").

Experiments involving manipulations of calcium and barium

concentrations, pharmacology and/or single-channel recordings will be necessary to clarify the mechanism of ionic selectivity and the identity of the transient and sustained current components.

Inactivation

The inactivation of the calcium current may have resulted from a current-dependent or a voltage-dependent mechanism. Current-dependent inactivation specific for calcium ions was unlikely to occur in the conditions used because both I_{Ca} and I_{Ba} showed identical voltage dependencies of inactivation (Table 3.3, Fig. 3.8B). As mentioned above, relief from calcium-dependent inactivation was unlikely to produce a slowing of the slowly inactivating I_{Ba} relative to I_{Ca} (Table 3.1; Fig. 3.3C) because of the coincidences this would involve. In addition, calcium-dependent inactivation usually affects rapid decay more readily than it does slow inactivation (Hennessey and Kung, 1985; Habuchi et al., 1990; Plummer et al., 1990). Mechanisms for calcium-dependent inactivation may have been present but undetectable under the conditions used because of buffering by EGTA in the electrode solution.

On the other hand, buffering by intracellular EGTA may have been too slow to inhibit a divalent-cation-dependent mechanism in SMNs, and current-dependent inactivation may have occurred. Chad et al. (1984) have proposed a model of calcium-dependent inactivation that may be applied to less specific mechanisms of current-dependent inactivation. They surmise that a complex time course of decay showing two exponentials and incomplete inactivation may result if the proportion of channels available for opening decays hyperbolically with increasing submembranous $[Ca^{2+}]$. Thus, rapid decay would result from the initial influx of divalent cations raising submembranous $[Ca^{2+}]$ to a level at which the mechanism causing inactivation is most sensitive. The more slowly decaying component would appear when the inactivation mechanism becomes saturated and responds with less sensitivity. Finally, the sustained component would occur at a level where calcium influx is balanced by calcium removal, and little submembranous calcium remains to elicit inactivation. The sustained current would therefore depend on the amount of intracellular divalent cation buffering and would be reduced by experimentally decreasing the buffering capacity of the cytosol.

The steady-state inactivation curve shows considerable inactivation at voltages where little current is elicited on the prepulse (compare Figs. 3.4A, 3.8B). If current-dependent inactivation were present, as described above, a

60

small influx would increase submembranous divalent cation concentration to within the steep, dynamic range of the inactivation mechanism, while much larger influx would elicit saturating inactivation. Depending on the capacity of the inactivation mechanism for bound divalent cations, and on the intracellular buffering, maximal inactivation will occur after different amounts of influx. Thus, the general lack of recovery from inactivation at positive prepulses, where a small but significant influx occurs, may indicate that the inactivation mechanism has a low capacity for divalent cations, or that the intracellular divalent cation buffer is saturated.

A mechanism of voltage-dependent inactivation can also produce features such as a complex time course of inactivation with incomplete inactivation, and significant inactivation at non-activating voltages. A double-exponential decay would result if a single channel population mediating only the HVA-t current showed two inactivated states reached by pathways with different rate constants. Alternately, if both the selective, HVA-t and non-selective, HVA-s currents were mediated by a single population of channels, then it would be necessary to invoke a gating mechanism involving two open states with different ionic selectivities and possibly an inactivated state from which channels can reopen to the non-selective state, giving the sustained current. Some combination of rate constants between the two open states and the inactivated state could produce a double-exponential decay. By its simplicity, the first mechanism is more amenable to testing.

Inactivation at voltages where few channels are activated could occur if channels can convert directly from the closed to the inactivated state, in a voltage-dependent manner. At activating voltages, inactivation likely occurs indirectly, via the activated states. Recovery from inactivation may also occur through the open state and may be visible as a reopening tail current in responses to sudden repolarizations (Slesinger and Lansman, 1990, 1991c). In SMNs, repolarizations to -80 mV produced slow and sustained tail currents that were selective for Ca^{2+} over Ba^{2+} (Fig. 3.3B), and may have arisen from reopenings of channels carrying the ion-selective HVA-t current. Repolarizations to -40 mV only elicited tail currents lasting less than 2 ms, with no sign of a sustained tail current, suggesting that recovery from inactivation at this voltage was mostly through transitions from inactivated to closed states. The inactivation and recovery from inactivation of the calcium channels may have occurred via direct and/or indirect pathways, and the relative contribution of each pathway to these processes remains to be determined. Much of the voltage dependence of inactivation may arise from the voltage dependence of transitions from

the closed to the open or inactivated states. According to this model, transitions between open and inactivated states don't have to be voltage-dependent.

Experimental manipulations of intracellular divalent cation buffering and single-channel recordings should help determine which particular mechanism of current- or voltage-dependent inactivation is at work in the SMNs of *Polyorchis*. Both mechanisms could contribute to this process (e.g., Brehm et al., 1980; Hennessey and Kung, 1985; Gutnick et al., 1989; Habuchi et al., 1990).

Nifedipine blockade

The concentration of nifedipine (100 µM) used to block the calcium currents of *Polyorchis* was larger than the effective doses of dihydropyridines used to block most vertebrate calcium channels (~0.1–10 µM; e.g., Plummer et al., 1989; Bean, 1989). Furthermore, the inhibitory effect of this drug on both the non-selective, sustained and the selective, slowly inactivating components suggests that the action was non-specific. Dihydropyridines are known to bind to calcium channels while they are open, producing an apparent inactivation (Lee and Tsien, 1983; Sanguinetti and Kass, 1984). This could spare the rapidly inactivating component, and block the slowly inactivating component more than the sustained current, as was observed. This result does not conclusively indicate how many HVA calcium channels are present in the membrane of *Polyorchis* SMNs.

Conclusions on the HVA currents

In summary it is probable that there are two HVA channel populations in SMNS of this jellyfish. The major objection to the existence of a single population of HVA channels is that whole-cell current would have to change from being ion-selective before inactivation, to non-selective after inactivation. There are no reports in the literature indicating that ionic selectivity depends on the state of inactivation of a channel.

These experiments have not provided sufficient evidence to demonstrate the predominance of either current- or voltage-dependent inactivation mechanisms of the HVA calcium currents.

Functions of the calcium currents

The calcium currents in swimming motor neurons of *Polyorchis penicillatus* play important roles in excitability and synaptic transmission in the electrically coupled network of the swimming motor neurons. The

high voltage of activation of these currents indicates they may accompany the sodium current (Chapter 4) in producing the relatively high spiking threshold found in these cells ($\sim V_m$ -20 mV). The sensitivity to Cd^{2+} of the rising slope of the action potential (Fig. 3.9B) suggests that the rapidly activating HVA-t may participate in the spike upstroke. HVA-s may contribute to the slow, spontaneous, membrane potential fluctuations observed *in vitro* (unpublished data).

Cadmium blockade of the action-potential plateau phase (Fig. 3.9B) indicates another role for the calcium current, probably associated with synaptic transmission (Spencer et al., 1989 [Appendix A]). The plateau duration changes consistently with baseline membrane voltage and the distance of spike propagation around the electrically coupled network of the SMNs (Spencer and Satterlie, 1980; Spencer, 1982). This is associated with changes in synaptic delay at the SMN-swim muscle junction that compensate for propagation time of the action potentials around the bell and synchronize contraction of all regions of the swimming bell. Understanding the relative contributions of HVA-t and HVA-s currents to this phenomenon awaits further pharmacological characterization.

While the swimming motor neurons have been studied most extensively in this jellyfish, other cells are also present that show different suites of voltage-dependent ionic currents. Neurons producing short-duration spikes *in vitro* are smaller than SMNs and more "neuron-like" (with distinct soma and neurites; Przysiezniak and Spencer, 1989 [Chapter 2]), and their activity resembles that of the identified "B" or "Burster" neurons observed in semi-dissected preparations (Arkett and Spencer, 1986). These cells showed very little calcium current, if any, in response to depolarizations from a holding potential of -80 mV to +10 mV (unpublished observations), which explains the absence of a spike plateau. *In situ*, myoepithelial cells produce plateau action potentials lasting about 170 ms (Spencer and Satterlie, 1981), arising from a negative resting potential (-75 mV; Spencer and Satterlie, 1981). Tetraethylammonium application lengthened the plateau phase (Spencer and Satterlie, 1981) of *in vivo* myoepithelial spikes. Such spikes may be maintained by a small, sustained calcium current and repolarized by a slowly arising potassium current. This type of calcium current also appears to be present in SMNs. Thus, the "repertoire" of calcium currents observed in SMNs is obviously specific to that cell type, but may be partly shared by other cells.

Taxonomic and evolutionary considerations

Recordings of calcium currents in jellyfish, anemones and their kin are recently becoming more common. Anderson (1987) demonstrated the presence of an HVA, rapidly activating ($T_{peak} \approx 2$ ms) and inactivating calcium current in neuronal somata of the scyphozoan jellyfish *Cyanea capillata*, which, with a fast sodium current, contributes to produce a short-duration spike. Recorded in high concentrations of external calcium (95 mM), this current was maximal at +35 mV. In normal calcium concentrations, the maximum current would likely occur at more negative voltages because of surface charge unscreening, making the voltage dependence more similar to that of *Polyorchis* currents. Dunlap et al. (1987) describe a calcium current in epithelial cells of a colonial hydroid, *Obelia*. This current serves as a source of calcium for bioluminescence in photocytes that are coupled through gap-junctions to these epithelial cells. It activates slowly ($T_{peak} \approx 60$ ms), inactivates slowly, and reaches a maximum around -5 mV in 40 mM barium. At more natural calcium concentrations, the I-V curve might be shifted to more negative voltages, as for a LVA current. Meech (1989) briefly describes a calcium current in the hydrozoan jellyfish *Aglantha digitale*, which activates rapidly, at low voltages. Most recently, Holman and Anderson (1991) have presented evidence for an inactivating calcium current in myoepithelial cells of the anemone *Calliactis tricolor*, resembling the HVA current found in *Polyorchis*. This current has the permeability sequence, $Ca^{2+} > Sr^{2+} > Ba^{2+}$, which is similar to that described here for the HVA-t current. While no LVA current could be clearly identified in the SMNs of *Polyorchis*, the small cadmium-insensitive current (Fig. 3.9A) may indicate its presence.

The HVA calcium currents of *Polyorchis penicillatus* share features with the three common classes of vertebrate calcium currents. Rapid activation and inactivation, and activation at relatively depolarized voltages make the HVA-t component similar to the "N" current (Nowycky et al., 1985; McCleskey et al., 1986). However, a positive voltage range of inactivation, as seen here, is not a feature of "N" currents, and neither is selectivity for calcium over barium, which has usually been described in transient, LVA, "T" channels (Durroux et al., 1988; Akaike et al., 1989; Hernández-Cruz and Pape, 1989). Interestingly, HVA currents in marine tunicate eggs are larger in calcium than barium (Okamoto et al., 1976), like the HVA-t current observed here. The HVA-s component behaved like the "L" current; it activated in a positive voltage range, inactivated slowly, if at all, and showed little steady-state inactivation at positive voltages (although 1 s prepulses may be too short to see this). However, its lack of ionic selectivity

64

makes it more similar to the "T" or "N" currents tha.. the "L" current (Durroux et al., 1988; Hirano et al., 1989; cf. Johansen et al., 1987). The absence of rundown of the HVA currents in *Polyorchis* makes them different from the HVA currents in vertebrates, and more similar to the LVA, "T" current (Durroux et al., 1988; Akaike et al., 1989). Insensitivity to blockade by dihydropyridines is not uncommon among invertebrate phyla (Ehrlich et al., 1988).

It appears that cnidarians can exhibit both LVA and HVA calcium currents. Two types of voltage-gated calcium channel, distinguished by their voltage ranges of activation, can also be recorded from the protozoan *Stylonychia* (Deitmer, 1984), the snail *Helisoma* (Haydon and Man-Son-Hing, 1988), and many vertebrate cells (see above). It is possible that protists, cnidarians, and other animals have evolved so much from their original ancestors that little evidence remains of the primitive traits of calcium channels among extant species. Thus, the present classes of LVA and HVA channels may have arisen several times in evolution, under the biophysical constraints requiring a calcium channel to regulate activity near the resting potential (LVA) and another channel acting more occasionally and briefly during periods of excitation (HVA). Alternately, the divergence of calcium channels into LVA and HVA classes may have occurred at an early stage of evolution, and would have determined the basic molecular structure of these channel types in extant metazoans. If this were the case, it is likely that the differences in amino-acid sequence between these two classes of channels would be more important than the molecular differences between channel types within each class. Molecular studies have already suggested that sodium channels have arisen from primitive HVA calcium channels (Hille, 1984; Catterall, 1988), indicating this class of calcium channel may be relatively primitive. The amino-acid sequences of HVA channels show much similarity within this class (Perez-Reyes et al., 1990; Mori et al., 1991; Snutch et al., 1991). However, a more satisfying conclusion regarding the evolutionary divergence of calcium channels will require a molecular description of LVA channels.

Table 3.1
Features of maximal calcium and barium currents in swimming motor neurons of *Polyorchis penicillatus*.

	I_{Ca}	I_{Ba}	P
Time to peak (ms)[a]	4.0 ± 0.3 (9/7)	4.3 ± 0.2 (9/5)	NS
Peak current (pA)[a]	-217 ± 23 (9/7)	-13? ± 14 (9/5)	0.001-0.01
Amplitude of fast decay (pA)[b]	-88.4 ± 7.9 (10/3)	-61.1 ± 5.1 (14/5)	0.001-0.01
τ of fast decay (ms)[b]	25.6 ± 2.8 (10/3)	20.9 ± 1.6 (14/5)	NS
Amplitude of slow decay (pA)[b]	-99.5 ± 9.0 (10/3)	-50.7 ± 4.5 (14/5)	<0.001
τ of slow decay (ms)[b]	187 ± 21 (10/3)	244 ± 60 (14/5)	NS
Current at 1 s (pA)[c]	-24.5 ± 5.0 (6/3)	-29.2 ± 7.2 (7/4)	NS
Sustained tail current 6.2 ms after 80 ms pulse (pA)[a]	-29.0 ± 3.5 (9/7)	-12.5 ± 1.5 (9/5)	<0.001

V_h was -80 mV, V_c was +10 mV. Data are expressed as mean ± standard error of the mean (nb. of cells/nb. of animals). P is the probability that the two parameters are statistically indistinguishable, from a two-tailed Student's *t*-test; only significant probabilities (≤0.05) are indicated. NS = not significant.
[a] Measured from responses to 80 ms pulses.
[b] Fitted to responses to 400 ms pulses.
[c] Measured from responses to 1 s prepulses of inactivation protocols.

Table 3.2

Parameters used to fit simulated I–V functions to average data for peak I_{Ca} and I_{Ba}.

	I_{Ca}	I_{Ba}	P
$V_{a,HV}$ (mV)	0.3 ± 0.6	3.0 ± 1.2	NS
$K_{a,HV}$ (mV)	6.3 ± 0.2	6.4 ± 0.4	NS
$P_{max,HV}$ (l/s)	$(2.03 \pm 0.22) \times 10^{-13}$	$(1.28 \pm 0.14) \times 10^{-13}$	0.01–0.02
$V_{a,VHV}$ (mV)	$+80.5 \pm 4.7$	$+66.0 \pm 10.2$	NS
$K_{a,VHV}$ (mV)	10.7 ± 0.8	9.7 ± 1.1	NS
$P_{max,VHV}$ (l/s)	$(6.05 \pm 2.09) \times 10^{-12}$	$(3.61 \pm 1.28) \times 10^{-12}$	NS

Data curves shown in Fig. 3.4A. Data from each of nine cells in each ionic condition were fitted with a combination of the Goldman-Hodgkin-Katz (GHK) constant-field equation (Hille, 1992) and two Boltzmann distributions: $I_D = (P_{HV}+P_{VHV}) \times Z^2 F^2 V/RT \times ([D]_{in} - [D]_{out} \times exp(-ZFV/RT))/(1 - exp(-ZFV/RT))$, where $P_{HV} = P_{max,HV}/(1 + exp[(V_{a,HV} - V)/K_{a,HV}])$ and $P_{VHV} = P_{max,VHV}/(1 + exp[(V_{a,VHV} - V)/K_{a,VHV}])$. The variables were V_a, the voltage of half-activation, K_a, the slope factor of the Boltzman function and P_{max}, the maximal permeability to Ca^{2+} or Ba^{2+}. V_a and K_a were fitted to the nearest 0.1 mV, P_{max} to the nearest 10^{-15} l/s. The constants were $[D]_{in} = 10^{-9}$ M, $[D]_{out} = 10^{-2}$ M, Z = 2, F = 96480 C/mol, R = 8314 mV x C/°K/mol, and T = 293 °K. A surface charge of zero was assumed in the GHK equation. At V = 0 mV and negligible internal calcium, the GHK equation reduced to $I_{D(0)} = P_D \times ZF \times (-[D]_{out})$. All fitting parameters were averaged over nine cells, except for VHV parameters in calcium (N = 8), which could not be fitted for one cell. Values are in mean ± SEM.

67

Table 3.3
Parameters used to fit Boltzmann curves to steady-state inactivation data for peak I_{Ca} and I_{Ba}.

	I_{Ca}	I_{Ba}	P
V_i (mV)	-23.4 ± 1.5	-22.0 ± 1.0	NS
K_i (mV)	9.2 ± 0.4	8.7 ± 0.7	NS
I_{max} (pA)	-192.6 ± 16.6	-126.8 ± 10.5	0.001-0.01
I_{min} (pA)	-31.2 ± 3.8	-30.8 ± 4.0	NS

Fitting was carried out on 6 (I_{Ca}) or 7 (I_{Ba}) recordings from different cells, in each ionic condition. Average fitting parameters ± SEM are presented. The equation fitted was $I_{test} = I_{min} + (I_{max} - I_{min})/\{1 + exp[(V_{pp} - V_i)/K_i]\}$. I_{test} was the peak current response to a test pulse following a 1 s prepulse to V_{pp}, I_{min} was the non-inactivating component available at positive V_{pp}, I_{max} was the maximal current available at negative V_{pp}, V_i was the voltage at half-inactivation, and K_i was the slope factor. For normalized curves, I_{min} was subtracted from I_{test} and the difference was normalized to ($I_{max} - I_{min}$).

68

0 mM Ca^{2+}, 9.5 mM Co^{2+}

100 pA
10 msec

Control, 9.5 mM Ca^{2+}
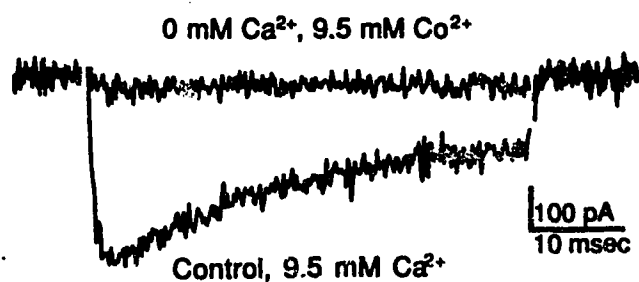
Figure 3.1 - Calcium current from an identified SMN of the jellyfish *Polyorchis penicillatus*. Current responses from one cell elicited by 50 ms voltage-clamp pulses, from a holding potential (V_h) of -40 mV to a command potential (V_c) of $+20$ mV, in normal conditions and with external Ca^{2+} replaced with Co^{2+}. Sampling interval was 100 μs. Subtraction carried out with a $-p/5$ protocol from -40 mV. Bath solution contained (in mM) MgSO$_4$, 5.7; MgCl$_2$, 23.3; CaCl$_2$ or CoCl$_2$, 9.5; KCl, 7.8; choline–Cl, 437; HEPES, 10; and KOH, 5.6. Electrode solutions contained (in mM) CsCl, 109; MgCl$_2$, 2; CaCl$_2$, 1; HEPES, 10; EGTA, 11; dextrose, 536; tetraethylammonium chloride, 100; and CsOH, 31. Initial, transient, outward was removed graphically.

69

Before perfusion

A

$I_{Na}+I_{Ca}$

I_{Na}

7 min of perfusion

B

I_{Ca}

I_{Na}

17 min of perfusion

C

I_{Ca}

100 pA
10 msec
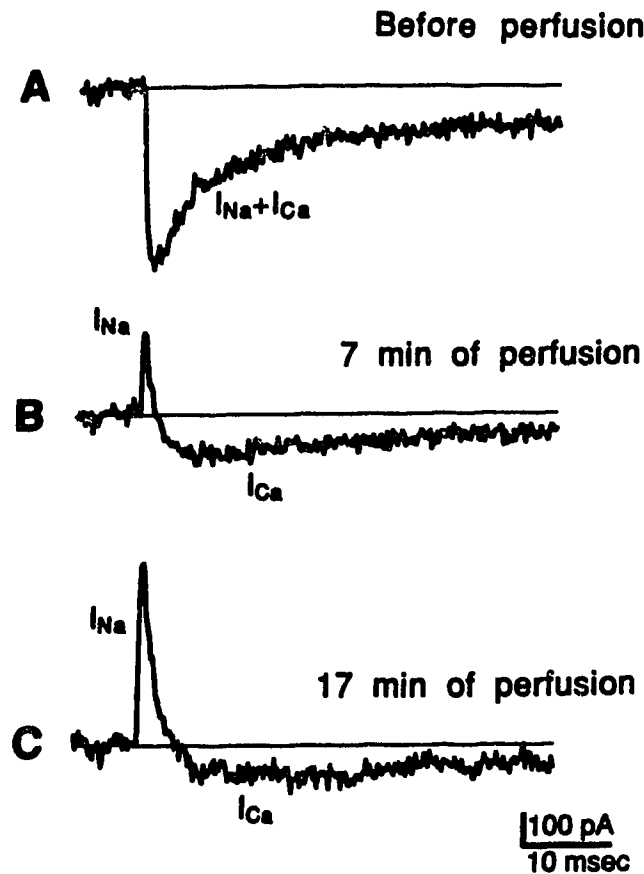
Figure 3.2 - Simultaneous recordings of sodium and calcium currents from one cell in conditions where both currents are of similar amplitude, showing they are carried through different channel populations. In control conditions, the bath contained 10 mM Ca^{2+}, 40 mM Mg^{2+}, 100 mM Na^+ and no K^+ (NMG substitution), while the electrode contained ~1 nM Ca^{2+}, 2 mM Mg^{2+}, 50 mM Na^+, and no K^+. The bath was superfused four times for short periods (30–120 s) with sodium-free solution, alternating with equilibration periods of 1–2 min. Traces were taken just before the first superfusion (A), after the second superfusion (B), and after the fourth (last) superfusion (C). Sampling interval was 200 μs. Voltage pulses were applied from V_h –80 mV to V_c +10 mV for A-C. Subtraction protocol was -p/4 from –80 mV. Data points during capacitive artifacts were set to zero, for clarity. The flat line is zero current in this and the following figures.

70
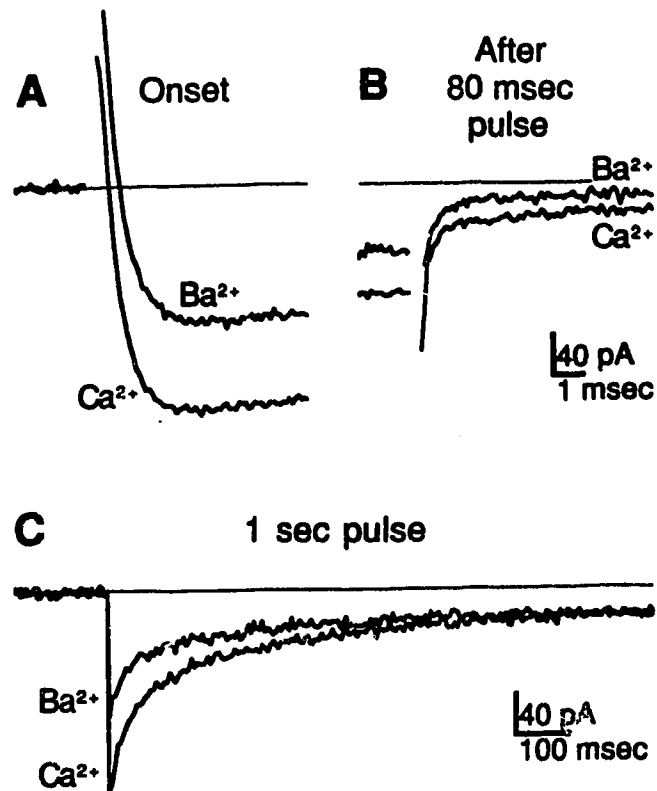
Figure 3.3 - Superimposed, maximal I_{Ca} and I_{Ba} responses elicited by voltage-clamp stimuli from V_h −80 mV to V_c +10 mV. *A. and B.* Currents at beginning and at end of responses to 80 ms pulses, respectively, averaged for 9 cells in each ionic condition. Sampling interval was 100 μs. The *scale* is the same for *A* and *B*. The initial, outward, transient currents in *A* were truncated for the first half millisecond, approximately, to remove the unsubtracted capacitive transient. *C.* Currents elicited by 1 s pulses, averaged for 6 cells in Ca^{2+} and 7 cells in Ba^{2+}, showing rapidly and slowly inactivating current components. Sampling was every 5 ms. Solutio⁻ are described in Materials and Methods.

Figure 3.4 - Current-voltage relationships of HVA–t (*A*) and HVA–s (*B*) currents recorded in calcium and barium. The HVA–t was carried by calcium more easily than by barium, over a wide voltage range, while the sustained component was indifferent to the ionic species. Data are plotted as mean ± SEM in this and the following graphs. *A*. Transient I_{Ca} and I_{Ba} versus voltage. An automatic peak-detection function was used to measure the largest current between 1.2 ms and 18.7 ms in recordings from 9 cells in each ionic condition. The *broken curves* are mathematical fits of Boltzmann and constant-field equations, calculated assuming only one current component, while the *solid curves* were calculated assuming two components. The equations are given in Table 3.2 notes. At very positive voltages, HVA–t is contaminated by the very-high-voltage-activated (VHVA) current. *B*. Sustained current. Measurements were taken near the end of 1 s, "steady-state inactivation" prepulses (cf. Fig. 3.8). Means from 6 cells in calcium, 7 in barium.

A

HVA–transient Current (pA)

Ba²⁺

Ca²⁺

V$_c$ (mV)

B

HVA-sustained Current (pA)

Ca²⁺

Ba²⁺

V$_c$ (mV)
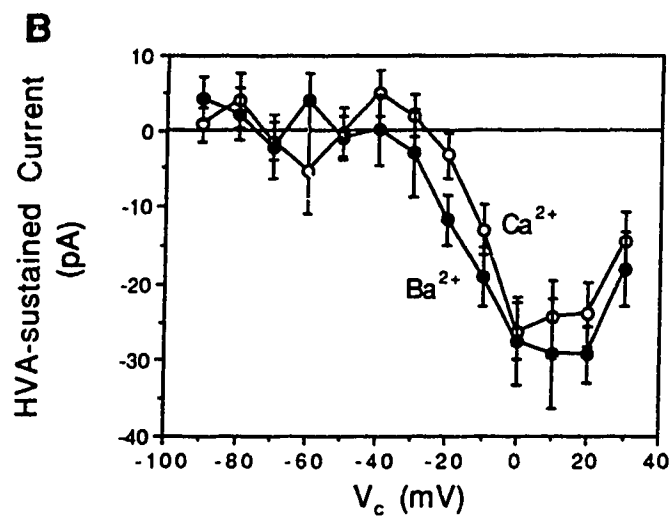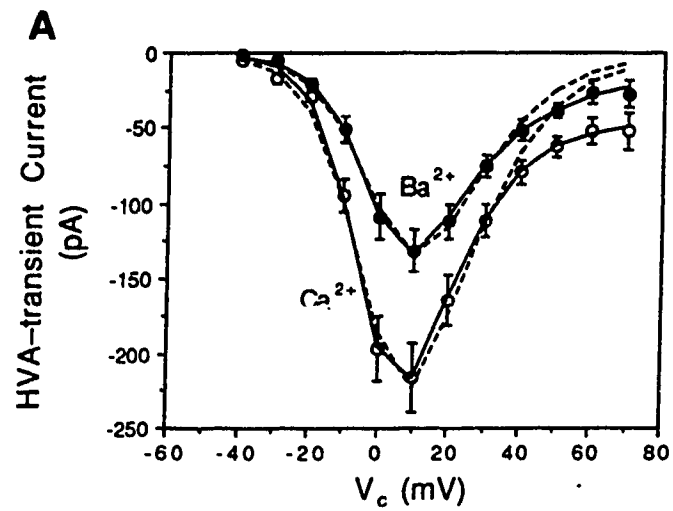
Figure 3.5 - Divalent cation current responses to depolarizing voltage pulses and the VHVA current. *A.* Superimposed I_{Ca} (*thick traces*) and I_{Ba} (*thin traces*) responses to graded, 80 ms voltage-clamp pulses, averaged for 9 cells in each condition. The stimulating voltages are indicated above the traces (in mV). The sampling interval was 100 µs. The currents at the voltage transitions were removed for clarity. The responses are selective for calcium over barium for most of the voltage range. At very positive voltages ($\sim$+50 mV), the slowly arising, non-selective VHVA current appears. *B.* I_{Ba} measured isochronally at 78 ms, as a function of stimulating voltage, showing a prominent shoulder around +50 mV, which indicates the presence of the VHVA current.
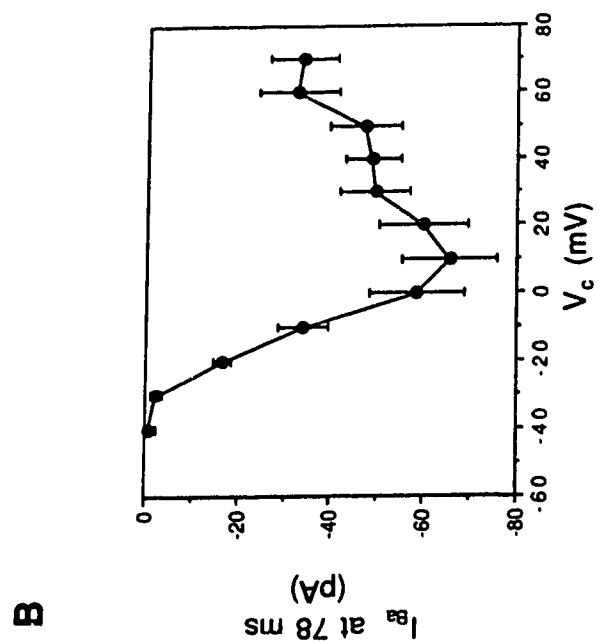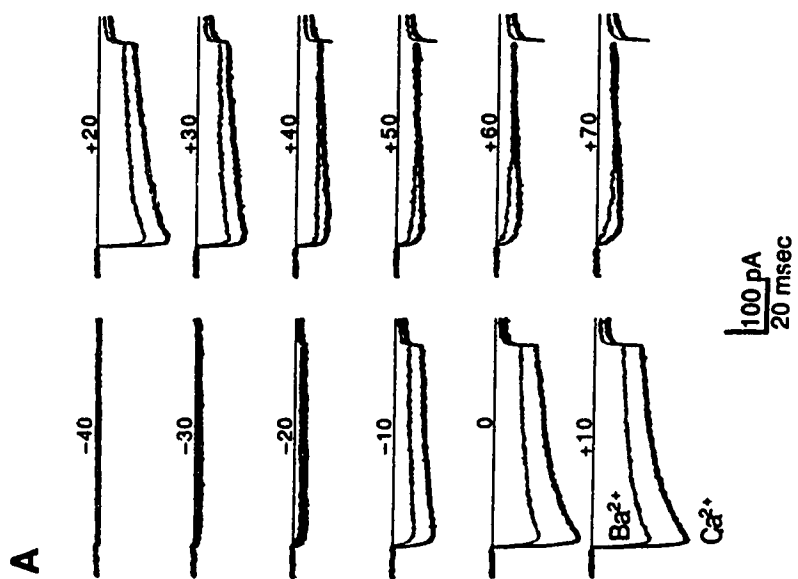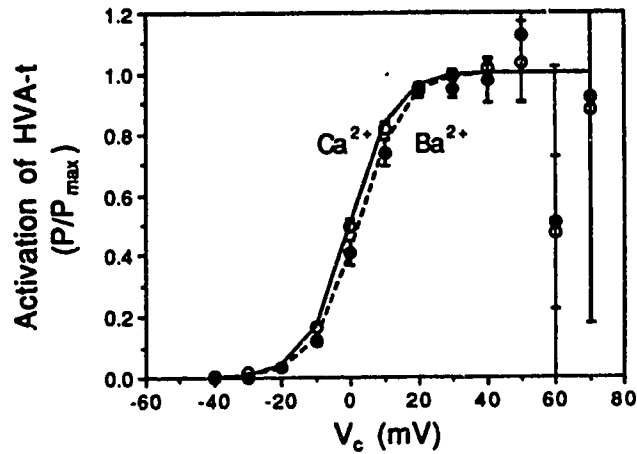
Figure 3.6 - Activation of HVA–t with voltage in calcium and barium, expressed as the ratio P/P_{max} calculated from the data in Fig. 3.4A and from simulated I–V curves fitted to this data. Points (Ca^{2+}, *open circles*; Ba^{2+}, *solid circles*) are mean ratios. *Solid* (Ca^{2+}) and *broken* (Ba^{2+}) *curves* are Boltzmann distributions with parameters from fits to the average I–V data, as shown in Table 3.2. To obtain activation data for the HVA current, total divalent cation permeability was calculated at each voltage using the GHK equation (Table 3.2), the expected permeability $P_{D,VHV}$ was calculated from the Boltzmann equation, and the latter was subtracted from the former to obtain $P_{D,HV}$. This was normalized to $P_{max,HV}$ and plotted.
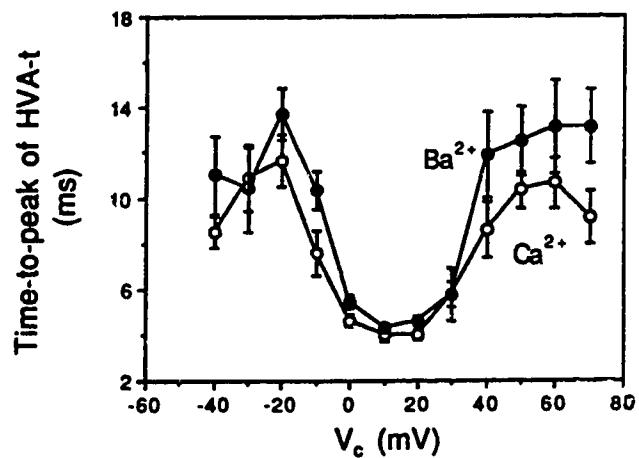
Figure 3.7 - Time to peak I_{Ca} and I_{Ba}, showing a U-shaped function of voltage, measured from data in Fig. 3.5. Automatic peak detection software was used. Note the insignificantly but consistently longer T_{peak} in barium relative to calcium.
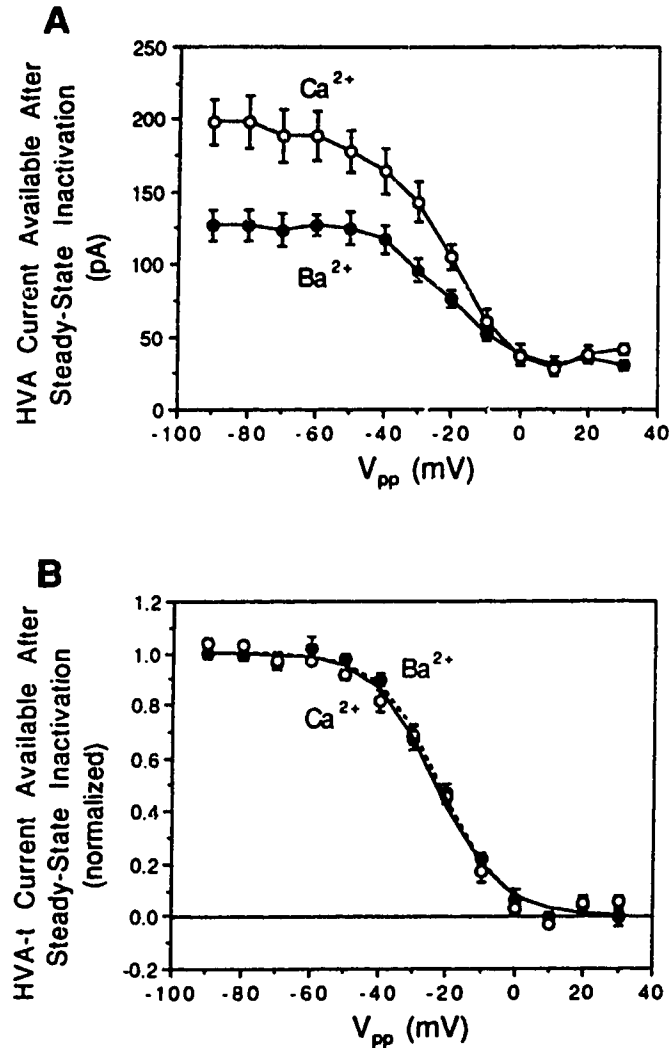
Figure 3.8 - Availability of divalent cation current after pulses causing steady-state inactivation. One-second prepulses to different voltages (V_{pp}, *abscissa*) were applied from –80 mV, followed immediately by a 35 ms test pulse to +10 mV. *Open* (Ca^{2+}) and *solid* (Ba^{2+}) *circles* are means (±SEM) from 6 cells in calcium, 7 in barium. *A*. Absolute calcium and barium test-pulse currents after steady-state inactivation (prepulse response to V_{pp} +10 mV is shown in Fig. 3.3*C*). Currents were measured with automatic peak detection, between 2.2 ms and 9.2 ms from the beginning of the test pulse. Prepulse voltages are indicated on the *abscissa*. *B*. Availability of transient I_{Ca} and I_{Ba} as a function of V_{pp}, after subtraction of the non-inactivating component and normalization of the data to fitted, maximal test-pulse current. *Solid* (Ca^{2+}) and *broken* (Ba^{2+}) *curves* are Boltzmann distributions extracted from fits to the average, raw data in *A*.

Figure 3.9 - Pharmacology of the divalent cation currents. *A.* Representative trace showing nearly complete blockade of I_{Ca} by 0.3 mM Cd^{2+}. The test pulse was applied from a V_h of -80 mV to a V_c of $+10$ mV just before and after 4 min of superfusion with 0.3 mM Cd^{2+}. Sampling interval was 200 μs. Subtraction protocol: +p/4 from -80 mV. *B.* Blockade of the action-potential plateau by 0.1 mM Cd^{2+}. Sampling interval was 100 μs. Bath solution contained (in mM) NaCl, 378; $MgCl_2$, 29; $CaCl_2$, 9.5; Na_2SO_4, 5.7; KCl, 13.4; choline–Cl, 42; HEPES, 10; NaOH, 5. Electrode solution contained (in mM) KCl, 105; $MgCl_2$, 2; $CaCl_2$, 2; HEPES, 1; HEPES, 10; EGTA, 11; dextrose, 740; KOH, 35. (*C*) Nifedipine blockade of I_{Ca}. Long test depolarizations ($V_h = -80$ mV, $V_c = +10$ mV for 400 ms) were applied every minute during superfusions with 100 μM nifedipine (vehicle: 0.05% DMSO + 0.9% ethanol), normal saline, and vehicle-containing saline. Traces were taken 3 min before (*initial*), during (*2 min* and *4 min*), and 2 min after nifedipine superfusion (*6 min*), at the end of the washing period (*washed*), and 2 min after vehicle application (*vehicle*). After washing, the recording became unstable. After a period of rest at V_h -40 mV, sufficient stability returned for vehicle application, which produced no change in peak I_{Ca}, but spurious changes in late I_{Ca} (not shown). Note that *control*, *wash* and *vehicle traces* coincide. Sampling interval was 500 μs.

A

+0.3 mM Cd²⁺

Control

30 pA
10 msec

B

Control

+0.1 mM Cd²⁺

10 mV
5 msec

C

4 min + 6 min
nifedipine

2 min
nifed.
100 μM

control +
washed +
vehicle

50 pA
50 msec
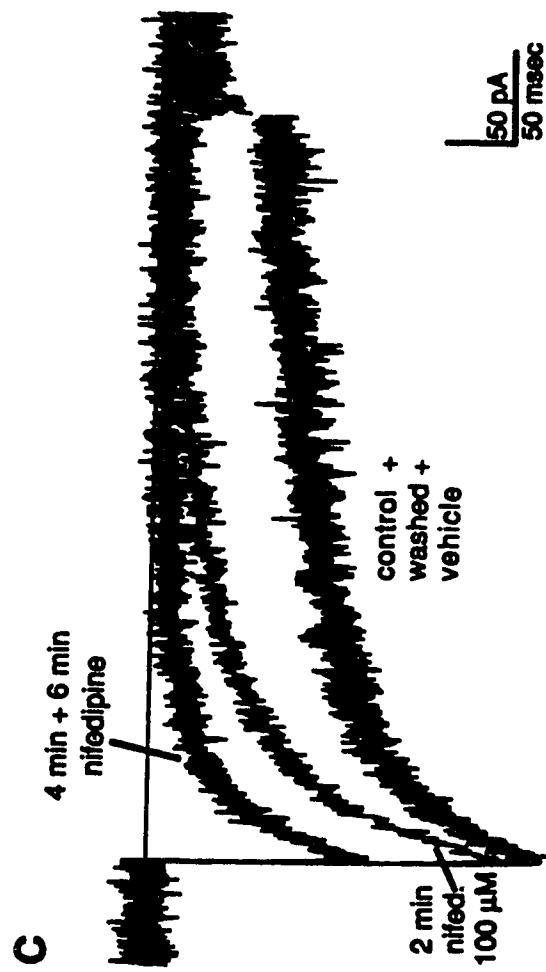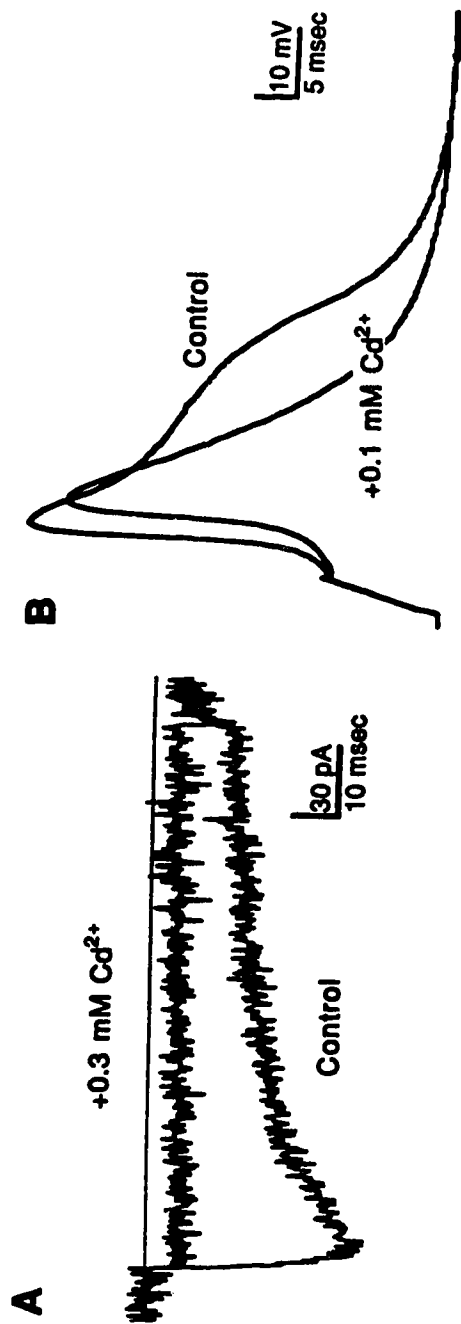
REFERENCES

Akaike N, Kostyuk PG, Osipchuk YV (1989) Dihydropyridine-sensitive low-threshold calcium channels in isolated rat hypothalamic neurons. J Physiol (Lond) 412: 181-195.

Almers W, McCleskey EW (1984) Non-selective conductance in calcium channels of frog muscle: calcium selectivity in a single-file pore. J Physiol (Lond) 353: 585-608.

Anderson PAV (1979) Ionic basis of action potentials and bursting activity in the hydromedusan jellyfish Polyorchis penicillatus. J Exp Biol 78: 299-302.

Anderson PAV (1987) Properties and pharmacology of a TTX-insensitive Na^+ current in neurons of the jellyfish, Cyanea capillata. J Exp Biol 133: 231-248.

Anderson PAV, Mackie GO (1977) Electrically coupled, photosensitive neurons control swimming in a jellyfish. Science 197: 186-188.

Arkett SA, Spencer AN (1986) Neuronal mechanisms of a hydromedusan shadow reflex. I- Identified reflex components, and sequence of events. J Comp Physiol A 159: 201-213.

Bean BP (1989) Classes of calcium channels in vertebrate cells. Annu Rev Physiol 51: 367-384.

Beaty GN, Cota G, Nicola Siri L, Sanchez JA, Stefani E (1987) Skeletal muscle Ca^{2+} channels. In: Structure and physiology of the slow inward calcium channel, Vol 1 (Triggle DJ, Venter JC, eds), pp 123-140 New York: Liss.

Brehm P, Eckert R, Tillotson D (1980) Calcium-mediated inactivation of calcium current in Paramecium. J Physiol (Lond) 306: 193-203.

Carbone E, Sher E, Clementi F (1990) Ca currents in human neuroblastoma IMR32 cells: kinetics, permeability and pharmacology. Pflügers Arch 416:

Catterall WA (1988) Structure and function of voltage-sensitive ion channels. Science 242: 50-61.

Chad J, Eckert R, Ewald D (1984) Kinetics of calcium-dependent inactivation of calcium current in voltage-clamped neurons of *Aplysia californica*. J Physiol (Lond) 347: 279-300.

Chesnoy-Marchais D (1985) Kinetic properties and selectivity of calcium-permeable single channels in *Aplysia* neurons. J Physiol (Lond) 367: 457-488.

Copello J, Simon B, Segal Y, Wehner F, Ramanujam VMS, Alcock N, Reuss L (1991) Ba^{2+} release from soda glass modifies single maxi K^+ channel activity in patch-clamp experiments. Biophys J 60: 931-941.

Deitmer JW (1984) Evidence for two voltage-dependent calcium currents in the membrane of the ciliate *Stylonychia*. J Physiol (Lond) 355: 137-159.

Dunlap K, Takeda K, Brehm P (1987) Activation of a calcium-dependent photoprotein by chemical signalling through gap junctions. Nature 325: 60-62.

Durroux T, Gallo-Payet N, Payet MD (1988) Three components of the calcium current in cultured glomerulosa cells from rat adrenal gland. J Physiol (Lond) 404: 713-729.

Ehrlich BE, Jacobson AR, Hinrichsen R, Sayre LM, Forte MA (1988) *Paramecium* calcium channels are blocked by a family of calmodulin antagonists. Proc Natl Acad Sci USA 85: 5718-5722.

Furman RE, Tanaka JC (1988) Patch electrode glass composition affects ion channel currents. Biophys J 53: 287-292.

Ganitkevich VY, Shuba MF, Smirnov SV (1988) Saturation of calcium channels in single isolated smooth muscle cells of guinea-pig taenia caeci. J Physiol (Lond) 399: 419-436.

calcium-dependent inactivation of calcium channel current in identified snail neurons. J Physiol (Lond) 412: 197-220.

Habuchi Y, Noda T, Nishimura M, Watanabe Y (1990) Recovery of the slow inward current from Ca^{2+}-mediated and voltage-dependent inactivation in the rabbit sinoatrial node. J Mol Cell Cardiol 22: 469-482.

Haydon PG, Man-Son-Hing H (1988) Low- and high-voltage-activated calcium currents: their relationship to the site of neurotransmitter release in an identified neuron of *Helisoma*. Neuron 1: 919-927.

Hennessey TM, Kung C (1985) Slow inactivation of the calcium current of *Paramecium* is dependent on voltage and not internal calcium. J Physiol (Lond) 365: 165-179.

Hernández-Cruz A, Pape H-C (1989) Identification of two calcium currents in acutely dissociated neurons from the rat lateral geniculate nucleus. J Neurophysiol 61: 1270-1283.

Hess P, Tsien RW (1984) Mechanism of ion permeation through calcium channels. Nature 309: 453-456.

Hille B (1984) Ionic channels of excitable membranes. Sunderland, MA: Sinauer.

Hirano Y, Fozzard HA, January CT (1989) Inactivation properties of T-type calcium current in canine cardiac Purkinje cells. Biophys J 56: 1007-1016.

Holman MA, Anderson PAV (1991) Voltage-activated ionic currents in myoepithelial cells isolated from the sea anemone *Calliactis tricolor*. J Exp Biol 161: 333-346.

Johansen J, Yang J, Kleinhaus AL. (1987) Voltage-clamp analysis of the ionic conductances in a leech neuron with a purely calcium-dependent action potential. J Neurophysiol 58: 1468.

Jones SW, Marks TN (1989) Calcium currents in bullfrog sympathetic neurons. II. Inactivation. J Gen Physiol 94: 169-182.

systems of a giant barnacle muscle fiber under membrane potential control. J Physiol (Lond) 229: 409-455.

Kostyuk PG, Mironov SL, Shuba YM (1983) Two ion-selecting filters in the calcium channel of the somatic membrane of mollusc neurons. J Membr Biol 76: 83-93.

Lansman JB, Hess P, Tsien RW (1986) Blockade of current through single calcium channels by Cd^{2+}, Mg^{2+}, and Ca^{2+}. Voltage and concentration dependence of calcium entry into the pore. J Gen Physiol 88: 321-347.

Lee KS, Tsien RW (1983) Mechanisms of calcium channel blockade by verapamil, D600, diltiazem and nitrendipine in single dialysed heart cells. Nature 302: 790-794.

Lux HD, Carbone D, Zucker H (1990) Na^+ currents through low-voltage-activated Ca^{2+} channels of chick sensory neurons: block by external Ca^{2+} and Mg^{2+}. J Physiol (Lond) 430: 159-188.

Marty A, Neher E (1983) Tight-seal, whole-cell recording. In: Single-channel recording (Sakmann B and Neher E, eds), Chapter 7. New York: Plenum.

McCleskey EW, Fox AP, Feldman D, Tsien RW (1986) Different types of calcium channels. J Exp Biol 124: 177-190.

Meech RW (1989) The electrophysiology of swimming in the jellyfish *Aglantha digitale*. In: Evolution of the first nervous systems (Anderson PAV, ed), pp 281-298. New York: Plenum.

Meves H, Vogel W (1973) Calcium inward currents in internally perfused giant axons. J Physiol (Lond) 235: 225-265.

Mori Y, Friedrich T, Kim M-S, Mikami A, Nakai J, Ruth P, Bosse E, Hofmann F, Flockerzi V, Furuichi T, Mikoshiba K, Imoto K, Tanabe T, Numa S (1991) Primary structure and functional expression from complementary DNA of a brain calcium channel. Nature 350: 398-402.

channels from brain incorporated into planar lipid bilayers. Nature 308: 77-80.

Nowycky MC, Fox AP, Tsien RW (1985) Three types of neuronal calcium channel with different calcium agonist sensitivity. Nature 316: 440-443.

Okamoto H, Takahashi K, Yoshii M (1976) Two components of the calcium current in the egg cell membrane of the tunicate. J Physiol (Lond) 255: 527-561.

Perez-Reyes E, Wei X, Castellano A, Birnbaumer L (1990) Molecular diversity of L-type calcium channels. Evidence for alternative splicing of the transcripts of three non-allelic genes. J Biol Chem 265(33): 20430-20436.

Plummer MR, Hess P (1991) Reversible uncoupling of inactivation in N-type calcium channels. Nature 351: 657-659.

Plummer MR, Logothetis DE, Hess P (1989) Elementary properties and pharmacological sensitivities of calcium channels in mammalian peripheral neurons. Neuron 2: 1453-1463.

Plummer MR, Kanevsky M, Hess P (1990) Multiple forms of inactivation of the N-type calcium current. Soc Neurosci Abstr 16: 622.

Przysiezniak J, Spencer AN (1989) Primary culture of identified neurons from a cnidarian. J Exp Biol 142: 97-113.

Regan LJ (1991) Voltage-dependent calcium currents in Purkinje cells from rat cerebellar vermis. J Neurosci 11: 2259-2269.

Saimi Y, Kung C (1982) Are ions involved in the gating of calcium channels? Science 218: 153-156.

Sanguinetti MC, Kass RS (1984) Voltage-dependent block of calcium channel current in the calf cardiac Purkinje fiber by dihydropyridine calcium channel antagonists. Circ Res 55: 336-348.

Satterlie RA, Spencer AN (1983) Neuronal control of locomotion in hydrozoan medusae. A comparative study. J Comp Physiol A 150: 195-

206.

Slesinger PA, Lansman JB (1990) Calcium channel reopenings at resting membrane potentials following prior depolarization. Soc Neurosci Abstr 16: 1174.

Slesinger PA, Lansman JB (1991a) Inactivation of calcium currents in granule cells cultured from mouse cerebellum. J Physiol (Lond) 435: 101-121.

Slesinger PA, Lansman JB (1991b) Inactivating and non-inactivating dihydropyridine-sensitive Ca^{2+} channels in mouse cerebellar granule cells. J Physiol (Lond) 439: 301-323.

Slesinger PA, Lansman JB (1991c) Reopening of calcium channels at negative membrane potentials depends on channel inactivation. Biophys J 59: 537a.

Snutch TP, Tomlinson WJ, Leonard JP, Gilbert MM (1991) Distinct calcium channels are generated by alternative splicing and are differentially expressed in the mammalian CNS. Neuron 7: 45-57.

Sokal RR, Rohlf FJ (1981) Biometry. 2nd edition. New York: Freeman.

Spencer AN (1978) Neurobiology of Polyorchis. I. Function of effector systems. J Neurobiol 9: 143-157.

Spencer AN (1979) Neurobiology of Polyorchis. II. Structure of effector systems. J Neurobiol 10: 95-117.

Spencer AN (1981) The parameters and properties of a group of electrically coupled neurons in the central nervous system of a hydrozoan jellyfish. J Exp Biol 93: 33-50.

Spencer AN (1982) The physiology of a coelenterate neuromuscular synapse. J Comp Physiol A 148: 353-363.

Spencer AN, Satterlie RA (1980) Electrical and dye coupling in an identified group of neurons in a coelenterate. J Neurobiol 11: 13-19.

Spencer AN, Satterlie RA (1981) The action potential and contraction in subumbrellar swimming muscle of *Polyorchis penicillatus* (Hydromedusae). J Comp Physiol 144: 401-407.

Spencer AN, Przysiezniak J, Acosta-Urquidi J, Basarsky TA (1989) Presynaptic spike broadening reduces junctional potential amplitude. Nature 340: 636-638.

Stanley EF (1989) Calcium currents in a vertebrate presynaptic nerve terminal: the chick ciliary ganglion calyx. Brain Res 505: 341-345.

Stockbridge NL (1987) EGTA Comput Biol Med 17: 299-304.

Swandulla D, Armstrong CM (1988) Fast-deactivating calcium channels in chick sensory neurons. J Gen Physiol 92: 197-218.

Tsien RW, Hess P, McCleskey EW, Rosenberg RL (1987) Calcium channels: mechanisms of selectivity, permeation and block. Ann Rev Biophys Biophys Chem 16: 265-290.

Yaari Y, Hamon B, Lux HD (1987) Development of two types of calcium channels in cultured mammalian hippocampal neurons. Science 235: 680-682.

Chapter 4

VOLTAGE-ACTIVATED SODIUM CURRENT IN IDENTIFIED MOTOR NEURONS FROM THE HYDROZOAN JELLYFISH, *POLYORCHIS PENICILLATUS*.[3]

INTRODUCTION

In multicellular animals, sodium currents often set the firing threshold and drive the rising phase of rapid action potentials, functions that are essential for the fast propagation of signals over long distances. Sodium channels are believed to have evolved from calcium channels (Hille, 1992), and are thought to replace the latter in multicellular animals, to allow spike propagation without the toxic effects of massive calcium influx. Fast sodium currents are also partly responsible for the "coding" of receptor potentials into trains of action potentials, and the rapid onset of fast chemical neurotransmission. While molecular biology can give a precise idea of the structural similarities between voltage-gated sodium and calcium channels, and between sodium channels in cnidarians and in other phyla, electrophysiological studies may indicate, albeit more coarsely, which functional sites have seen the most, and the least evolutionary change.

In the Cnidaria, rapid, sodium-dependent action potentials have been observed in current clamp (Anderson and Mackie, 1977; Roberts and Mackie, 1980; Satterlie and Spencer, 1983; Anderson and Schwab, 1983). The voltage-clamp study of cnidarian, voltage-dependent sodium currents is still in its infancy. Anderson has described a TTX-insensitive sodium current in neurons of the scyphozoan jellyfish, *Cyanea capillata*(Anderson, 1987).

In the hydrozoan jellyfish, *Polyorchis penicillatus*, the action potentials of swimming motor neurons (SMNs) have been demonstrated to be sodium-dependent and TTX-insensitive (Anderson, 1979) and their *in vivo* behavior has been studied extensively using the current-clamp technique (Anderson and Mackie, 1977; Spencer and Satterlie, 1980; Spencer, 1981; Spencer and Arkett, 1984). A primary culture technique (Przysiezniak and Spencer, 1989 [Chapter 2]) has been developed to isolate SMNs from the

---

[3] A version of this chapter has been submitted for publication to the Journal of Neuroscience.

electrically-coupled network that they form with each other, and from the epithelial cells that ensheath them. This has allowed the application of the tight-seal, whole-cell voltage-clamp technique with sufficient spatial control of membrane voltage to study the time course, voltage dependence and pharmacology of the sodium current in isolated SMNs.

MATERIALS AND METHODS

Animals were collected in Bamfield Inlet (Vancouver Island, British Columbia) from the surface by dip netting, or at depth by scuba divers using plastic bags. The jellyfish were maintained in a recirculating, refrigerated (10°C) aquarium containing a mixture of Rila Marine Mix and seawater from Bamfield Inlet, on a cycle of 12 h of light, 12 h of dark. The animals were fed newly hatched brine shrimp larvae once or twice a week.

Cultures were prepared as described by Przysiezniak and Spencer (1989, 1992 [Chapters 2, 3]). Nerve-ring tissue was dissected into artificial seawater (ASW), then incubated 5 min in 10% ASW, 15 min in calcium- and magnesium-free ASW, and 3–7 h in collagenase type I (Sigma) at 1000 U/ml. All incubations were at room temperature. After a brief rinse in ASW, the tissue was triturated and plated onto mesoglea-coated culture dishes (Falcon 1008; preparation described in Przysiezniak and Spencer, 1989). Cultures were kept at 10°C.

Recordings were carried out on cells in 0 to 5 day-old cultures using the tight-seal, whole-cell recording technique. Cells ranged in size from 35 to 150 μm on the long axis, and from 20 to 50 μm on the shorter axis. In most experiments, the solutions had the following ionic compositions. The <u>bath</u> solution contained (in mM) NaCl, 378; $MgCl_2$, 29; $CoCl_2$, 9.5; Na_2SO_4, 5.7; KCl, 13.4; choline–Cl, 42; HEPES, 10; NaOH, 4.5. For two cells, external KCl was replaced with CsCl, mole for mole, with no observable difference in the resulting recordings. The <u>electrode</u> solution contained (in mM) CsCl, 369; $MgCl_2$, 2; $CaCl_2$, 1; NaCl, 50; HEPES, 10; EGTA, 11; dextrose, 116; CsOH, 31. This solution was also used to prepare 4–5% (w/w) agar in the salt bridge for the Ag/AgCl ground electrode wire. For all solutions described in these methods, pH was adjusted to 7.5 ± 0.05.

When caesium currents through sodium channels were recorded, the bath solution contained the following (in mM) $MgSO_4$, 5.7; $MgCl_2$, 23.3; $CoCl_2$, 9.5; KCl, 7.8; choline–Cl, 437; HEPES, 10; KOH, 5.6. The electrode solution contained (in mM) CsCl, 109; $MgCl_2$, 2; $CaCl_2$, 1; HEPES, 10; EGTA, 11; D-glucose, 536; TEA-Cl, 100; CsOH, 31.

In all pharmacological experiments on total current (Fig. 4.6), except for those with procaine, solutions were as follows. The bath contained (in mM) NaCl, 394; $MgCl_2$, 30; $CaCl_2$, 10; Na_2SO_4, 5.7; KCl, 15; N-methyl-D-glucamine/HCl (1:1), 30; HEPES, 10; NaOH, 5. For the procaine experiments, the bath solution was identical to that used for isolated I_{Na} recordings, except that calcium replaced cobalt so that the total inward current was studied. The electrode solution used for pharmacology contained (in mM) KCl, 365; $MgCl_2$, 2; $CaCl_2$, 1; NaCl, 50; HEPES, 10; EGTA, 11; choline–Cl, 60; KOH, 35. Pharmacological solutions applied to the cells were made up in bath solutions diluted to between 80% and 99%, except for some tetrodotoxin (TTX) experiments, where the applied solution was made up in distilled water, and some saxitoxin experiments (see below). TTX was obtained from Sigma. The saxitoxin (STX) powder obtained from Calbiochem contained acetic acid at 100 times the molar amount of toxin. Once STX was solubilized to 1 mM in distilled water, its pH was adjusted to between 6 and 7 using a pH strip. The concentration was halved with bath solution for a stock solution of 0.5 mM STX (50 mM acetic acid). Hille (1968) has shown that the potency of STX was as strong at a pH of 7.5 as at more acid pH values.

The voltage offset caused by the liquid junctional potential between the electrode and bath solutions was corrected electronically with the electrode tip in the bath. This offset correction was checked at the end of some recordings, after the electrode was removed from the cell, and was found to have deviated by only 2–3 mV. During most recordings, the composition of the bath solution was not changed (except in Fig. 4.1 and in pharmacological experiments), so it is unlikely that the voltage measurements were contaminated by changes in the junctional potential between bath and electrode solutions. However, it is possible that very slowly diffusing anionic proteins, which may be present in the cytoplasm, produced a liquid junctional potential between the electrode tip and the bulk of the cytoplasm (see Discussion on E_{rev}; Marty and Neher, 1983). In this case, it would be likely that all voltage measurements were more positive than the true voltages.

Electrodes made from non-heparinized hematocrit tubing (Fisher) had resistances of 1–2 MΩ, as measured with ±10 mV test pulses. Passive pulses of 40 mV were used to measure leakage resistance (R_{leak}) and series resistance (R_{ser}), and were applied from –80 mV when depolarizing, or from –40 mV when hyperpolarizing. R_{leak} measured 0.5 to 1.3 MΩ, averaging 0.7 MΩ.

The R_{ser} was estimated either from the back-extrapolated amplitude of single-exponential fits to the capacitive currents, or from the value of series conductance indicated on the amplifier R_{ser} compensation dial. These values ranged from 2.3 MΩ to 7.5 MΩ, averaging 4.2 MΩ. In all but the pharmacological experiments, R_{ser} was compensated by 70–75%, leaving an estimated, residual R_{ser} of 0.7 to 1.9 MΩ, averaging 1.2 MΩ. The membrane capacitance ranged from 19 to 54 pF, and the calculated time constant of the membrane charging after R_{ser} compensation ($\tau = R_{ser} \times C_m$) ranged from 23 to 81 μs. Charging to 95% thus occurred in less than 250 μs.

The voltage error caused by ionic current flowing through R_{ser} was important. At maximal, inward, sodium current, the voltage drop across the residual R_{ser} (V_{Rser}) ranged from 5 mV to 12 mV, causing the tip of the electrode to be at a more positive voltage than the expected command potential (V_c). At any given voltage, R_{ser} caused a 10–30% error in the estimation of current and level of activation (see Results, Table 4.2). The membrane voltage for current-voltage relationships was corrected with the following equation:

$$V_{corr} = V_c - (I_{peak} + V_{corr}/R_{leak}) \times R_{ser}$$

where the second term in the brackets is the "reconstituted" leakage current, assumed to reverse at 0 mV, and I_{peak} is the peak, sodium current at the true command voltage, V_{corr}. This equation can be solved for V_{corr}, giving:

$$V_{corr} = [V_c - (I_{peak} \times R_{ser})] \times R_{leak} /(R_{leak} + R_{ser}) \tag{1}$$

The usefulness of this mathematical correction of V_{Rser} is greatest when the current has reached steady state. While its application to peak current entailed some underestimation of current amplitude at a given voltage, it nonetheless improved the results by adjusting the command voltages to more realistic values.

The effect of V_{Rser} was unlikely to have been important in the experiments using constant test pulses eliciting maximal current ($\sim+10$ mV, uncorrected) to measure steady-state inactivation and recovery from inactivation. In both types of experiments, changes in R_{ser} during the test pulses caused the voltage at the electrode tip to vary by about 10 mV around the voltage eliciting maximal current. Therefore, currents measured were within 10% of the true, maximal current amplitude. The prepulse voltage was probably measured with little V_{Rser} error because the prepulse current

reached steady state at a low amplitude.

The rapid inactivation of I_{Na} truncated the current onset and thus contaminated the voltage dependence of peak current with that of the inactivation process. The corrected, steady-state activated current was obtained by graphically removing the inactivation phase. A double-exponential function was fitted to the decay phase and back-extrapolated to the beginning of the pulse. The initial amplitude of this function, plus that of the fitted offset (mostly composed of the slowly decaying current), predicts the steady-state activated current in the absence of inactivation.

The pharmacological data were usually gathered without R_{ser} compensation, to prevent ringing during bath exchanges. As a consequence, membrane capacitance charging was slow. The slowly arising voltage commands reached 95% of their final value after 150 to 1000 μs, assuming C_m values ranging from 20 pF to 45 pF. This likely resulted in a slowly arising current, partially truncated by rapid inactivation. Thus, changes in peak current amplitude reflected not only pharmacological effects but also changes in R_{ser}. The latter were monitored with the amplitudes of capacitive transients during passive current responses elicited before and after drug applications.

All recordings were made at room temperature with an L/M-EPC7 amplifier (List Medical, Darmstadt, Germany). Passive responses were low-pass filtered at 10 kHz, while active responses in all but the pharmacological experiments were filtered at 3 kHz, with a three-pole Bessel filter. Voltage pulses were produced and data were acquired through a Labmaster TL-1 interface connected to a modified IBM-PC using pCLAMP software (Axon Instruments, versions 5.03 and 5.5). Leakage and capacitive currents were subtracted online from active responses, using summed responses to 4 or 5 scaled-down, passive pulses preceding the active responses ("+p/4" or "+p/5" protocols). All measurements of peak current were made with an automatic peak detection procedure included in the pCLAMP software (Clampan program).

Data analysis was carried out on recordings that met the following criteria: 1) Cells were identified as SMNs by their large size and clear cytoplasm (Przysiezniak and Spencer, 1989 [Chapter 2]), and by the plateau action potentials recorded in current clamp when all external calcium was replaced by cobalt. Cells that produced no plateau action potentials were not used. It was likely that a slowly decaying sodium current was present that produced the plateau spikes. 2) The leakage resistance measured before and/or after an experimental protocol had to be, on average, larger than or

equal to 0.5 GΩ. 3) The series resistance must be compensated for electronically. 4) The active current could not exhibit a "threshold" voltage beyond which a test voltage pulse elicited an "all-or-none" current response. 5) Recordings must be stable, with no signs of seal disruption.

Exponential fitting to the capacitive transients, inactivation phases and tail current decays was carried out with the Clampfit program of the pCLAMP software. Fitting to the I–V and steady-state inactivation curves was carried out with C-language (Turbo C, Borland) programs. The equations used are given in the legends to Tables 2 and 3, respectively. Recovery from inactivation was fitted with a single exponential using a C–language program. With fits done using either pCLAMP or Turbo C programs, fitting was done by maximizing the following value:

$$R_{fit} = 1 - [\Sigma(I - I_{fitted})^2 / \Sigma(I - I_{overall\ mean})^2] \qquad (2)$$

where the sum, Σ, is taken over all points in the record. Parameters obtained from fitting were used only if $R_{fit} \geq 0.8$, except for one column in Table 4.2 (see legend).

All data were expressed as mean ± standard error of the mean, except where specified. Statistical comparisons were carried out using the Student's t test, assuming a significant difference if P was smaller than 5%.

RESULTS

Time course of maximal responses

To record the sodium current (I_{Na}), external calcium was replaced with cobalt and caesium was substituted for internal potassium. Rectangular voltage pulses to +10 mV applied from a holding potential (V_h) of –80 mV elicited a large, rapidly activating inward current that inactivated with a rapid, bi-exponential time course (Fig. 4.1, 4.2A; Table 4.1). Long pulses revealed an additional, slowly decaying phase that reached a low, sustained level (Table 4.1). A slowly decaying tail current could be observed upon repolarization to –80 mV (Fig. 4.2A), following I_{Na} responses lasting 45 ms.

Both the transient and slowly inactivating components of the inward current became outward when 99% of external sodium was replaced with choline (Fig. 4.1); thus both components were carried by sodium ions.

The channels carrying the transient component may also pass caesium ions. Recordings were obtained from two cells using solutions where

internal and external sodium, potassium and calcium were replaced with supposedly impermeant ions. Caesium was substituted for internal potassium. These cells exhibited a transient, outward current (not shown) that arose very rapidly and decayed e-fold in 0.8–1 ms, a time course very similar to that of the transient I_{Na}. At +10 mV, the transient caesium current measured about 200 pA. The permeability ratio, P_{Cs}/P_{Na} was calculated using the Goldman-Hodgkin-Katz constant field equation and was approximately 0.02.

Potassium current recordings (Chapter 5; $P_K/P_{Na} \approx 0.1$) exhibited a contaminating current that resembled I_{Na} in time course and voltage dependence of steady-state inactivation. Thus, the sodium channels are probably also permeable to potassium ions.

Voltage dependence of activation

A series of sodium current responses was elicited by 45 ms pulses to different voltages, from a holding potential of –80 mV, at 5 s intervals (Fig. 4.2A). The time to peak (T_{peak}) was extremely variable at barely activating voltages, measuring 9.03 ms ± 1.51 ms at –20 mV ($N = 9$), while above 0 mV it decreased to less than 1 ms and became much less variable (Table 4.1).

Peak, transient current amplitudes were averaged for 9 cells and plotted against step command potentials in Fig. 4.2B (solid circles with error bars). The average I–V data were fitted with a function composed of a Boltzmann distribution and Ohm's law (in legend to Table 4.2), represented by the solid curve in Fig. 4.2B. The fully activated sodium conductance was assumed to be ohmic because the I–V curve was linear around the reversal potential. A simulated function composed of a Boltzmann distribution and the Goldman-Hodgkin-Katz equation was not used because its reversal potential did not match that of the results and it was curvilinear at positive voltages. Individual data sets were also fitted in this way and the average parameters are given in Table 4.2 with SEMs. There was little difference between the parameters of curves fitted to data gathered with ascending and descending voltage series (data not shown), indicating little effect of cumulative inactivation (but see below). Only data from ascending series were used, because the few experiments with descending series did not meet the data selection criteria given in the Materials and Methods. Peak, corrected I_{Na} first activated between –30 mV and –20 mV. It increased sigmoidally with voltage, reached a maximum at about +10 mV and decreased quasi-linearly as the step potential progressed toward the reversal potential (E_{rev}). E_{rev} for I_{Na} (+62 mV) was 10 mV more positive than the expected Nernst equilibrium potential for sodium (E_{Na} = +52 mV) in these

ionic conditions.

The series resistance error (V_{Rser}) caused by the large peak current, and the truncation of peak current by rapid inactivation skewed the I–V data in opposite directions, and in almost equal amounts. As the inward current through the electrode became larger, the electrode tip became more positive than the expected command voltage; thus a corrected I–V relationship should exhibit a more positive maximum than the original data. Mathematical compensation for V_{Rser} was carried out as described in the Materials and Methods, on the data sets from individual cells. Data from the 9 cells were pooled and fitted with a simulated I–V function. In Table 4.2, the parameters fitted to the data corrected for V_{Rser} reflected a shallower and more positive voltage dependence than that for uncorrected data. The differences were significant for the voltage of half-activation, V_a, and the slope factor, K_a, but not the reversal potential. The calculated voltage of maximal current, V_{max}, was also more positive by about 9 mV.

The rapid inactivation of I_{Na} truncated the current onset and thus contaminated the voltage dependence of peak current with that of the inactivation process. The corrected, steady-state activated current was obtained by graphically removing the inactivation phase (see Materials and Methods). The steady-state I–V curve had a slightly steeper voltage dependence, reached a maximum at a more negative voltage and was ~80% greater in amplitude than the original data (Table 4.2). When both types of correction were combined, V_a and V_{max} were similar to those for the original data, while K_a and the current amplitude were larger.

The voltage dependence of the slowly decaying current, shown in Figure 4.2B with a fitted function (broken curve), was significantly shallower than the peak, doubly-corrected data ($0.02 < P < 0.05$) and reversed at a less positive voltage (+42 mV; Fig. 4.2B; Table 4.2) than the expected E_{Na}. A slowly arising outward current (Fig. 4.2A) probably caused the premature reversal of the slowly decaying I_{Na}.

Voltage dependence of the time course of inactivation

Double-exponential functions were fitted to the rapid inactivation phase of the I_{Na} responses described above. The shorter and longer time constants were named τ_1 and τ_2, respectively. At negative voltages (~–10 mV), not all traces could be fitted and τ_1 was variable (Fig. 4.3). At more depolarizing voltages, τ_1 decreased e-fold in 9.2 mV and became less variable. The longer τ_2 behaved similarly to τ_1 at voltages below +40 mV, decreasing e-fold for every 11.0 mV of depolarization. Beyond that, however, τ_2 showed

a steep increase in size and variability (points offscale). This was paralleled with a reduction in the quality of the fits (not shown), a decrease of the amplitude of the smaller exponential component at voltages near the reversal potential, and an increase of the slowly rising, outward current.

Voltage dependence of steady-state inactivation

The dependence of peak I_{Na} availability on prepulse voltage was measured in 8 cells, using a two-step protocol applied every 20 s. A two-second, conditioning prepulse was applied to various membrane potentials to cause steady-state inactivation. The amount of inactivation was measured by the availability of the peak, transient I_{Na} in response to 20 ms test pulses to +10 mV, applied after the prepulse without any interval. Because the prepulses were very long, these results reflect the behavior of both rapid and slowly inactivating components. The peak, test currents, averaged for 8 cells, are plotted in Fig. 4.4 against prepulse voltage, using normalized amplitudes. The availability of I_{Na} for activation decreased sigmoidally as the prepulse potential became more positive. A Boltzmann function (described in the legend to Table 4.3) was fitted to the average, transient current data and is plotted as a solid curve in Fig. 4.4. Fitting parameters for ascending and descending prepulse series are given in Table 4.3. The descending series showed a significantly shallower voltage dependence and a significantly smaller maximal current than the ascending series. These changes could have resulted from cumulative inactivation, which would have caused a reduction of responses as the protocol progressed.

The slowly decaying current at the end of the test responses showed a similar dependence on prepulse voltage to that of the transient current (Fig. 4.4; Table 4.3), although the voltage of half-inactivation, V_i, was significantly more positive than for the transient current, and the test responses decreased after prepulses to below –40 mV.

Recovery from inactivation and cumulative inactivation

A two-pulse protocol was applied in 4 cells to measure the time course of recovery of the sodium current from inactivation. A 100 ms prepulse to +20 mV was applied, followed by an interval of variable duration at –80 mV, and a second depolarizing pulse, the test pulse, to +10 mV, lasting 20 ms. The normalized data were plotted in Figure 4.5, and showed little variability between cells. Single exponentials fitted the data well and showed that inactivation recovered with a time constant of about 111 ms at –80 mV. The time constant of recovery from inactivation was measured at different

voltages in only one cell (Fig. 4.5, open triangles), where recovery was 2.6 times faster at –80 mV than at –40 mV ($\tau \approx 102$ ms vs 268 ms, respectively).

The sodium current elicited by the prepulses decreased gradually as the two-pulse protocol progressed. In one cell, the prepulses were applied every 10 s, and the total reduction in I_{Na} was 26%. In two other cells, intervals of 20 s caused a reduction of 24%, on average, while in a fourth cell, a slight increase of I_{Na} was observed with 30 s inter-stimulus intervals. These preliminary results suggest that the cumulative inactivation of I_{Na} was dependent on the stimulation rate.

Pharmacology

Organic and inorganic pharmacological agents were applied during recordings of total current, to determine if they inhibited I_{Na} specifically. I_{Na} was assumed to be the major component of the inward current (I_{in}), since the inward, calcium current seldom exceeded 500 pA (Przysiezniak and Spencer, 1992 [Chapter 3]). The data described below were not selected according to the criteria listed in the Materials and Methods, because the series resistances often changed during drug applications. However, R_{ser} was monitored using passive test responses recorded before and after drug applications, and drug effects were judged valid only if they occurred independently of changes in R_{ser}.

None of the organic compounds showed any effect on, or specificity for the inward current. The classical sodium channel blocker, tetrodotoxin (TTX) had no effect at all on the inward current in 3 cells, even at final concentrations of up to 140 μM (Fig. 4.6A). Both the transient and slowly decaying components of isolated I_{Na} were found, in 3 other cells, to be insensitive to TTX between 10 μM and 33 μM (data not shown). The TTX used in these experiments was found to be active when tested on neurons from the central ganglia of the nudibranch mollusc Hermissenda. Another compound known to act like TTX, saxitoxin (STX), incompletely and reversibly blocked both inward and outward components in 4 cells, at concentrations between 45 μM and 100 μM, and revealed an inactivating outward current (Fig. 4.6B). It is unclear whether the high concentration of acetate in the STX solutions (4.5 mM to 10 mM; see Materials and Methods) contributed in any way to this non-specific blockade. Procaine, a known sodium channel blocker, was applied at final concentrations of 1 mM to 3 mM in 5 cells and blocked total current incompletely, with no specificity for either component (Fig. 4.6C). The calcium current in 3 cells was also inhibited by this drug (not shown), confirming the absence of any specific

effect.

Five, divalent, inorganic cations were applied as the chloride salts (Fig. 4.6D-H). The effects upon application were too large to be accounted for by calcium current blockade alone (cf. Przysiezniak and Spencer, 1992 [Chapter 3]). Most of the ions caused some reduction of both inward and outward current components, and a slowing of their onset kinetics. Three out of the five ions tested showed some specificity for I_{in}. These were cadmium, zinc and cobalt. All three ions showed a transient blockade and often a reversal of I_{in} upon the application of a bolus of stock solution (10 mM for Cd^{2+} and Zn^{2+}, 100 mM for Co^{2+}). This was followed by some recovery of I_{in}, as the applied solution became diluted to its final concentration.

The effect of bath-applied cadmium was the most specific, with a bolus of 10 mM Cd^{2+} blocking the transient I_{in} and slightly enhancing I_{out} (Fig. 4.6D). However, after dilution of the bolus to a lower final concentration, estimated to be 0.4 to 0.9 mM, peak I_{in} usually (in 4/8 cells) recovered to approximate its initial amplitude, suggesting that it was probably sensitive to a concentration of cadmium above 1 mM. I_{out} remained enhanced after dilution. The enhancement of I_{out} may have resulted from an inhibition of the slowly inactivating I_{Na}. In three cells where a more concentrated (50 mM) stock solution was applied for a final $[Cd^{2+}]$ above 1.5 mM, I_{out} showed some reduction (20–50%), while I_{in} reversed. In 6 cells where ionically isolated sodium currents were recorded (external Ca^{2+} replaced with Co^{2+}), Cd^{2+} superfused into the bath at a concentration of 0.5 mM caused no effect that was distinguishable from spontaneous changes in the current caused by changes in series resistance (data not shown). For example, in one cell, the slowly decaying current was unaffected by cadmium while the transient current showed a gradual reduction that was not reversed after washing. These behaviors could be explained by changes in R_{ser}. Thus, experiments with total currents and with isolated sodium currents agree in showing that Cd^{2+} was potent at concentrations higher than 1 mM.

Zinc exerted a less specific blockade than did Cd^{2+}. When a stock solution of 10 mM (2 cells) or 100 mM (3 cells) was applied, I_{out} was reduced to about 40% while I_{in} was usually reversed. The application of Zn^{2+} tended to make the recordings unstable, so the recovery of I_{in} after dilution of the stock solution could be followed in only 1 of the 5 cells tested. This cell was accessed while it was exposed to 0.6 mM Zn^{2+}, and it exhibited a large I_{in} (Fig. 4.6E, control trace), suggesting that this concentration of zinc was relatively ineffective. With the application of a bolus of 10 mM zinc, I_{in} momentarily reversed and I_{out} was reduced. After dilution, both I_{in} and I_{out} were still inhibited by at least one half (Fig. 4.6E), while the expected, final bath

concentration of zinc (0.8 mM) had only increased by 0.2 mM. The onset of the inward current was visibly slowed by zinc.

Cobalt was applied to 3 cells as a 100 mM stock solution to give calculated, final bath concentrations of 0.6 mM to 3.2 mM. When large volumes (15 μl or more) of the stock solution were applied the boluses caused transient elimination of I_{in} or reversal of the current (Fig. 4.6F). In these cases when the final concentration was 1 mM or more, I_{out} was inhibited by 50–80%, indicating some specificity of action. Cobalt also slowed the onset of the inward current. However when cobalt replaced calcium at 9.5 mM in the bath there was no apparent effect on the isolated sodium current.

Two other ions, manganese and nickel (Fig. 4.6G,H), caused a more gradual reduction of both I_{in} and I_{out} than did Cd^{2+}, Zn^{2+} or Co^{2+} and never caused the reversal of I_{in}. The onset of I_{in} was slowed by these cations. In 2 cells, Mn^{2+} was applied at 100 mM to a final concentration of 3.2 mM, and inhibited I_{in} and I_{out} by 65% and 45%, respectively. Nickel was applied at 20 mM (2 cells) or 100 mM (1 cell) to final concentrations of 0.6 mM or 6.3 mM, respectively. The lower concentration inhibited the I_{in} and I_{out} by 60% and 35%, respectively, similar to the effect of 3.2 mM Mn^{2+}, while the higher concentration exerted 80% and 60% blockade, respectively.

The divalent cations can be placed in a tentative ranking of specificity in blocking I_{Na}, as follows: $Cd^{2+} > Zn^{2+}$, $Co^{2+} > Mn^{2+}$, Ni^{2+}. Because the true concentration of applied ions around the cells was not measured, and most of the divalent cations were effective at concentrations around or above 1 mM, a potency order was difficult to establish.

Location of sodium channels

The distribution of sodium channels on the SMNs was examined in one SMN. Using a pipette tip, the cell was separated into two relatively equally sized pieces containing mostly soma, and mostly material from a large, lamellipodial structure. Tight-seal, whole-cell voltage clamp of these pieces revealed that the inward current appeared in the soma but not in the rounded lamellipodium.

Other currents

Other cells seen *in vitro*, namely the "short-spike neurons" (Chapter 2), produced spikes of "conventional" duration, but exhibited an inward current that tended to run-down a few minutes after access. This may represent a second type of sodium current in *Polyorchis*.

DISCUSSION

The results describe an inward sodium current that activated rapidly (T_{peak} = 0.8–9 ms), inactivated rapidly with two exponential phases ($\tau \approx$ 1 ms, 8 ms) and exhibited a slowly decaying component ($\tau \approx$ 240 ms). The rapidly inactivating component could also be carried by potassium ($P_K/P_{Na} \approx$ 0.1) and caesium ions ($P_{Cs}/P_{Na} \approx$ 0.02). This transient current was half activated around 0 mV, reached a maximum between +1 mV and +17 mV, depending on whether the data were corrected for errors introduced by the series resistance and the rapid inactivation, and reversed at +62 mV, above the sodium Nernst potential. It was half inactivated by 2 s prepulses to –26 mV and recovered e-fold from full inactivation in approximately 100 ms, at –80 mV. Both the transient and the slowly decaying components were reversed by a reversal of the sodium gradient, and both were insensitive to TTX. In total-current recordings, the transient, inward current was blocked more effectively than was the outward current by millimolar concentrations of the divalent cations cadmium, zinc and cobalt.

The slowly decaying current exhibited a significantly shallower voltage sensitivity than did the transient current, and reversed at +42 mV, below the sodium Nernst potential. It was half inactivated at a slightly but significantly more positive voltage than the transient current.

The transient and slowly decaying sodium current components

The slowly decaying component appeared to be similar to the transient component, in its I–V relationship and its voltage dependence of steady-state availability, and may have been mediated by the same channel population. However, certain discrepancies were observed and must be explained before this conclusion can be accepted.

The slowly decaying current activated with a shallower voltage dependence than did the peak, transient current, even after the latter data were mathematically corrected for series resistance error and rapid inactivation. The presence of an outward current in the later phase of the sodium current responses likely masked some of the slowly decaying I_{Na} and caused it to increase less steeply with voltage than it should have. This may account for the remaining difference between the slope factors fitted to the data of the two components.

The reversal potential of the slowly decaying current was more negative than the reversal potential of the transient current. This difference is partly

explained by contamination of the slowly decaying current by the outward "creep" current, and suggests that the latter is carried by ions such as caesium, chloride, or residual potassium, whose reversal potentials are more negative than E_{Na}.

The reversal potential of the transient current was more positive than E_{Na}. This difference may have several causes. First, a liquid junctional potential between the cytoplasmic and electrode solutions could be generated by any large, negatively charged, proteins lingering in the cytoplasm (Marty and Neher, 1983). These would drive an electrochemical gradient centered at the electrode tip, such that the voltage in the bulk of the cytoplasm was more negative than that at the electrode tip. Marty and Neher (1983) found a junctional potential of $\sim$–10 mV or less in adrenal chromaffin cells. Thus, the reversal potential in the bulk cytoplasm would be closer to E_{Na} than E_{rev} measured at the electrode tip. As the slowly diffusing proteins became diluted in the electrode solution, this junctional potential would subside. In small neurons ($C_m \approx 5$ pF), such a dilution may take about 15 min (Marty and Neher, 1983), but in the large SMNs ($C_m \approx 35$ pF), the reduction in the junctional potential may be much slower so the discrepancy could persist through the recording period (15–30 min). Second, the discrepancy between E_{rev} and E_{Na} could have arisen if E_{Na} were underestimated. Such an error would translate to an underestimate of $[Na^+]_{out}$ by $\sim$200 mM or an overestimate of $[Na^+]_{in}$ by 16 mM. The former is improbable because the bath sodium around the cell would rapidly be replenished even after a massive influx. However, the latter may be possible if the exchange of cellular and electrode solutions were slow and no sodium-calcium exchange were present, as was the case here, in the absence of external calcium. Third, the difference between E_{rev} of the transient component and E_{Na} probably was not the result of contamination by an inward current, because the only other bathing cations with reversal potentials more positive than E_{Na}, magnesium and cobalt, are known not to permeate the calcium or sodium channels of these cells in the absence of calcium and sodium (Przysiezniak and Spencer, 1992 [Chapter 2], Fig. 1). The discrepant reversal potential of the transient current may have resulted from an inhomogeneous space clamp. A depolarization to E_{Na} at the electrode tip may have clamped electrically distant parts of the cell at a more negative voltage, at which there remained a significant, inward driving force on sodium ions. However, there was little correlation between cell length or width and the reversal potential ($N = 9$) and it remains unclear whether space-clamp error caused the transient current to reverse beyond E_{Na}.

The voltage of half-inactivation of the slowly decaying I_{Na} was significantly more positive than that of the transient current. This, and the reduction of the maximal test current after prepulses below −40 mV, could result from contamination by a fast potassium channel current, I_{K-fast}, described elsewhere (Chapter 5). The gradual increase of I_{Na} as the prepulses approached −40 mV from more negative values may reflect the voltage-dependent inactivation of the contaminating I_{K-fast}. Some I_{K-fast} still remaining after prepulses to −40 mV may have suppressed the slowly decaying I_{Na}, causing an underestimate of the maximal and half-maximal current amplitudes, resulting in a positive shift of the apparent voltage of half-inactivation. Among the 8 cells tested, the linear slope of the curve from −70 mV to −40 mV, representing I_{K-fast}, and the voltage of half-inactivation showed a positive correlation ($r^2 = 0.682$), further suggesting that both phenomena were linked. The potassium channel current was likely carried by caesium, assuming that the cytoplasmic electrolytes had equilibrated with the pipette solution.

Thus, the differences in voltage dependencies between the transient current and the slowly decaying current were probably artifacts of outward current contamination. Although their voltage dependencies were very similar, it remains unclear whether these currents were mediated by the same or by different channel populations.

It has been shown elsewhere (Przysiezniak and Spencer, 1992 [Chapter 3]) that the transient sodium current in the SMNs is mediated by channels that are selective for sodium over calcium, when both of these ions are present in the bath, and is distinct from the transient calcium current described in the SMNs. This current probably drives the action-potential upstroke, as Anderson (1979) has shown in an *in vivo*, current-clamp, ion-replacement study. Furthermore, because the transient sodium current takes 0.8 to 1 s, at physiological resting potentials, to recover almost completely from full inactivation ($\tau \approx 250$ ms at −40 mV), it is well suited to limit the SMN spiking frequency, which reaches a maximum between 1 and 3 Hz (Spencer and Satterlie, 1980, Fig. 3; Spencer, 1981, Fig. 2).

The selectivity of the slowly decaying sodium current is unknown. Furthermore, its time course of inactivation ($\tau \approx 240$ ms), and its voltage dependencies of activation and inactivation are similar to those of the slowly inactivating phase ($\tau \approx 190$ ms) of the transient calcium current in SMNs (Przysiezniak and Spencer, 1992 [Chapter 3]). Finally, the presence of plateau action potentials in current-clamp recordings in the absence of external calcium suggests that the slowly decaying sodium current can have

a similar role to the calcium current in these cells, and may be carried through the same channels.

Pharmacology

The lack of specific effect of tetrodotoxin and saxitoxin on the inward current confirms the current-clamp study by Anderson (1979), who found that the action potentials of *in vivo* swimming motor neurons were TTX-insensitive. In contrast, the swimming muscle cells of *Polyorchis* produce action potentials that are sensitive to high concentrations of TTX (Spencer and Satterlie, 1981), suggesting that there may be two types of sodium current occurring in different tissues of this animal.

The divalent cations applied reduced the inward current amplitude and all, except cadmium, caused a delay in the time to peak. Since all of these ions, except cadmium, also inhibited some of the outward current, the delay in time to peak may have resulted from the unmasking of the later part of the inward current. This does not preclude a direct pharmacological effect of divalent cations on the sodium current kinetics (cf. Hanck and Sheets, 1992).

Some evidence suggests that the effective concentrations of the applied divalent cations were a few to a few tens of mM greater than the calculated, final, bath concentrations. The inward current in total-current recordings was blocked by cobalt applied to a calculated, final concentration of 2.3 mM from a stock solution of 100 mM, while the isolated sodium current appeared full-sized and untouched by the 9.5 mM cobalt replacing the bath calcium. The greater effectiveness of applied cobalt than of cobalt integrally present in the bath suggests that incomplete dilution of the stock solution in the pharmacological experiments produced a final concentration of cobalt higher than 9.5 mM. Similarly, the presence of I_{Na} with 0.6 mM zinc in the bath and its halving upon the application of 10 mM stock solution suggests that the effective concentration was greater than the calculated, final 0.8 mM. Incomplete dilution may have been aided if the ions that bound to cell receptors upon application dissociated very slowly once the applied cation became diluted. Assuming that all the divalent cations bound with similar mechanisms, or had similar diffusion coefficients, it is likely that the final bath concentrations of all divalent cations were underestimated.

The effective concentration of cadmium for blockade of the transient, inward, sodium current (>1 mM) was greater than that for blockade of the transient calcium current (usually ~0.5 mM; Przysiezniak and Spencer, 1992 [Chapter 3]), which supports the evidence distinguishing these currents.

103

Taxonomic comparisons

Several features of the transient sodium current in *Polyorchis* resemble those found in other cnidarians. A rapid sodium current, similar in time course to that in *Polyorchis*, was described by Anderson (1987) in motor neurons of the scyphozoan jellyfish, *Cyanea capillata*, and found to be unaffected by 100 μM TTX, but partially inhibited by 5 mM cadmium. Its I–V curve reached a maximum around +5 mV and reversed around +60 mV, resembling that in *Polyorchis*. Its steady-state availability reached 50% after prepulses to -15 mV, which was more positive than in *Polyorchis*. This difference may have occurred if a slowly decaying component was present in *Cyanea* and was insufficiently inactivated by the 50 ms prepulses used. The stenotele cnidocytes of the hydroid, *Cladonema* sp. (Anderson and McKay, 1987) exhibited a sodium current that reached a peak in about 2 ms and barely inactivated, but showed an I–V curve like that of I_{Na} in *Polyorchis* ($V_{max} \approx +20$ mV, $E_{rev} \approx +65$ mV). This current was unaffected by 1 μM TTX but was suppressed by 2–5 mM cadmium. In the hydromedusa *Aglantha*, a sodium-dependent action potential was found to be TTX-insensitive (Meech, 1989).

The sodium current of *Polyorchis* differed from that of most other, non-cnidarian animals in that its voltage dependencies of activation and inactivation occurred at generally more positive voltages (cf. Kostyuk et al., 1977; Byerly and Leung, 1988; García et al., 1990; Visentin et al., 1990). Relatively positive voltage dependencies were also seen in *Cyanea* motor neurons (Anderson, 1987), and could be inferred from the high-threshold, sodium action potentials in the giant motor neurons of *Aglantha*(Mackie and Meech, 1985). The motor neurons of these jellyfish and the SMNs drive swimming in these jellyfish, so a high spiking threshold may be an adaptation to limit the mean firing frequency and allow the adequate relaxation of the swimming muscle and complete refilling of the swimming bell.

The transient sodium current in *Polyorchis* swimming motor neurons was similar in several of its features to I_{Na} in various invertebrates and vertebrates. Its selectivity ratios for potassium (Chapter 5) and caesium relative to sodium, calculated from current amplitudes and the Goldman-Hodgkin-Katz constant field equation, were similar to those measured with reversal potentials in squid axon (Chandler and Meves, 1965) and in frog node of Ranvier (Hille, 1972). Thus, sodium selective channels may have evolved in an ancestor common to the Cnidaria and other Metazoa. Alternately, they may have evolved several times independently from

calcium channels (Hille, 1992), under the selective pressures for rapid propagation without massive, damaging, calcium influx. Sodium-selective channels dependent on calcium are present in the cilia of the freshwater protozoan, *Paramecium* (Saimi, 1986; review by Hennessey, 1989), and of the marine ciliate, *Euplotes vannus* (Krüppel and Lueken, 1990). Both slow and transient sodium channels may be present in the heliozoan protozoan *Actinocoryne contractilis*, which exhibits sodium-dependent receptor and action potentials (Febvre-Chevalier et al., 1986). These protozoan currents may represent some of the earliest evolutionary "experiments" in sodium selectivity.

The rapid time course of the transient I_{Na} in *Polyorchis* is comparable to that in leeches (García et al., 1990), snails (Kostyuk et al., 1977) and squid (Hodgkin and Huxley, 1952), fruit fly (Byerly and Leung, 1988), salamander (Lukasiewicz and Werblin, 1988) and guinea-pig (Visentin et al., 1990), among others. This general similarity of transient, sodium current time courses may be the result of stringent selective pressures on different groups of animals to evolve analogous mechanisms for rapid impulse generation and propagation, and maximum information transmission as frequency coded messages. It may also reflect a common evolutionary origin of all metazoan, voltage-gated sodium channels. This is reflected in the conservation of crucial amino-acid residues in regions of the sodium channel proteins controlling voltage-dependent activation and rapid inactivation (reviewed in Catterall, 1992; however, see George et al., 1992).

Tetrodotoxin-insensitive sodium currents and their resulting potentials appear throughout metazoan phylogeny in the flatworms (Koopowitz, 1989), molluscs (Kostyuk et al., 1977), and vertebrates (Bossu and Feltz, 1984; Visentin et al., 1990). This feature of sodium channels was likely of selective advantage for marine, plankton-feeding jellyfish, which may be exposed to "blooms" of dinoflagellates (Taylor and Seliger, 1979) producing TTX analogs such as saxitoxin. In less primitive animals not normally exposed to TTX or its analogs, the presence of sodium channels with a "receptor" for these drugs may reflect the relative absence of selective pressure against such channels, and the phylogenetic relationship between these animals and the more primitive planktivores. Recent molecular evidence shows that the TTX and divalent cation sensitivities of sodium channels are affected in opposite directions by single amino-acid substitutions in at least two different sites of the SS2 linker between the S5 and S6 transmembrane segments (Terlau et al., 1991; Heinemann et al., 1992; Satin et al., 1992; Backx et al., 1992; Catterall, 1992). For example, single-point mutations of the rat heart sodium channel, replacing a Cys residue at

position 374 to a Tyr residue caused its TTX sensitivity to increase almost a thousand-fold and its cadmium sensitivity to decrease about 30-fold (Satin et al., 1992). Thus, the balance of TTX-sensitive and insensitive sodium channels in vertebrates may also depend on the evolutionary importance, if any, of sodium channel blockade by external, divalent cations such as calcium (Nilius, 1988; Chahine et al., 1992). That cnidarian neuronal sodium channels show both TTX insensitivity and cadmium sensitivity (Anderson, 1987; this study) suggests that they may be structurally similar and phylogenetically related to TTX-insensitive, voltage-dependent sodium channels in less primitive metazoans.

Sodium channels are believed by some (Hille, 1984,1992; Schreibmayer and Waller, 1991) to have evolved from calcium channels, through a change in ionic selectivity and gating kinetics. The conversion of calcium-selective to sodium-selective channels may have required at least one appropriate mutation, since one of the sites responsible for TTX sensitivity in the vertebrate sodium channel, a lysine residue at position 1422 (in the SS2 segment), is known to be important in determining the ionic selectivity of the sodium channel (Terlau et al., 1991; Heinemann et al., 1992), and its conversion to a glutamate residue renders the channel selective for calcium over sodium. Furthermore, assuming that the two sites described in this and the previous paragraph must bear the appropriate amino acids for sodium channels to be TTX-sensitive, then it is possible that sodium selectivity of voltage-dependent channels arose first with a mutation at "position 1422" while TTX sensitivity arose afterwards, through a point mutation at "position 374". Thus, the voltage-sensitive sodium channels of the Cnidaria may reflect the first of these molecular transitions from calcium channels to TTX-sensitive sodium channels.

The apparently simple nature of the molecular changes necessary to convert a sodium channel to a calcium channel, that is, a substitution from lysine to glutamate at position 1422, may suggest that multiple, parallel, evolutionary events could have given rise to sodium channels a number of times. However, the natural occurrence of a point mutation at a specific codon in the genome, yielding a specific amino acid substitution, has a low probability (at least 3×10^{-9} x 1/20 x freq. of random germ cell mutation). Thus, the simplicity of point mutations is only apparent and the evolution of sodium channels from calcium channels may have occurred only once.

Molecular studies in progress will help verify this conclusion. If sodium channel evolution was monophyletic, it may have occurred in a more primitive group than the Cnidaria, such as the Porifera (sponges), perhaps

106

the Placozoa or even the kingdom Protozoa.

Table 4.1
Features of maximal sodium current in swimming
motor neurons of *Polyorchis penicillatus*.

Time to peak	0.84 ± 0.04 ms
Peak current	-7.2 ± 0.6 nA
Fast τ_{off-1}	1.12 ± 0.04 ms
Fast decay 1 amplitude[a]	-10.9 ± 1.1 nA
Fast τ_{off-2}	8.0 ± 0.5 ms
Fast decay 2 amplitude[a]	-1.6 ± 0.7 nA
Slow τ_{off}[b]	241 ms
Slowly decaying current at 44.7 ms	-560 ± 90 pA
Sustained current at 2 s[c]	-57 ± 2 pA
Tail current τ after 45 ms	2.1 ± 0.2 ms

For all entries except the slow τ_{off} and the sustained current:
Averaged for 9 cells from 3 animals. Pulses lasted 45 ms and were
applied from V_h = -80 mV to V_c = +10 mV. All errors are SEM.
[a] Amplitudes were obtained from the double-exponential fits to
the traces, back-extrapolated to the voltage transition.
[b] Responses lasting 2 s at -20 mV were averaged from 8 cells and
fitted.
[c] Same recordings as b. Twenty samples taken from 1.84 s to 2.0 s
were averaged.

Table 4.2
Parameters used to fit simulated I-V functions to raw and mathematically-corrected I_{Na} data.

	Peak[a]	Slow Decay[a] (P^f)	V_{Rev} corr.[b] (P)	St-state corr.[c] (P)	Both corr.[d] (P)
V_a (mV)	-2.6 ± 0.9	-1.1 ± 1.7 (NS)	+5.4 (<0.001)	-9.5 (<0.001)	-2.5 (NS)
K_a (mV)	4.6 ± 0.2	8.7 ± 0.9 (<0.001)	6.9 (<0.001)	4.1 (NS)	6.5 (<0.001)
E_{rev} (mV)	+62.6 ± 1.3	+42.2 ± 2.0 (<0.001)	+62.5 (NS)	+63.1 (NS)	+62.6 (NS)
G_{max} (nS)	152 ± 14	20.8 ± 1.5 (<0.001)	192 (0.01-0.02)	248 (<0.001)	313 (<0.001)
V_{max} (mV)[e]	+8.3	+8.2	+17.2	+1.4	+10.2
I_{max} (nA)[e]	-7.6	-0.53	-7.4	-14.3	-14.4

[a] Uncorrected data for each cell were fitted with a combination of a Boltzmann equation and Ohm's law: $I = G_{max} \times (V_c - E_{rev}) / (1 + exp[(V_a - V_c)/K_a])$, where V_c is the command voltage, G_{max} is the maximal conductance to sodium, E_{rev} is the fitted reversal potential of the current, V_a is the voltage of half-activation and K_a is the slope factor of the activation curve in mV per e-fold change. G_{max} was fitted to the nearest 0.1 nS. All other parameters were fitted to the nearest 0.01 mV. The parameters fitted to 9 data sets from different cells were averaged and are given as means ± SEM.

[b] For each current measurement, in every cell, the command voltage was corrected by subtracting from it the voltage drop across the series resistance (V_{Rev}; see Materials and Methods). All data were pooled and fitted as in a. No error is given because there were no standard voltage values after correction.

[c] The steady-state current was obtained from the amplitude of a bi-exponential function fitted to the decay of each trace and back-extrapolated to the voltage transition. This was equivalent to graphically removing the inactivation phase of the responses. Steady-state activated currents at the most negative and positive voltages could not be obtained in this way because they were too small for satisfactory curve-fitting.

[d] The correction methods in b and c were used together. The quality of the fitting (R_{fit}) in this column was below the criterion given in the Materials and Methods (0.8): $R_{fit} = 0.72$.

[e] These values were calculated by setting the derivative of the equation in a to zero and rearranging it to obtain V_c or I from the parameters in the table.

[f] Two-tailed, Student's t-test probability of comparisons to the raw, peak data in the first column. "NS" indicates $P \geq 0.05$.

Table 4.3
Parameters used to fit Boltzmann curves to the steady-state inactivation data for I_{Na}, measured with ascending and descending prepulse series.

	Ascending	Descending (P^a)	Slowly decaying (P)
V_i (mV)	-26.1 ± 0.6	-29.8 ± 3.4 (NS)	-21.2 ± 1.2 (0.001–0.01)
K_i (mV)	4.8 ± 0.3	6.7 ± 0.8 (<0.05)	4.6 ± 0.5 (NS)
$I_{test,max}$ (nA)	-7.0 ± 0.8	-4.3 ± 0.4 (0.02)	-0.77 ± 0.11 (<0.001)
Nb. of cells	8	3	8

Steady-state inactivation data were fitted with the following equation: $I_{test} = I_{test,max} / \{1 + \exp[(V_{pp} - V_i)/K_i]\}$, where I_{test} is the peak current amplitude expected on the test pulse response, $I_{test,max}$ is the maximal current fitted at non-inactivating prepulse voltages, V_{pp} is the prepulse voltage, V_i is the prepulse voltage causing half-inactivation, and K_i is the slope of the inactivation curve in mV per e-fold change. The test-pulse current was assumed to reach zero at positive prepulse voltages; this reduced the possibility of obtaining a spurious fit. I_{max} in all columns was fitted to the nearest 0.1 pA. V_i and K_i were fitted to the nearest 0.1 mV for peak current and 0.01 mV for the slowly decaying current.

a Probabilities that the values are the same as those in the first column, determined with a Student's t-test.
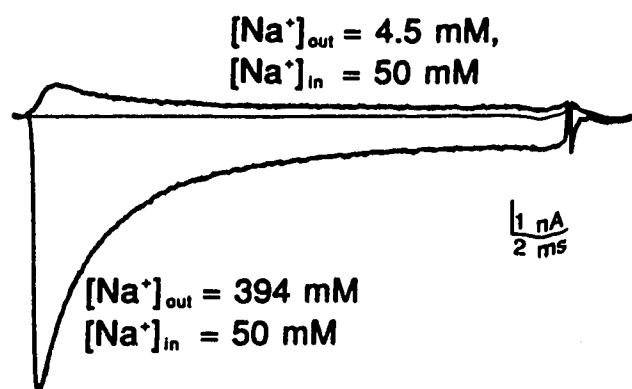
Figure 4.1 - Sodium current responses reversed with a reversed sodium gradient. Maximal I_{Na} responses from one swimming motor neuron (SM^N) were elicited by 20 ms pulses from a holding potential (V_h) of -80 mV to a command voltage (V_c) of $+10$ mV. The lower trace of I_{Na} was recorded with the bath and electrode solutions described in the Materials and Methods (Na^+ concentrations are indicated below the trace). The top trace was recorded when the response had stabilized after 3 minutes of superfusion with low-sodium solution of the following composition (in mM) $MgCl_2$, 23.3; $CoCl_2$, 9.5; $MgSO_4$, 5.7; KCl, 13.4; choline–Cl, 432; HEPES, 10; NaOH, 4.5. Leakage and capacitive current subtractions were carried out online using a +P/5 protocol. No series resistance (R_{ser}) compensation was used. Samples during residual capacitive transients were set to zero.

Figure 4.2 - The voltage dependence of I_{Na}. **A.** Representative sodium current responses from one SMN. Depolarizations lasting 45 ms were applied from a V_h of –80 mV, to a series of command voltages (V_c) incremented from –40 mV to +70 mV in steps of +10 mV. Responses at +10 mV and +70 mV are labelled. Samples for 250 µs after depolarizing and repolarizing voltage steps were set to zero current to remove capacitive transients. **B.** Current-voltage (I–V) relationships of the transient and slowly decaying components of I_{Na}. The uncorrected, peak amplitudes of I_{Na} responses such as those in A were averaged for nine cells and plotted as *solid circles* with accompanying error bars (SEM). An automatic peak detection routine was applied to samples between 0.4 ms and 18.4 ms from the beginning of the stimulus. The *solid curve* is a function fitted to the averaged data, combining the Boltzmann equation and Ohm's law (see legend to Table 4.2 for description). The *open squares* are an I–V plot of the current measured isochronally at the end (44.7 ms) of the responses described in A, representing the slowly decaying component of I_{Na}. These amplitudes were scaled 12.825 times so the maximum (–560 pA at +10 mV) matched that of the peak current. The *broken curve* is a fitted Boltzmann/Ohm function.

A

+70 mV

1 nA
5 ms

+10 mV

B

Slowly decaying

Transient
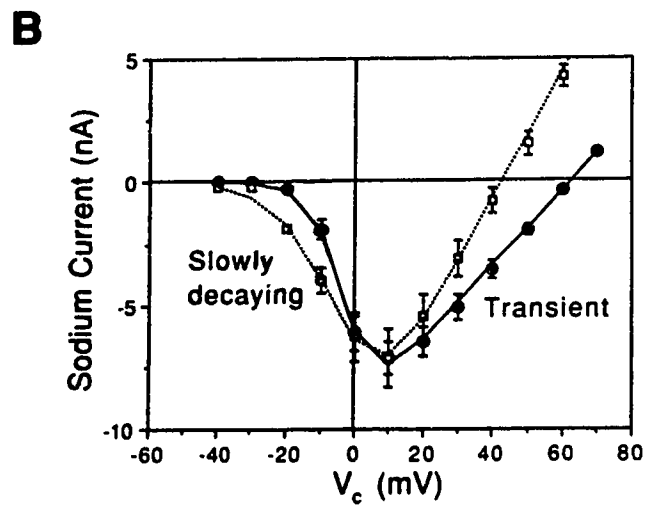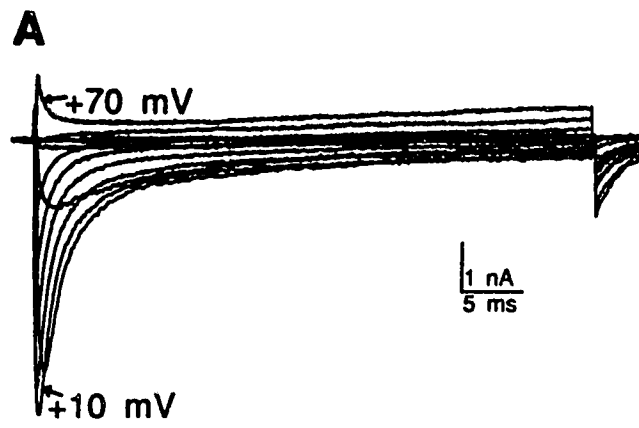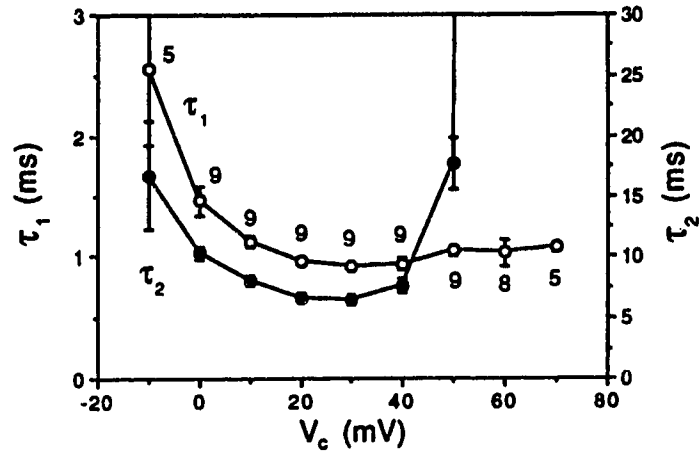
Figure 4.3 - The time constants of rapid inactivation of I_{Na} as a function of V_c. Double-exponentials were fitted to the rapid decay phase of I_{Na} responses described in Figure 4.2 and the shorter (τ_1, *open circles, left ordinate*) and longer (τ_2, *solid circles, right ordinate*) time constants are plotted against the command voltage. Some of the traces with small amplitudes could not be fitted in this way. The number of cells used to obtain the averages is indicated near points at each voltage and is the same for both time constants. Above +50 mV, τ_2 is offscale.

114
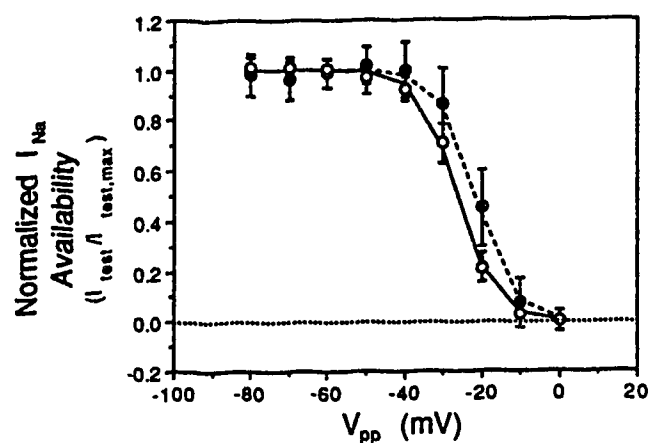
Figure 4.4 - Voltage dependence of I_{Na} availability after inactivating prepulses. The availability of the sodium conductance for activation was measured using a 20 ms test pulse to +10 mV following a 2 s, inactivating prepulse to an ascending series of voltages (V_{pp}). Currents measured at peak (*open circles*) and after 19.7 ms (*solid circles*) were averaged from 8 cells, normalized and plotted with standard deviations (N.B.), and are superimposed with fitted Boltzmann curves (*solid* or *broken lines*, respectively). The fitting parameters and equation are given in Table 4.3. Straight, dotted line shows zero availability.

115
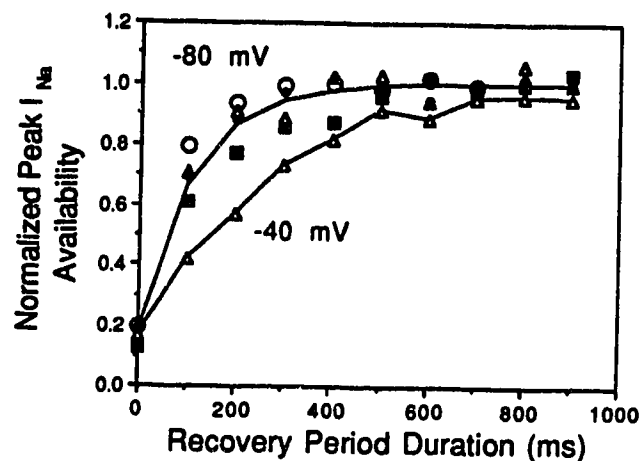
Figure 4.5 - Time course of recovery from inactivation. The recovery of the sodium current from inactivation was tested in four cells using a two-pulse protocol composed of an inactivating prepulse lasting 100 ms, applied from a V_h of -80 mV to a V_c of $+20$ mV, a recovery period of variable duration at -80 mV (and -40 mV in one cell, represented by *open triangles*), and a test pulse to $+10$ mV, lasting 20 ms. To compensate for cumulative inactivation, peak test-pulse responses were normalized to the peak, prepulse responses. Because of undersampling, the prepulse measurements were taken ~4 ms after peak, by which time I_{Na} had partially inactivated, so the normalized test responses were often larger than 1. To compare the recovery from inactivation between different cells, test responses were normalized again, to the fully recovered amplitudes obtained from fitting single exponentials to the results from each cell. These twice-normalized data were plotted as a function of the recovery period duration, with different symbols for each cell. For recovery at -80 mV, the *solid line* is a single-exponential fit to the averaged data ($N = 4$). One cell used in this average also yielded data on recovery at -40 mV; both data sets from this cell are plotted with *open triangles*.

116

Figure 4.6 - Representative traces illustrating the pharmacology of the total, voltage-dependent current, to find a specific blocker of I_{Na}. The inward current (I_{in}) is predominantly composed of I_{Na}. All responses were elicited with depolarizing test pulses from a V_h of -80 mV to a V_c of +10 mV. All panels have the same time base as A. Vertical scale bars on all panels represent 2 nA. All concentrations given with the experimental or *diluted* traces were calculated assuming the full dilution of the applied stock solutions. In several traces, the residual capacitive transients were removed. *A.* Tetrodotoxin (TTX) at a final concentration of 140 μM did not affect I_{in} or I_{out}. Traces were taken 1.5 min before the first application of TTX, and 11 min after the beginning of the first application or 3 min after the second and last addition of TTX. The solution applied was 1 mM TTX in distilled water. *B.* Saxitoxin (STX) at a final concentration of 45 μM reversibly blocked inward and outward components non-specifically, and unmasked a rapidly inactivating outward current. Traces were taken one minute after the beginning of STX application, 8 min after the end of STX application (before washing), and at the end of a 2.5 min wash. The solution applied was 0.5 mM STX in 50 mM acetic acid and 50% bath solution, at a pH between 6 and 7. *C.* Procaine applied to a final concentration of 1.7 mM exerted a non-specific blockade. Traces were at 1 min before the first application, and 9.5 min after the beginning of the first application, (i.e. 3 min after the second addition). The stock solution was 20 mM procaine in bath solution. R_{ser} compensation was used in this particular experiment. *D.* Cadmium applied at a stock concentration of 10 mM blocked I_{in} much better than I_{out} but once diluted to 0.6 mM Cd^{2+}, exerted only weak blockade. Traces were taken 1.5 min before, 1 min after and 7.5 min after Cd^{2+} addition. *E.* Zinc was applied to a cell that was already bathing in 0.6 mM Zn^{2+}. At a stock concentration of 10 mM, the freshly applied Zn^{2+} blocked both I_{in} and I_{out}, causing the transient reversal of I_{in}. Partial recovery of both components followed, as the bolus was diluted into the bath. The calculated, final bath concentration of Zn^{2+} was 0.8 mM. Traces were taken 1.5 min before, 3 min after and 15 min after Zn^{2+} application. *F.* Cobalt applied as a 100 mM stock solution caused the reversal of I_{in} with the inhibition of I_{out}, followed by the partial recovery of both currents. The final bath $[Co^{2+}]$ was calculated to be 2.3 mM. Traces were taken immediately before, 30 s after, and 6.5 min after Co^{2+} addition. *G.* Manganese non-specifically inhibited both components of total current. The final concentration was 3.2 mM. Traces were taken 1.5 min before and 3.5 min after the addition of Mn^{2+}. Stock solution was 100 mM Mn^{2+} in bath solution. *H.* Nickel also blocked I_{in} and I_{out} equally, at a final concentration of 0.6 mM. Traces were taken 2 min before and 3 min after the addition of Ni^{2+}. The stock solution was 20 mM nickel in bath solution.

A TTX
control
140 µM

B STX
wash
control
45 µM

C Procaine
1.7 mM
control

D Cd²⁺
dil.
cont. add.
addition (10 mM)
diluted (0.6 mM)
control

E Zn²⁺
addition (10 mM)
diluted (0.8 mM)
control (0.6 mM)

F Co²⁺
addition (100 mM)
diluted (2.3 mM)
control

G Mn²⁺
3.2 mM
control

H Ni²⁺
0.6 mM
control

2 nA
1 ms

REFERENCES

Anderson PAV (1979) Ionic basis of action potentials and bursting activity in the hydromedusan jellyfish *Polyorchis penicillatus*. J Exp Biol 78: 299-302.

Anderson PAV (1985) Physiology of a bidirectional, excitatory, chemical synapse. J Neurophysiol 53: 821-835.

Anderson PAV (1987) Properties and pharmacology of a TTX-insensitive Na^+ current in neurons of the jellyfish, *Cyanea capillata*. J Exp Biol 133: 231-248.

Anderson PAV, Mackie GO (1977) Electrically coupled, photosensitive neurons control swimming in a jellyfish. Science 197: 186-188.

Anderson PAV, McKay MC (1987) The electrophysiology of cnidocytes. J Exp Biol 133: 215-230.

Anderson PAV, Schwab WE (1983) Action potential in neurons of the motor nerve net of *Cyanea* (Coelenterata). J Neurophysiol 50: 671-683.

Backx PH, Yue DT, Lawrence JH, Marban E, Tomaselli GF (1992) Molecular localization of an ion-binding site within the pore of mammalian sodium channels. Science 257: 248-251.

Bossu JL, Feltz A (1984) Patch-clamp study of the tetrodotoxin-resistant sodium current in group C sensory neurons. Neurosci Lett 51: 241-246.

Byerly L, Leung H-T (1988) Ionic currents of *Drosophila* neurons in embryonic cultures. J Neurosci 8: 4379-4393.

Catterall WA (1992) Cellular and molecular biology of voltage-gated sodium channels. Physiol Rev 4: S15-S48.

Chahine M, Chen L-Q, Kallen RG, Barchi RL, Horn R (1992) Expressed Na channel clones differ in their sensitivity to external calcium concentration. Biophys J 62: 37-40.

Chandler WK, Meves H (1965) Voltage-clamp experiments on internally perfused giant axons. J Physiol (Lond) 180: 788-820.

Febvre-Chevalier C, Bilbaut A, Bone Q, Febvre J (1986) Sodium-calcium action potential associated with contraction in the heliozoan *Actinocoryne contractilis*. J Exp Biol 122: 177-192.

Frelin C, Cognard C, Vigne P, Lazdunski M (1986) Tetrodotoxin-sensitive and tetrodotoxin-resistant Na channels differ in their sensitivity to Cd^{2+} and Zn^{2+}. Eur J Pharmacol 122: 245-250.

García U, Grumbacher-Reinert S, Bookman R, Reuter H (1990) Distribution of Na^+ and K^+ currents in soma, axons and growth cones of leech Retzius neurons in culture. J Exp Biol 150: 1-17.

George AL Jr, Knittle TJ, Tamkun MM (1992) Molecular cloning of an atypical voltage-gated sodium channel expressed in human heart and uterus: evidence for a distinct gene family. Proc Natl Acad Sci USA 89: 4893-4897.

Hanck DA, Sheets MF (1992) Extracellular divalent and trivalent cation effects on sodium current kinetics in single canine cardiac Purkinje cells. J Physiol (Lond) 454: 267-298.

Heinemann SH, Terlau H, Stühmer W, Imoto K, Numa S (1992) Calcium channel characteristics conferred on the sodium channel by single mutations. Nature 356: 441-443.

Hennessey TM (1989) Ion currents of *Paramecium*: Effects of mutations and drugs. In: Evolution of the first nervous systems (Anderson PAV, ed), pp 215-235. New York: Plenum.

Hille B (1968) Pharmacological modifications of the sodium channel of frog nerve. J Gen Physiol 51: 199-219.

Hille B (1972) The permeability of the sodium channel to metal cations in myelinated nerve. J Gen Physiol 59: 637-658.

Hille B (1992) Ionic channels of excitable membranes. 2nd ed. Sunderland,

MA: Sinauer.

Hodgkin AL, Huxley AF (1952) A quantitative description of membrane current and its application to conduction and excitation in nerve. J Physiol (Lond) 116: 449-472.

Kerfoot PAH, Mackie GO, Meech RW, Roberts A, Singla CL (1985) Neuromuscular transmission in the jellyfish *Aglantha digitale*. J Exp Biol 116: 1-25.

Koopowitz H (1989) Polyclad neurobiology and the evolution of central nervous systems. In: Evolution of the first nervous systems (Anderson PAV, ed), pp 315-328. New York: Plenum.

Kostyuk PG, Krishtal OA, Shakhovalov YA (1977) Separation of sodium and calcium currents in the somatic membrane of mollusc neurons. J Physiol (Lond) 270: 545-568.

Krüppel T, Lueken W (1990) Calcium-dependent sodium current in the marine ciliate *Euplotes vannus*. J Membr Biol 116: 79-86.

Lukasiewicz P, Werblin F (1988) A slowly inactivating potassium current truncates spike activity in ganglion cells of the tiger salamander retina. J Neurosci 8: 4470-4481.

Mackie GO, Meech RW (1985) Separate sodium and calcium spikes in the same axon. Nature 313: 791-793.

Marty A, Neher E (1983) Tight-seal, whole-cell recording. In: Single-channel recording (Sakmann B and Neher E, eds), Chapter 7. New York: Plenum.

Meech RW (1989) The electrophysiology of swimming in the jellyfish Aglantha digitale. In: Evolution of the first nervous systems (Anderson PAV, ed), pp 281-298. New York: Plenum.

Nilius B (1988) Calcium block of guinea-pig heart sodium channels with and without modification by the piperazinylindole DPI 201-106. J Physiol (Lond) 399: 537-558.

121

Przysiezniak J, Spencer AN (1989) Primary culture of identified neurons from a cnidarian. J Exp Biol 142: 97-113.

Przysiezniak J, Spencer AN (1992). Voltage-activated calcium currents in identified neurons from a hydrozoan jellyfish, Polyorchis penicillatus. J Neurosci 12: 2065-2078.

Roberts A, Mackie GO (1980) The giant axon escape system of a hydrozoan medusa, Aglantha digitale. J Exp Biol 84: 303-318.

Satin J, Kyle JW, Chen M, Bell P, Cribbs LL, Fozzard HA, Rogart RB (1992) A mutant of TTX-resistant cardiac sodium channels with TTX-sensitive properties. Science 256: 1202-1205.

Satterlie RA (1979) Central control of swimming in the cubomedusan jellyfish Carybdea rastonii. J Comp Physiol 133: 357-367.

Satterlie RA, Spencer AN (1983) Neuronal control of locomotion in hydrozoan medusae. A comparative study. J Comp Physiol A 150: 195-206.

Saimi Y (1986) Calcium-dependent sodium currents in Paramecium: Manipulations and effects of hyper- and depolarization. J Membr Biol 92: 227-236.

Schreibmeyer W, Waller M (1991) Domain specialization in voltage-dependent Na^+ and Ca^{2+} channels. J Theor Biol 151: 141-143.

Spencer AN (1981) The parameters and properties of a group of electrically coupled neurons in the central nervous system of a hydrozoan jellyfish. J Exp Biol 93: 33-50.

Spencer AN, Arkett SA (1984) Radial symmetry and the organization of central neurons in a hydrozoan jellyfish. J Exp Biol 110: 69-90.

Spencer AN, Satterlie RA (1980) Electrical and dye coupling in an identified group of neurons in a coelenterate. J Neurobiol 11: 13-19.

Spencer AN, Satterlie RA (1981) The action potential and contraction in

subumbrellar swimming muscle of *Polyorchis penicillatus* (Hydromedusae). J Comp Physiol 144: 401-407.

Taylor DL, Seliger HH, eds (1979) Toxic dinoflagellate blooms. Developments in marine biology, v.1. Proceedings of the second international conference on toxic dinoflagellate blooms. New York: Elsevier/North-Holland.

Terlau H, Heinemann SH, Stühmer W, Pusch M, Conti F, Imoto K, Numa S (1991) Mapping the site of block by tetrodotoxin and saxitoxin of sodium channel II. FEBS Lett. 293(1,2): 93-96.

Visentin S, Zaza A, Ferroni A, Tromba C, DiFrancesco C (1990) Sodium current block caused by group IIb cations in calf Purkinje fibers and in guinea-pig ventricular myocytes. Pflügers Arch 417: 213-222.

Chapter 5

VOLTAGE-ACTIVATED POTASSIUM CURRENTS IN ISOLATED MOTOR NEURONS FROM THE JELLYFISH *POLYORCHIS PENICILLATUS*.

INTRODUCTION

Voltage-activated potassium currents serve numerous functions in the excitable cells of multicellular animals, including the repolarization of the action potential and control of its duration (delayed rectifier; Hodgkin and Huxley, 1952), the stabilization of the resting membrane potential (inward rectifier; Hille, 1992, p. 128) and the regulation of firing frequency (A current; Connor and Stevens, 1971b). What functions are served by different potassium currents depend on the kinetics and voltage dependencies of their activation and inactivation.

In the Cnidaria, potassium channels have diversified into a number of phenotypes with distinct activation and inactivation kinetics and voltage dependencies (Hagiwara et al., 1981; Anderson, 1989; Meech et al., 1989; Spencer et al. [Appendix A], 1989; Holman and Anderson, 1991). However, there have been no detailed studies of the voltage-activated potassium currents of a well-described neuronal type.

The current-clamp electrophysiology of "swimming motor neurons" (SMNs) from the hydrozoan jellysish *Polyorchis penicillatus* has been described extensively *in vivo* (Anderson and Mackie, 1977; Spencer, 1981, 1982). Recently, a primary culture technique (Przysiezniak and Spencer, 1989b [Chapter 2]) has allowed the isolation of these neurons and their characterization using the tight-seal, whole-cell, voltage-clamp technique. Rapidly and slowly arising potassium currents are present in the SMNs. In this article, the time course and voltage dependence of these currents is described and some evidence is provided regarding their ionic dependence and pharmacology.

MATERIALS AND METHODS

Animals were collected in Bamfield Inlet (Vancouver Island, British Columbia) from the surface by dip netting, or at depth by scuba divers using

plastic bags. The jellyfish were maintained in a recirculating, refrigerated (10°C) aquarium containing a mixture of Rila Marine Mix and seawater from Bamfield Inlet, on a cycle of 12 h of light, 12 h of dark. The animals were fed newly hatched brine shrimp larvae once or twice a week.

Cultures were prepared as described by Przysiezniak and Spencer (1989b, 1992 [Chapters 2, 3]). Nerve-ring tissue was dissected into artificial seawater (ASW), then incubated 5 min in 10% ASW, 15 min in calcium- and magnesium-free ASW, and 3–7 h in collagenase type I (Sigma) at 1000 U/ml. All incubations were at room temperature. After a brief rinse in ASW, the tissue was triturated and plated onto mesoglea-coated culture dishes (Falcon 1008; preparation described in Przysiezniak and Spencer, 1989b). Cultures were kept at 10°C.

Table 5.1 lists the salt compositions of different bath and electrode solutions, respectively, used in potassium current recordings. Bath solutions BSD and BSD2, which differed only in sulfate content, were used in most of the experiments described below, unless otherwise specified. To mimic normal intracellular conditions, the standard electrode solution contained potassium concentrations that ranged from 40 to 400 mM (solutions ESE, ESE2, ESE3 and ESD) and a calcium/EGTA buffer producing a final calcium concentration of approximately 1 nM (Stockbridge, 1987). The pH of all solutions was adjusted to 7.5 ± 0.05.

Four–aminopyridine (4–AP) was made up in bath solution as a 100 mM stock, which was added in small volumes to the bath. Stock solutions of divalent cations were dissolved in distilled water.

Recordings were carried out on cells in 0 to 5 day-old cultures using the tight-seal, whole-cell technique, at a room temperature of 20 to 25°C. The isolated SMNs were recognized by their large size, wide processes, clear cytoplasm and membranous inclusions around the nucleus (Przysiezniak and Spencer, 1989b). For recordings with adequate space clamping, cells were chosen that were relatively compact, with few or short (<50 μm) processes. Cells ranged in length from 30 to 150 μm and in width from 15 to 50 μm.

The voltage offset caused by the liquid junctional potential between the electrode and bath solutions was corrected electronically with the electrode tip in the bath. This offset correction was checked at the end of some recordings, after the electrode was removed from the cell, and was found to have deviated by only 2–3 mV. During most recordings, the composition of the bath solution was not changed (except in pharmacological experiments), so it is unlikely that the voltage measurements were contaminated by

changes in the junctional potential between bath and electrode solutions. However, it is possible that very slowly diffusing anionic proteins, which may be present in the cytoplasm, produced a liquid junctional potential between the electrode tip and the bulk of the cytoplasm (see Discussion on E_{rev}; Marty and Neher, 1983). In this case, it would be likely that all voltage measurements were more positive than the true voltages.

The ground electrode was a silver wire coated with silver chloride, inserted into an agar bridge (4–5% agar in ESD described in table 5.1). Whole-cell recording electrodes were made of soft-glass hematocrit tubing (Fisher), pulled with a two-stage puller (Narishige PP-83), polished to resistances ranging from 0.8 to 2.0 MΩ and coated with Sigmacote. Series resistances (R_{ser}) ranged from 1 MΩ to 8.3 MΩ. R_{ser} compensation of 60–80% was used in most recordings that were included in the analyses. In many recordings where the electrode solution contained 40 mM potassium, no compensation was used. The voltage error across R_{ser}, (V_{Rser}) calculated using the amplitude of voltage-clamp responses at +50 mV, ranged from 2.3 mV to 17.0 mV after compensation, with 43/48 recordings having less than 10 mV of error. Data obtained in early experiments (e.g., recovery from inactivation) were collected with higher resistance electrodes (1.5 to 4 MΩ).

Voltage pulses were produced and data were acquired through a Labmaster TL-1 (Axon Instruments) interface connected to an IBM-PC or IBM clone modified with an Enhanced Graphics Adaptor (ATI Technologies Inc.) and a math coprocessor, using pCLAMP software (Axon Instruments). Leakage and capacitive currents were subtracted online using P/4 or P/5 protocols. Earlier data (collected with high resistance electrodes) were recorded on chart paper and processed manually.

The following criteria were normally used to select data that were of sufficient quality (exceptions are noted in the text):

1) Cells must produce long action potentials in current clamp, in total-current conditions, or at least outward current responses in voltage clamp that did not show a shoulder or "notch" at 10–20 ms from the beginning of the voltage step (see Discussion on other cell types).

2) Leakage resistance must not be lower than 0.5 GΩ.

3) R_{ser} must be smaller than 10 MΩ.

4) R_{ser} must be compensated for unless the electrode solution contained 100 mM potassium or less.

5) Recordings must be stable, with no signs of seal disruption.

Data were digitally filtered at 1 kHz before current amplitude measurements. The latter were obtained using an automatic peak detection function of the pCLAMP software (Clampan), or from isochronal samples

(e.g., I–V data of currents at the end of the pulses).

Curve fitting was carried out using a least squares program in C language (Turbo C, Borland), to the precision indicated in the data tables (Tables 2, 3). The equations fitted are given in the table notes. Fitted functions were accepted only if the proportion of the variance of the data accounted for by the fit (the R_{fit} value) was ≥ 0.8. R_{fit} was defined as follows:

$$R_{fit} = 1 - [\Sigma(I - I_{fitted})^2 / \Sigma(I - I_{overall\ mean})^2]$$

where the sum, Σ, is taken over all points in the record. Data measurements are expressed as mean $\pm$ standard error of the mean (SEM), or as ranges of measurements. Statistical comparisons were carried out using two-tailed Student's t tests. Most data were collected into small sets of 1 to 4 samples, because of differences in stimulation protocols and recording solutions. Statistical comparisons were usually not done between such small data sets.

Possible sources of error

Series resistance error, inhomogeneous space clamp, and small sample sizes were the principal causes of inaccuracies in the results. Series resistance error, or V_{Rser}, was largest when currents were largest, i.e. at high $[K^+]_{in}$. The features most affected by V_{Rser} were the voltage dependence of activation, and possibly the time course of current decay at very positive voltages. Features such as the time to peak and the voltage dependence of steady-state inactivation showed no obvious dependence on the current amplitude.

The voltage dependence of activation was made shallower by any significant V_{Rser} because the current flowing into the cell through the electrode and access resistance (= R_{ser}) generated a voltage drop and caused the cell interior to be more negative than the back of the electrode, where the command voltage (V_c) was applied. When $[K^+]_{in}$ was 100 mM or smaller, the effect of V_{Rser} was likely unimportant, since currents were rarely larger than 3 nA.

The decay of large responses to very positive commands (i.e. above +50 mV) may have been affected by V_{Rser}. For example, at peak current, V_{Rser} was maximal for that response and Vm was more negative than the expected V_c. When channels inactivated, the outward current decreased (as did V_{Rser}) and caused V_m to approach V_c, activating a greater number of channels. The superposition of current through inactivating channels and

channels activated by decreased V_{Rser} may then have produced a response with a decay slower than the true inactivation rate.

It is possible that with the large conductance changes underlying potassium currents, the space constant of the cell was reduced considerably, so that effective voltage clamp was restricted to the membrane around the electrode. However, the extent of this type of error was not evaluated.

RESULTS

Overview

Three outward currents were distinguished when swimming motor neurons (SMNs) were voltage clamped. Figure 5.1 shows these currents, in conditions where potassium was the only permeant ion available. When the internal potassium concentration, $[K^+]_{in}$, was 100 mM and $[K^+]_{out}$ was 13.4 mM, responses to voltage steps from a holding potential (V_h) of -80 mV to a command potential (V_c) of $+50$ mV arose rapidly and decayed with two exponential phases (Fig. 5.1A, large response). This response was composed of two currents, I_{K-fast} and I_{K-slow}, with distinct time courses of onset. The rapid onset of I_{K-fast} was obvious using short-duration voltage steps from a V_h of -80 mV (Fig. 5.1B), while the slow onset of I_{K-slow} (Fig. 5.1A, small response) was revealed when V_h was -30 mV. An additional, transient, outward current arose before I_{K-fast}, and produced a notch or shoulder 1 to 2 ms after the beginning of the response (Fig. 5.1B). This current, I_{trans} ("transient outward"), is briefly described in the section below.

Initial, transient, outward current (I_{trans})

In the absence of internal and external sodium or calcium, certain characteristics of I_{trans} were reminiscent of the sodium current observed in the SMNs (Przysiezniak and Spencer, 1989a; Chapter 4). This can be shown by superimposing an inverted and scaled I_{Na} response on I_{trans} (Fig. 5.2A). The shorter time constants of bi-exponential functions fitted to the decay phases of I_{trans} (0.93 ± 0.28 [SEM] ms at $+50$ mV; $N = 4$) and I_{Na} (0.92 ± 0.03 ms at $+30$ mV; $N = 9$) were essentially identical. Also, the steady-state inactivation of I_{trans} reached 50% around -25 mV (Fig. 5.2B), as did that for I_{Na}, although the steepness of the relationship appeared greater for I_{Na} than for I_{trans}. Thus, I_{trans} may be carried by potassium ions through sodium channels, in the absence of sodium.

I_{K-fast} and I_{K-slow}

In the following sections the behavior of the potassium current responses will be described, and elements of this behavior will be attributed to the underlying I_{K-fast} or I_{K-slow}. The time courses and the ionic dependencies of the currents, and their voltage dependencies of activation and inactivation are described in detail in each of these sections. Preliminary pharmacological data are also presented.

Time course of I_{K-fast} and I_{K-slow}

In this section, "total outward" current refers to currents produced by command pulses to +50 mV applied from a holding potential of -80 mV, while I_{K-slow} responses result from pulses to +50 mV from a V_h of -30 mV. I_{K-fast} and I_{K-slow} could be easily distinguished from one another by their time courses of onset. In recordings of total outward currents, I_{K-fast} could be seen immediately following I_{trans} (Fig. 5.1B), arising rapidly with a time to peak (T_{peak}) of 6.7 ± 1.4 ms (N = 7). In one recording where $[K^+]_{in}$ was 400 mM and the sampling rate was high, I_{trans} was relatively small and did not mask the sigmoidal onset of I_{K-fast} (data not shown). A fourth order power function (τ = 0.86 ms) fitted the time course of the response at +50 mV slightly better than did a third order function.

The onset of I_{K-slow} was revealed when I_{K-fast} was inactivated by a V_h of -30 mV (Fig. 5.1A, smaller trace). The slow onset did not exhibit a sigmoidal time course, and at +50 mV, it could be fitted with a single time constant of 68.0 ± 5.0 ms (N = 6). Additionally, an initial, rapid phase of onset could clearly be observed in the recordings, although the slow digital sampling rate made it difficult to fit with an exponential function. This rapid onset was likely contributed by the remaining I_{K-fast} that was not inactivated by the relatively positive holding potential.

The decay of total outward current appeared to be multi-exponential (Fig. 5.1A, larger trace). When the $[K^+]_{in}$ was 400 mM, the fast and slow decays could best be fitted with two exponentials having time constants with ranges of 49 to 92 ms and 680 to 1270 ms, respectively (N = 3). The fast decay can only be attributed to I_{K-fast}, because I_{K-slow} had not activated substantially by the time the fast decay was apparent. The slow decay may also result from I_{K-fast} inactivation, because it was absent from I_{K-slow} responses. I_{K-slow} decayed little (2 to 9%, N = 3) during pulses to +70 mV lasting 1 s.

Following total outward current and I_{K-slow} responses lasting 20 ms, tail currents deactivated rapidly with time constants of 1–1.5 ms at -80 mV (N = 5). Following responses longer than 100 ms, the tail current exhibited a

more slowly decaying component (τ = 12–45 ms; N = 8).

Ionic dependence of I_{K-fast} and I_{K-slow}

In this and the following sections, all measurements of the total, outward current at its peak was assumed to reflect the amplitude of I_{K-fast} almost exclusively, since this current activated 10 to 20 times faster than did I_{K-slow}.

The peak amplitude of I_{K-fast} at +50 mV exhibited a linear dependence on $[K^+]_{in}$, with a slope of 19.2 pA/mM (r^2 = 0.889) and an ordinate of –634 pA (Fig. 5.3). Note that each point in this figure was measured from a different cell, at a fixed value of $[K^+]_{in}$. Thus, this relationship represents the behavior of a population of neurons. The linearity of this relationship contrasts with the saturation of current through potassium channels at high potassium concentrations seen in other preparations (cf. Coronado et al., 1980).

To measure reversal potentials (E_{rev}), tail currents were elicited with step repolarizations to different voltages following fixed test pulses to +50 mV, applied from a V_h of –80 mV and lasting 20 or 150 ms. The internal potassium concentration was 100 mM. Data for 20 ms and 150 ms test pulses were combined because no significant difference was observed between these two groups (N = 3 in each group). Tail current amplitudes were measured 1.5 to 2.0 ms after repolarization. E_{rev} measured -40.2 mV ± 1.7 mV (N = 6) and was significantly more positive than the Nernst potential in these conditions (-50.8 mV; 0.001 < P < 0.01; $[K^+]_{out}$ = 13.4 mM). E_{rev} measurements obtained when $[K^+]_{in}$ was 40 mM (–33.7 mV) and 400 mM (–75.8 mV) were not replicated and were thus unreliable.

Voltage dependence of activation of I_{K-fast} and I_{K-slow}

Total, outward currents elicited at various command voltages showed that the onset of I_{K-fast} accelerated as V_c became more positive (Fig. 5.4A). T_{peak} values averaged from 7 cells were relatively constant from –20 mV to 0 mV (15.9 ms ± 1.0 ms [SEM] at –10 mV), and decreased almost linearly to +50 mV, where T_{peak} measured 6.7 ms ± 1.4 ms. The activation kinetics of I_{K-fast} were more accurately quantified in one cell (same as in Fig. 5.4A) where power functions could be fitted to the activation phase. The time constants of the fourth-order functions ranged from 3.13 ms (–10 mV) to 0.71 ms (+70 mV), showing an exponential voltage dependence that decreased with a slope factor of 26.1 mV per e-fold change in the time constant.

Figure 5.4B shows the normalized relationships of peak I_{K-fast} to stimulating voltage, at different values of $[K^+]_{in}$. The holding potential was

-80 mV. I_{K-fast} increased approximately sigmoidally with voltage. It first activated just above -30 mV, with the slope conductance first increasing, then decreasing gradually beyond about +20 mV. Except for data at 40 mM, which were noisy, the results were similar regardless of the internal potassium concentration. A Boltzmann function was combined with Ohm's law and fitted to the data at 100 mM. The equation and the fitted parameters are given in Table 5.2. A function composed of a Boltzmann distribution and the Goldman-Hodgkin-Katz constant field equation, which was expected to model the fully activated potassium conductance more realistically, fitted the data poorly at positive voltages because it exhibited a slope increase.

The voltage dependence of I_{K-slow} onset could not be measured in a data set that fulfilled the selection criteria described in Materials and Methods. However, one recording of I_{K-slow} at different command voltages (Fig. 5.5A), made without R_{ser} compensation and with R_{leak} smaller than 0.5 GΩ was used because it showed a similar time course of onset to that of I_{K-slow} responses fulfilling the selection criteria. The onset of I_{K-slow} could best be fitted with two exponentials. Single-exponential fits gave time constants with an erratic voltage dependence and were not used. The shorter time constant ranged from 10.5 ms at -10 mV to 1.6 ms at +70 mV, while the longer time constant decreased from 247 ms to 65 ms, respectively. The faster time constant probably reflected the presence of residual I_{K-fast}. The slower time constant showed an exponential voltage dependence, with a slope factor of 13.1 mV per e-fold change in time constant.

The amplitude of I_{K-slow}, measured at 380 ms after the beginning of the pulse in the recordings from Fig. 5.5A, followed a voltage dependence that did not level off with positive commands (Fig. 5.5B, open circles), and was more positive and less steep than that for peak I_{K-fast}. This difference in voltage dependence was apparent at voltages (-10 mV, 0 mV) where currents were too small to cause a voltage error across R_{ser}. The voltage dependence of I_{K-slow} could be fitted with a Boltzmann/Ohm function (parameters in Table 5.2). The voltage of half-activation and the slope factor reflected the positively shifted and more shallow voltage dependence of I_{K-slow} relative to I_{K-fast}. The following data suggest that the above results adequately represent the behavior of I_{K-slow} in most SMNs.

Since the potassium current at the end of 1 s pulses likely contained a greater proportion of I_{K-slow} than the peak current did, the voltage dependence of this "late" current should reflect that of I_{K-slow} more than would the voltage dependence of the peak current. Figure 5.5B presents the I–V relationship of the current at 980 ms (open squares). The late

current behaved like I_{K-slow} in that it activated at more positive voltages and with a more shallow voltage dependence than did I_{K-fast}, and exhibited almost no levelling off at positive voltages. Thus, the late current after 1 s was likely composed of a large proportion of I_{K-slow}.

The tail current following total, outward current responses exhibited a voltage dependence that was intermediate to that of I_{K-fast} and I_{K-slow} (Table 5.2), and likely represented a combination of both. Tail currents were elicited upon repolarization to –80 mV, after 40 ms or 400 ms test pulses to different voltages, when $[K^+]_{in}$ was 100 mM. The tail current amplitudes measured 1 ms after the repolarization step were never larger than 0.6 nA, so any effect of series resistance error on the voltage was likely negligible. Since the repolarization voltage was constant, the driving force on potassium ions during tail currents was constant, and the increase in tail current amplitude with V_c directly reflected the activation of the potassium conductance or permeability elicited by the voltage pulse. Thus tail current data could be compared to the normalized conductance of I_{K-fast} and I_{K-slow} calculated from the I–V data and the driving force.

Single Boltzmann functions were fitted to the tail current voltage dependencies measured after 40 ms and 400 ms pulses (Table 5.2). The parameters in both cases lay between those measured for I_{K-fast} and I_{K-slow}. Furthermore, the fitted parameters did not differ substantially whether the tail currents were elicited after 40 ms or 400 ms pulses. Such a difference might be expected if the relative contributions of I_{K-fast} and I_{K-slow} to the tail current differed depending on the duration of the test pulse.

Two, summed, Boltzmann functions fitted the tail current data better than single funtions (Table 5.2), and each component followed the voltage dependence of I_{K-fast} or I_{K-slow}. Since no measurement of E_{rev} was necessary to obtain these fits, the parameters were more reliable than those fitted to I_{K-fast} and I_{K-slow} I–V data. The value of the slope parameter for the more steeply voltage-dependent component of the tail current at 40 ms resembled that obtained from a Boltzmann/Ohm fit to the I_{K-fast}–V relationship. In addition, both fitted functions were more positive and shallower for tail currents at 400 ms compared to 40 ms, reflecting the increased importance of I_{K-slow} at later times on the test pulse (Table 5.2). Thus, tail currents likely reflected the deactivation of both I_{K-fast} and I_{K-slow} channels.

The decay of total, outward current during 1 s voltage-clamp pulses became slower with increasingly positive command potentials, when $[K^+]_{in}$ equalled 400 mM (Fig. 5.6). This was unconventional since the inactivation rate of potassium currents is either insensitive to voltage (Connor and

Stevens, 1971a) or is accelerated at depolarizing voltages (Furukawa et al., 1992). This particular behavior of the total, outward current decay likely reflected the distinct but overlapping voltage dependencies of activation of I_{K-fast} and I_{K-slow}, as explained in the discussion.

Voltage dependence of inactivation of I_{K-fast} and I_{K-slow}

The voltage dependence of inactivation of the total, outward current was studied using a two-pulse voltage protocol. A prepulse to different voltages was applied for one second before testing the availability of the potassium current with a pulse to +50 mV. In a representative recording from one cell, where the test pulse lasted 800 ms and $[K^+]_{in}$ was 400 mM (Fig. 5.7A), a graded series of depolarizing prepulses caused the rapidly arising I_{K-fast} to be reduced and the slowly arising I_{K-slow} to be unmasked. I_{K-fast} showed no change in its time course of onset as I_{K-slow} was revealed, suggesting that the two currents arose through distinct kinetic mechanisms, likely in separate ion channel populations. Furthermore, both the fast and slow inactivation phase of the total outward current was gradually removed by depolarizing prepulses, suggesting that both phases resulted from the inactivation of I_{K-fast} and not of I_{K-slow}.

In Figure 5.7B, isochronal measurements of peak current and late current from the response in Fig. 5.7A are shown as a function of prepulse voltage. Data were normalized to the maximal current amplitude after the non-inactivating component was subtracted. With prepulses more negative than –70 mV I_{K-fast} availability appeared weakly voltage-dependent. With more positive prepulses, the current availability became steeply voltage-dependent. Around –30 mV, the peak, test current levelled off to a non-zero amplitude representing a combination of I_{K-slow} and residual I_{K-fast} (Fig. 5.7A). The similarity of the voltage dependencies of peak and late current availability strongly suggests that slow inactivation is a feature of I_{K-fast} and not of I_{K-slow}. These data were representative of steady-state inactivation in other cells. When the normalized availabilities of peak current were averaged for 8 cells, the results overlapped completely with those presented above.

Because the prepulses used in these experiments were only 1 s long, and because the inactivation of the outward current did not reach a true steady state within this time, these data only represent a quasi-steady-state relationship. With longer prepulses, I_{K-fast} inactivation would be more complete than with the protocols used here, and the relationship between current availability and prepulse voltage would be shifted to more negative potentials.

Modified Boltzmann functions were fitted to the peak data from the representative cell above (Fig. 5.7A; Table 5.3) and 7 other cells, assuming the presence of a non-inactivating component. The averaged fit parameters are given in Table 5.3. The tail current, measured 1-2 ms after repolarization of a test pulse lasting 20 ms, inactivated with a voltage dependency similar to that of peak I_{K-fast} (Table 5.3).

The recovery from inactivation of I_{K-fast} or I_{K-slow} was estimated coarsely in early experiments using a protocol with two, 2 s pulses. No cumulative inactivation of I_{K-fast} was observed using intervals of 1 s at -80 mV, whereas I_{K-slow} showed marked cumulative inactivation (65%) with 1 s intervals at -30 mV. Full recovery of I_{K-slow} from inactivation could be obtained if a 500 ms hyperpolarization to -60 mV was inserted halfway through the recovery interval.

Voltage dependence of I_{K-fast} inactivation and action-potential broadening

The following data suggest that I_{K-fast} is an important determinant of swimming motor neuron action-potential duration. The action potentials of SMNs usually showed three phases of repolarization (Fig. 5.8, inset). One was rapid and immediately followed the peak; it was not always present. The second repolarization phase was slow and progressed toward a shoulder, beyond which the third phase repolarized rapidly. Voltage slope measurements in current clamp are a reflection of the amplitude of the ionic currents flowing during the action potential (dV/dt = $[I_K+I_{Ca}+I_{Na}+I_{leak}+...]/C_m$), and their behavior can be roughly compared to that of currents measured in voltage clamp. The slow, or "plateau", repolarization slope (S_{repol}) that precedes the shoulder reflects the time necessary for the outward currents to counteract the inward currents and initiate the rapid repolarization, and is thus an important determinant of spike duration. Figure 5.8 shows that as the voltage preceding the spike increased, S_{repol} decreased almost exponentially. The reduction in S_{repol} was steepest around the voltage of half-inactivation for I_{K-fast}, and levelled off around -40 mV, where the availability of I_{K-fast} after inactivation was 10-20%.

Pharmacology of potassium currents

The pharmacological effects of several organic and inorganic compounds on outward currents were examined. The preliminary data used in the following description did not necessarily meet the criterion of minimum R_{leak} (0.5 GΩ) given in the Materials and Methods. In most cases R_{ser}

compensation was not used, because changing solutions levels often caused the compensation circuitry to ring. However, R_{ser} never exceeded the 10 MΩ criterion used in the remainder of the results.

A current-clamp recording of action potentials matched for baseline membrane potential (Fig. 5.9) showed that the repolarization was delayed after application of 4-aminopyridine (4-AP) to a final bath concentration of 10 mM. In early voltage-clamp experiments (Spencer et al., 1989 [Appendix A]), 5 mM 4-AP was seen to block I_{K-fast} more effectively than I_{K-slow}, in responses elicited from holding potentials of -80 mV and -30 mV, respectively ($N = 3$; data not shown). This effect was found to take more than 10 min to become visible. In recent voltage-clamp experiments where the effect of 10-40 mM 4-AP was studied on responses elicited from a V_h of -80 mV ($N = 3$), the peak current and the current at 400 ms were equally and weakly affected in two cells (inhibited by 15% after 13 min) and unaffected in one cell. The effect was difficult to distinguish from that of spontaneous changes in the series resistance. This is difficult to reconcile with the current-clamp data. However, such inconsistency likely arose from experimental variation, because recent work by Grigoriev (unpublished) indicates that 4-AP is effective in blocking I_{K-fast}. Its effect on I_{K-slow} remains unclear.

Tetraethylammonium applied internally at 10 or 100 mM ($N = 3$) partially blocked both I_{K-fast} and I_{K-slow}. Preliminary results show that when applied externally, this drug strongly increased action-potential duration (A. N. Spencer, unpublished) and reduced both I_{K-fast} and I_{K-slow} (N. G. Grigoriev, unpublished).

Two multivalent cations, barium and lanthanum, were found to inhibit the potassium current. The effect of 0.5 mM to 15 mM extracellular barium chloride ($N = 8$; solutions BS, ES) on total-current responses at +10 mV was to produce a consistently greater blockade of the peak outward current (65% inhibition, on average) than of the late outward or inward currents (25%, 5%, respectively). In sodium- and calcium-free conditions, recordings from 2 cells showed that exposure to 5-50 mM barium caused a gradual slowing of the onset of the total, outward, potassium current at +70 mV (Fig. 5.10, 50 mM). This effect was reversible. Since the effect was visible with 5 mM barium in the bath and the inward, barium current was smaller than 1 nA when $[Ba^{2+}]_{out}$ was 10 mM (Przysiezniak and Spencer, 1992 [Chapter 3]), it is unlikely that the superposition of an inward barium current caused the slowing of the potassium current onset. When maximally blocked by 50 mM barium, total outward current onset at +70 mV could be fitted with bi-exponential functions with time constants of 3.5 ms and 20.7 ms.

Furthermore, the voltage dependence of the potassium current in the presence of 25 mM barium, measured in one cell at 16 ms from the beginning of the voltage pulse (data not shown), was shifted by about 20 mV in the positive direction relative to that of unblocked, peak I_{K-fast} (Fig. 5.4B used for comparison). Since I_{K-fast} onset at +50 mV, in the absence of barium (T_{peak} = 6.7 ms; see section on voltage dependence of activation), was faster than that in the presence of barium at 20 mV more positive, i.e. +70 mV (T_{peak} > 20 ms), the slowing of I_{K-fast} onset by barium cannot be accounted for completely by a shift in voltage dependence, and must therefore be mediated by some other mechanism.

Lanthanum nitrate (Fig. 5.11) inhibited the outward current more than the inward current, at final concentrations of 0.1 to 0.7 mM (N = 4). The effect, monitored with test pulses eliciting total membrane currents, was usually visible after a delay of about 5 min from the application of a concentrated stock solution. In total-current responses at +10 mV (V_h −80 mV), the inward current was initially blocked (it reversed when large quantities of lanthanum were added), but recovered partially, while the outward current underwent a more progressive and lasting inhibition by 85%, on average. An I–V series was recorded from one cell bathed in 0.3 mM lanthanum, and showed a residual, outward current that activated slowly (T_{peak} ≥35 ms, τ = 8–12 ms; Fig. 5.11, inset), with a voltage dependence shifted +30 mV relative to that of I_{K-fast} (Fig. 5.4B used for comparison). Thus, lanthanum exerted an effect qualitatively similar to that of barium, but was about 100-fold more potent.

Location of potassium channels

The distribution of potassium channels on the SMNs was examined in only one SMN. Using a pipette tip, the cell was divided into two roughly equal sized pieces. One piece contained mostly soma, and the other, mostly material from a large, lamellipodial structure. Tight-seal, whole-cell voltage clamp of these pieces revealed that the total, outward current appeared in both the soma and in the rounded lamellipodium.

DISCUSSION

The results presented here indicate that there are at least two distinct potassium currents in the swimming motor neurons of *Polyorchis*. One current, I_{K-fast}, turned on rapidly (T_{peak} = 6–15 ms), was half-activated at −10

to 0 mV, decayed with two exponential phases and was half-inactivated by prepulses around –53 mV. The other current, I_{K-slow}, exhibited a slow onset (τ = 65–250 ms) when V_h was –30 mV, was half-activated around +24 mV, exhibited a shallower voltage dependence than I_{K-fast}, and did not inactivate. A third, outward current, I_{trans}, was unlikely to be physiological.

Transient, outward current (I_{trans})

The transient, outward current, I_{trans}, was likely carried by potassium ions through sodium channels, as suggested by the similarities of its time course and voltage dependence of steady-state inactivation to those described for I_{Na} in the same neurons (Przysiezniak and Spencer, 1989a; Chapter 4). The permeability of I_{trans} channels to sodium relative to potassium, P_K/P_{Na}, was about 1/10 as estimated from the current amplitudes, the concentrations of permeant ions and the command voltages using the Goldman-Hodgkin-Katz constant field equation. Hille (1992, p.351) reviewed vertebrate and invertebrate studies, noting that P_K/P_{Na} for sodium channels ranged from 0.05 to 0.09, thus supporting the above hypothesis.

It remains possible that I_{trans} is a true potassium channel current, comparable in time course to the I_A recorded in frog node of Ranvier, squid axon and crab walking leg (reviewed by Rudy, 1988). However, I_{trans} inactivates in a considerably more positive range of prepulse voltages than do most I_A currents, and its similarity to the I_{Na} described in *Polyorchis* is probably not coincidental.

A last possibility is that I_{trans} was a gating current. The integral of I_{trans}, divided by as many as 6 gating charges per channel, suggests there would need to be more than 100,000 channels in one cell to produce such a current. Assuming a spherical cell with a diameter of 30 μm, the channel density would be ~35 per μm^2 or more, which is a realistic estimate (Hille, 1992, p.330). I_{trans} arose too rapidly to represent the opening of K–slow channels, and too slowly to represent the opening of sodium channels in these cells. Although the time course of I_{trans} could conceivably reflect the opening of K–fast channels, its voltage dependence of steady-state inactivation suggests I_{trans} is carried by potassium ions through sodium channels.

Separation of I_{K-fast} and I_{K-slow}

The features that allow the separation of I_{K-fast} from I_{K-slow} will be the focus of this section. The strongest evidence for the presence of two, distinct, potassium currents is the difference in their voltage dependencies of inactivation. Following a 1 s prepulse to –30 mV, I_{K-fast} inactivated

almost completely while I_{K-slow} persisted. Furthermore, the perfect overlap of the voltage dependencies of steady-state inactivation of the peak and late currents strongly suggests that both the rapid and slowly inactivating phases could be attributed to I_{K-fast}. Finally, that I_{K-fast} did not completely inactivate during 1 s prepulses to -30 mV also indicates that it bore a slowly inactivating component. This evidence shows that I_{K-slow} was unlikely to exhibit any inactivation. In contrast, earlier evidence (Spencer et al., 1989 [Appendix A]) suggests that I_{K-slow} had an inactivating component. Voltage steps from a holding potential of -30 mV to $+70$ mV elicited an I_{K-slow} that decayed to ~60% in 2 s. Unlike the present recordings, these recordings were made with hard glass electrodes, which may have favored the maintenance of I_{K-fast} and its greater prominence in the residual current after inactivating prepulses. The soda glass electrodes used in the present experiments tapered more steeply and probably caused a rapid loss of cytoplasmic components necessary for the full activity of I_{K-fast} channels. Chemical influences from the soda glass may also have inhibited I_{K-fast} (Cota and Armstrong, 1988; Copello et al., 1991).

Another prominent distinguishing feature of these two potassium currents, is their time course of activation. The onsets of I_{K-fast} and I_{K-slow} were distinct regardless of the prepulse voltage, indicating that these currents were mediated by separate kinetic mechanisms, likely in separate ion channel populations. It remains possible that this behavior represents the existence of two different gating modes in a single channel population (cf. Artalejo et al., 1991, for calcium channels; Duval et al., 1992, for sodium channels). For simplicity, however, the more conservative hypothesis will be adopted, that is, that multiple onset rates in the same voltage-clamp response indicate multiple channel populations.

The distinct but overlapping voltage dependencies of I_{K-fast} and I_{K-slow} serve to separate these currents and can explain the unconventional slowing of the total, outward current decay with depolarization. Since the onset of I_{K-slow} ($\tau \approx 68$ m... a time course almost complementary to the fast decay phase of I_{K} ... ms to 65 ms above $+20$ mV), it may have masked the latter s... at positive voltages where I_{K-slow} was most prominent. Th... the ...ent slowing of the total, outward current decay was likely a result of I_{K-fast} and I_{K-slow} superposition.

A quantitative estimate of the relative contributions of I_{K-fast} and I_{K-slow} to the late current was difficult to obtain. The steady-state inactivation data suggest that the inactivating I_{K-fast} represented a larger proportion (~75%) of the late current than did I_{K-slow} (~25%). In contrast, the I-V curve of the late current was more similar to that of I_{K} ... than that of I_{K} ... suggesting that

I_{K-slow} was prominent in the late current. One possible explanation for this contradiction is that the I_{K-slow}–V data, gathered from a single cell, was not accurately representative and may have been shifted to more negative voltages compared to those in other cells. This would falsely enhance the similarity between the late current I–V and that of I_{K-slow}. I_{K-slow} measurements taken from other data that did not fulfull the selection criteria (R_{leak} too low, no R_{ser} compensation) indicate that this may be the case.

Functions of the potassium currents in action-potential repolarization

The overlap of the voltage dependencies of spike repolarization rate and I_{K-fast} inactivation is consistent with the hypothesis proposed by Spencer et al. (1989 or Appendix A), that I_{K-fast} determines the duration of the action potential in swimming motor neurons of *Polyorchis penicillatus*. These results are not coincidental, because other than I_{K-fast}, no other current described in these cells exhibited a voltage dependence of inactivation in the appropriate voltage range (Chapters 3 to 5 and Table 6.1). The distinct time courses of onset of I_{K-fast} and I_{K-slow} probably allows them to share the job of action-potential repolarization. While I_{K-fast} serves to regulate spike durations around 20 ms, I_{K-slow} sets the upper limit for the plateau duration. I_{K-slow} probably contributes to the slower, subthreshold activity of SMNs, regulating the rate of spontaneous depolarizations, and generally stabilizing the membrane potential.

Other currents and other cell types

Preliminary evidence suggests that a third potassium current may be expressed in another cell type of *Polyorchis*. Certain other neurons found in these cultures produced only short-duration action potentials ("short spike neurons"; Przysiezniak and Spencer, 1989b [Chapter 2]) and exhibited voltage-clamped outward currents with a notch or inflexion point around 10–20 ms after onset (J.Przysiezniak, unpublished). The current preceding the notch arose like the I_{K-fast} seen in SMNs. However, the current following the notch arose more slowly than I_{K-fast} but more rapidly than I_{K-slow} ($\tau \approx 16$ ms at +50 mV). The onset of this "intermediate" current resembled that of the barium-insensitive potassium current in SMNs. This similarity may have been coincidental, or it may indicate that SMNs also express the intermediate current. Unpublished observations from short-spike neurons suggest that this current is depressed in the absence of external calcium (T.A. Basarsky, unpublished).

Permeation

The dependence of peak I_{K-fast} on the concentration of internal potassium was almost linear. This contrasts with recordings from single potassium channels, which often show unitary currents or conductances that saturate at unphysiologically high potassium concentrations (Coronado et al., 1980). This is generally interpreted to show that ions interact as they permeate through the channel i.e. permeation involves non-independent ion fluxes. The linearity of the current-concentration curve may be interpreted in different ways. First, assuming the data from swimming motor neurons are representative, the linear relationship may indicate that the permeation of potassium ions through K-fast channels followed the principle of independence, as predicted by the Goldman-Hodgkin-Katz constant field equation (Hille, 1992, p.341). Second, the data may be incomplete and I_{K-fast} may saturate at values of $[K^+]_{in}$ that were not studied. Third, the data may not only represent the effect of intracellular potassium concentration, but also that of the substituting ion, choline, which is a quaternary ammonium ion and may act like its analog, tetraethylammonium, partially blocking the K-fast channels from inside. Thus, saturation of the current at high $[K^+]_{in}$ may be masked by inhibition of the current at lower $[K^+]_{in}$ i.e. higher choline concentrations.

The reversal potential measured with tail currents when $[K^+]_{in}$ was 100 mM was significantly more positive than the expected Nernst potential for potassium ions (E_K). At least two mechanisms could explain this discrepancy. First, a junctional potential between the cytoplasmic and electrode solutions could be generated by any large, negatively charged, proteins lingering in the cytoplasm. These would drive an electrochemical gradient centered at the electrode tip, such that the voltage in the bulk of the cytoplasm was more negative than that at the electrode tip. Marty and Neher (1983) observed such a junctional potential of ~-10 mV or less, in chromaffin cells. As the slowly-diffusing proteins became diluted in the electrode solution, this junctional potential would subside. In small neurons ($C_m \approx 5$ pF, in Marty and Neher, 1983), such a dilution may take 15 min, but in the large SMNs (Cm $\approx$ 35pF), the reduction in the junctional potential may be much slower. Second, the discrepancy between reversal potential and the Nernst potential for potassium may have resulted from contamination of the tail currents by a current with a reversal potential more positive than E_K. This current would be voltage-dependent, otherwise, the leakage subtraction protocol would have removed it. This current could be carried by chloride ions, which occurred in large and nearly

equal concentrations on either side of the cell membrane. Anderson and McKay (1985) describe a proton-activated but voltage-insensitive chloride current in motor neurons of the jellyfish *Cyanea capillata*. The pH buffering conditions in the experiments described here would have prevented the detection of a similar current. Calcium-activated chloride currents (Barish, 1983) were probably undetectable in these experiments because of strong intracellular buffering by EGTA and the absence of added, external calcium.

Some evidence from calcium current recordings (Przysiezniak and Spencer, 1992 [Chapter 3]) suggests that the slow potassium channels can pass caesium ions. In these recordings, intracellular potassium was replaced with caesium, and a slowly arising, outward current contaminated the late phase of I_{Ca}, masking the late component of I_{Ca} and causing the premature reversal of I_{Ca} at very positive voltages (Spencer et al., 1989; Materials and Methods in Przysiezniak and Spencer, 1992). The contaminating outward current was removed when caesium was replaced with the more impermeant ion, N-methyl-D-glucamine. Thus, Cs^+ ions may permeate the potassium channels mediating I_{K-slow}.

Pharmacology

Both barium and lanthanum shifted the voltage dependence of I_{K-fast} to more positive voltages, and slowed the onset of I_{K-fast}. The shift in voltage dependence could be caused by a screening of external, negative, membrane surface charges by the multivalent cations. Consequently, the apparently slowed onset of the blocked potassium current at a given voltage should correspond to the slower onset of a control current elicited at more negative voltages. However, the blocked responses arose more slowly than any of the control responses, so the slowing of potassium current onset by multivalent cations could not be accounted for entirely by a surface-charge screening mechanism.

The slowing of I_{K-fast} onset may have been accentuated by two other mechanisms. On the one hand, the multivalent cations may bind to the external pore of the closed K–fast channels, but be dislodged by sudden membrane depolarization and the efflux of potassium ions through the opened channel, just as internal TEA molecules are "pushed out" by inward potassium currents (Armstrong, 1971). The gradual unbinding of the blocking ion from the channel may produce a visibly slowed onset of I_{K-fast}, and its rate would depend on the dissociation constant of the blockade and on the blocking ion concentration. On the other hand, lanthanum or

barium binding may modify the conformational changes of the K–fast channel, slowing its opening transition (Spires and Begenisich, 1992). Consequently, a greater depolarization would be needed to force the channel open, resulting in a positively-shifted voltage dependence. These two mechanisms are not mutually exclusive.

Comparisons with other coelenterates

Work on other coelenterates (Cnidaria and Ctenophora) reveals the presence of a variety of types of potassium currents that can be classified according to their fast or slow kinetics. Here, the terms I_{K-fast} and I_{K-slow} only refer to the currents observed in *Polyorchis*.

Some work on cell-attached patches of the giant motor axons of the hydromedusa, *Aglantha digitale* suggests the existence of at least four, kinetically distinct potassium channel populations with time courses ranging from that of a transient, A-like current to that of a sustained, delayed rectifier (Meech et al., 1989; Mackie and Meech, 1989). All four currents exhibited the same unitary conductance, although each kinetic type persisted for up to 2 h. The authors suggested these were distinct channel types expressed from one gene family. The potassium currents in whole-cell recordings activated at voltages below –40 mV (Meech, 1989); in this respect they differ from the currents in *Polyorchis*. Details of the kinetics of these currents remain unpublished.

Anderson (1989) described three outward currents in neurons of the scyphomedusa *Cyanea capillata*. Because the currents were not well separated, it was difficult to determine the voltage at which the inactivating currents first activated. The sustained component, which masked the others, first activated around –20 to –15 mV. A rapidly and a slowly decaying current both activated more rapidly than did I_{K-fast} and were not inactivated by holding potentials more negative than 0 mV.

Non-neuronal cells of other cnidarians also express voltage-activated potassium currents. Holman and Anderson (1991) observed four components of outward current in myoepithelial cells from the anemone *Calliactis parasitica*. An A-like current arose and decayed within ~3 ms, first activated around 0 mV and was half-inactivated by prepulses to about –20 mV. A slower component rose to peak in 3.2 ms and decayed "slowly" ($\tau \approx 20$ ms), with first activation at –20 mV and half-inactivation with prepulses to potentials of ~–10 mV. Both these currents showed faster kinetics than the potassium currents in *Polyorchis*, although the slower of the two showed an I–V curve similar to that of I_{K-fast}. A third, sustained component represented ~40% of the peak current, although no strong

evidence indicates it represented a separate channel population. A fourth component decayed slowly and was dependent on external calcium.

Hagiwara et al. (1981) found rapidly and slowly arising, outward potassium currents in the egg cell of the hydrozoan, *Renilla koellikeri*, with onset kinetics and voltage dependencies that were similar to those of I_{K-fast} and I_{K-slow}, respectively. However, the transient component in *Renilla* inactivated much more rapidly (τ = 10–20 ms) than did I_{K-fast}, and showed no second, slowly inactivating phase, while the slowly arising component activated at a voltage ~10 mV more positive than did I_{K-slow}. As seen with I_{K-fast}, the conductance of the fast component showed little saturation at a $[K^+]_{in}$ of 200 mM. An inwardly rectifying, potassium current was also found by these workers.

Dunlap et al. (1987) observed an A-like potassium current in photocytes from the colonial hydrozoan *Obelia geniculata*. This current first activated at voltages above –20 mV, reaching a peak in 10–20 ms, and inactivated e-fold in about 100 ms, making it similar to I_{K-fast}.

Anderson and McKay (1987) demonstrated the presence of transient and slowly decaying potassium currents in the cnidocytes of the scyphozoan *Chrysaora quinquecirrha* and of the hydroid *Cladonema* sp. These currents showed more rapid onset and decay kinetics than did the currents of *Polyorchis penicillatus*. The voltage dependencies resembled those of *Polyorchis* currents, except that the slow component in *Chrysaora* activated at more positive voltages than did I_{K-slow} in *Polyorchis*.

Thus, most potassium currents in the Cnidaria showed onset and decay kinetics that were more rapid, and voltage dependencies that covered more positive voltage ranges than those of I_{K-fast} and I_{K-slow} in *Polyorchis*. Even in *Renilla* eggs, where onset kinetics of the fast and slow currents resembled those of I_{K-fast} and I_{K-slow}, respectively, the inactivation kinetics of the fast current were 4 to 10 times faster than for I_{K-fast}. It is likely that the differences in kinetics and voltage dependence between potassium currents of *Polyorchis* motor neurons and those of other cnidarian cells reflect functional differences. For example, *Polyorchis* shows a particular mode of neuromuscular modulation, where motor action-potential duration controls the amount of transmitter released and hence synaptic delay (Spencer et al., 1989 [Appendix A]).

Two groups have studied potassium currents in another phylum of coelenterates, the ctenophores. Bilbaut et al. (1988) described a fast current in longitudinal, smooth muscle of *Beroe ovata*, and both the same fast and a slow current in radial muscle. The slow current predominated in the

radial muscle, reaching a peak in more than 30 ms. The fast current reached a peak in 5–10 ms, decayed with a time constant of around 20 ms and was half-inactivated by prepulses to –55 mV. It first activated below –15 mV. The time to peak of the fast current in *Beroe* was similar to that of I_{K-fast}, as was the voltage of half-inactivation. However, just as for most of the cnidarian potassium currents, the rate of inactivation in *Beroe* was faster than in *Polyorchis*. Dubas et al. (1988) found two cation-sensitive and two cation-insensitive outward currents in the smooth muscle of the ctenophore *Mnemiopsis leydii*. The latter two currents were more similar to *Polyorchis* currents than were the currents of cnidarians. The fast current in *Mnemiopsis* rose to a peak in 10–30 ms, decayed with a time constant around 50 ms, first activated at about –35 mV and was half-inactivated at voltages more negative than –40 mV. All four of these features corresponded roughly to measurements made of I_{K-fast}. The slow current in *Mnemiopsis* was first activated by pulses around –5 mV and arose more slowly than did I_{K-slow}, reaching a peak beyond 500 ms.

It seems that potassium currents in the smooth muscles of ctenophores generally gated more slowly than those in neurons, myoepithelial cells and cnidocytes of most cnidarians studied, thus resembling I_{K-fast} and I_{K-slow} described in *Polyorchis*. Because smooth muscle is associated with the slow feeding behavior of these ctenophores (Bilbaut et al., 1988), whereas neurons and cnidocytes typically experience rapid electrical or mechanical activity, the differences in current kinetics may reflect the functional differences of the currents in different cells rather than their phylogenetic differences. Thus, neurons producing rapid action potentials should exhibit more rapidly arising potassium currents than neurons producing longer-duration spikes. This seems to be the case when *Cyanea* neurons, which produce short spikes, are compared to the swimming motor neurons of *Polyorchis*, which exhibit plateau action potentials.

With the present data on potassium currents scattered among different cell types in different species of coelenterates, it is difficult to draw conclusions about the tissue-specific expression of potassium channels. Such data are important since the Cnidaria are the most ancient, extant phylum to have evolved a body plan with organization at the tissue level, and probably are the first to have evolved mechanisms for tissue-specific ion channel expression.

Comparisons with other metazoa

Rudy (1988) defines three classes of potassium currents in a review of

some fifty potassium currents found in various organisms ranging from yeast to mammals. The delayed rectifiers arise slowly, decay slowly and are inactivated by relatively positive prepulses. These were first described by Hodgkin and Huxley (1952) in squid giant axon. The A currents arise and decay rapidly and are inactivated by depolarizing prepulses. They were first described by Connor and Stevens (1971a) in neurons of the nudibranch *Anisodoris*. The transient currents that differ from A currents, which will be referred to as atypical currents, also arise rapidly, but usually decay more slowly than A currents. The voltage dependencies of activation and inactivation of these atypical currents occur at more positive voltages than for A currents.

I_{K-fast} could not be neatly classified into the traditional A current or delayed rectifier categories, although it shared features from both. The voltage of first activation of I_{K-fast} was around -30 mV, and lay within the range of values given for delayed rectifiers or atypical currents, and was more positive than that for most A currents. The rapid decay of I_{K-fast} resembled that of A currents more than that of the other classes of current. The slowly decaying phase of I_{K-fast} matched the inactivation of delayed rectifiers and atypical currents and was slower than that of all A currents listed by Rudy (1988). The voltage of half-inactivation lay between the ranges of values given for A currents and atypical currents. Thus, I_{K-fast} could best be classified as an atypical, inactivating potassium current, with more similarity to the delayed rectifiers than to the A currents.

I_{K-slow} differed from known potassium currents more than did I_{K-fast}. While its voltage of first onset (~0 mV) was similar to those listed by Rudy for delayed rectifiers and atypical currents, it was more positive than that of most A currents. Its time course of onset was slower than that of nearly all currents reviewed by Rudy.

Recent molecular evidence (T. Jegla, N. G. Grigoriev, unpublished) shows that one potassium channel expressed from *Polyorchis* has considerable homology with the Shaker family of channels (cf. Wei et al., 1990), suggesting that potassium channels, and probably other voltage-gated channels in cnidaria, evolved from ancestors common to all multicellular animals.

Conclusion

It appears from the last sections of this discussion that the range of potassium current phenotypes in the Cnidaria may be as broad as that in other metazoans. Thus, the radiation of potassium channels is likely to have taken place before or with the occurrence of tissue organization in

multicellular animals. It is possible that several key sequences in the amino acids of potassium channels, which determined the particulars of voltage dependency and kinetics, evolved early and were later assembled, in a relatively conserved form, into various combinations to produce potassium channels with assorted properties. Molecular studies may show that the Cnidaria were the laboratory for such mix-and-match evolutionary experiments.

Table 5.1
Compositions of recording solutions (in mM)

| | BATH | | | | | ELECTRODE | | | | |
| | K⁺ current | | Tot. current | | | K⁺ current | | | | Tot. current | |
	[BSD	BSD2]	[SAL	BS]		[ESE	ESE2	ESE3	ESD]	[ESA	ES]
NaCl	--	--	378	394		--	--	--	--	50	50
KCl	6.8	6.8	13.4	15		5	65	165	365	365	365
Na$_2$SO$_4$	--	--	5.7	5.7		--	--	--	--	--	--
MgSO$_4$	5.7	--	--	--		--	--	--	--	--	--
MgCl$_2$	23.3	29	29	30		2	2	2	2	2	2
CaCl$_2$	--	--	9.5	10		1	1	1	1	1	1
CoCl$_2$	9.5	9.5	--	--		--	--	--	--	--	--
EGTA	--	--	--	--		11	11	11	11	11	11
Choline-Cl	437	434	42	--		470	410	310	110	60	--
NMG.HCl[b]	--	--	--	30		--	--	--	--	--	60
HEPES	10	10	10	10		10	10	10	10	10	10
KOH	6.6	6.6	--	--		35	35	35	35	35	35
NaOH	--	--	5	5		--	--	--	--	--	--
[K⁺]	13.4	13.4	13.4	15		40	100	200	400	400	400
[Cl⁻]	509	518	510	519		481	481	481	481	481	481

[a] Solution names between brackets are used for the same type of recording, indicated above the names.

[b] N-methyl-D-glucamine and HCl in a 1:1 molar ratio. Concentrations given are same for each.

Table 5.2
Parameters used to fit Boltzmann functions to I–V and tail current data for the potassium currents.

	V_a (mV)	K_a (mV)	E_{rev} (mV)	G_{max} (nS)	I_{max} (pA)	$[K^+]_{in}$ (mM)	N
Peak I_{K-fast} [a]	-10.11	6.78	-40	10.3		100	7
I_{K-slow} (V_h-30) [a]	+23.66	18.69	-76	24.4		400	1
Tail, 40 ms [b]	-0.72	12.85			-461.2	100	4
Tail, 400 ms [b]	-0.88	12.18			-571.2	100	3
Tail, 40 ms [c]	-11.73	6.10			-288.0	100	4
	+14.58	15.94			-200.0		
Tail, 400 ms [c]	-7.67	8.20	.		-227.8	100	3
	+33.68	16.74			-407.2		

[a] These data were fitted with the following combination of a Boltzmann equation and Ohm's law: $I = (G_{max} \times [V_c - E_{rev}])/(1 + \exp[(V_a-V_c)/K_a])$, where G_{max} is the maximal conductance, V_c is the command voltage at which the conductance was half-activated, V_c is the command voltage, and K_a is the slope factor, in mV per e-fold change in conductance. The parameter E_{rev} was fixed for fitting.
[b] The equation fitted to these data was as in a, but the numerator was replaced with I_{max}.
[c] The sum of two equations as in b was fitted to the tail current. The parameters for one fit occupy two lines. The quality of the double fits to the tail currents following 40 ms pulses was $R_{fit} = 0.99934$ compared to 0.99327 for the single fits.
All data: The fitting procedure was iterated until G_{max} or I_{max} varied within 0.1 unit, and until V_a and K_a varied within 0.01 mV. All data but that for I_{K-slow} were averaged before fitting, thus no statistical errors are given with the parameters.

Table 5.3
Parameters used to fit Boltzmann functions to steady-state inactivation data for the potassium current.

	V_i (mV)	K_i (mV)	$[K^+]_{in}$ (mM)	N
Peak, 800 ms test[a]	-52.4	7.1	400	1
End, 800 ms test[a]	-52.8	6.9	400	1
Average I_{K-fast} (± SEM)[b]	-53.5 ± 0.8	8.7 ± 0.8		8
Tail, 20 ms test[c]	-53.2	7.4	100	4

All data were fitted with the following Boltzmann equation: $I = (I_{max} - I_{min}) /(1 + exp[(V_{pp}-V_i)/K_i]) + I_{min}$, where I_{max} was the largest current on the test pulse after non-inactivating prepulses, I_{min} was the smallest test-pulse current after fully-inactivating prepulses, V_{pp} was the prepulse voltage, V_i was the prepulse voltage at which half of the inactivating current remained and K_i was the slope factor in mV per e-fold change in availability. I_{min} and I_{max} were not included in the table since they depended on $[K^+]_{in}$ and were not useful to the comparisons made. The fitting procedure was iterated until I_{max} varied within 0.1 pA, and the other parameters varied within 0.01 unit.

[a] Data from Fig. 7.
[b] Individual data sets were fitted, and the fitting parameters were averaged. None of the parameters in other rows differed significantly from the averaged parameters.
[c] These data were averaged before fitting, hence the absence of error values.
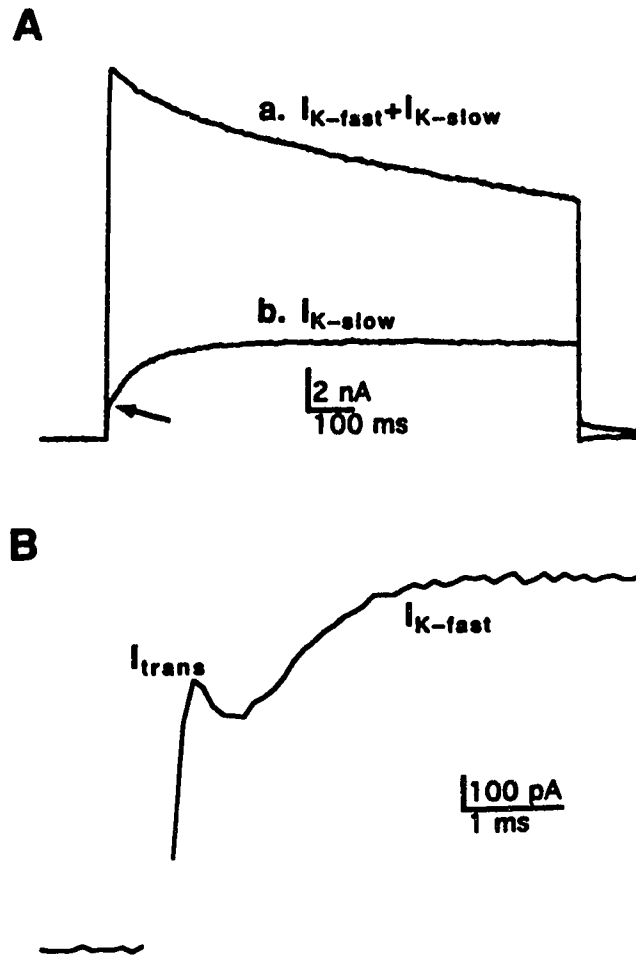
Figure 5.1 - Voltage-sensitive outward currents in the swimming motor neurons (SMNs) of *Polyorchis*. *A*. Total, outward current (I_{K-fast} + I_{K-slow}, trace a) and I_{K-slow} (trace b) in one cell. Total, outward current was elicited with 1 s pulses to +50 mV, from a holding potential (V_h) of –80 mV. I_{K-slow} was elicited at the same command voltage applied from a V_h of –30 mV. The internal potassium concentration ($[K^+]_{in}$) was 400 mM. Because of the slow sweep speed, the transient, outward current, I_{trans}, was not visible. The *arrow* at the beginning of the I_{K-slow} response indicates the end of the onset of residual I_{K-fast}, which was not completely inactivated by the depolarized holding potential. These data were representative but were not included in the quantitative analysis because R_{leak} was 0.3 GΩ and R_{ser} (2.2 MΩ) was not compensated for. *B*. Faster sweep showing I_{trans} and the onset of I_{K-fast}, elicited by a command step to +50 mV from a V_h of –80 mV. $[K^+]_{in}$ = 100 mM. The trace is an average of recordings from 4 cells. The capacitive transient was blanked out for 300 μs after the voltage step.

Figure 5.2 - I_{trans} resembled the sodium current from SMNs. **A.** Traces of I_{trans} and I_{Na} are scaled to match peak and steady-state currents. I_{trans} was elicited by test pulses to +50 mV following a 1 s prepulse to –30 mV, which removed most of I_{K-fast}. Four traces were averaged, each from a different cell. I_{Na} was elicited by test pulses to +30 mV from a V_h of –80 mV. The average of 9 traces was scaled and inverted to match I_{trans}. Note that the baseline preceding I_{trans} was shifted offscale in the negative direction, so that the steady-state of I_{trans} matched that of I_{Na}. The top and bottom amplitudes on the scale bar are for I_{trans} and I_{Na}, respectively. **B.** Graph to show the similarity of the voltage dependencies of availability of I_{trans} and the sodium current (I_{Na}) after inactivating prepulses. Peak I_{Na} was measured on test pulses to +10 mV after 2 s prepulses to the voltages indicated on the *abscissa*. Peak I_{trans} data were measured on test pulses to +50 mV after 1 s prepulses. Measurements were normalized to the largest current amplitude. The number of cells included in the plotted averages are indicated in the graph legend. I_{Na} data in traces and inset were collected with internal potassium replaced by caesium and external calcium replaced by cobalt. Internal and external sodium concentrations were 50 mM, 394 mM, respectively.
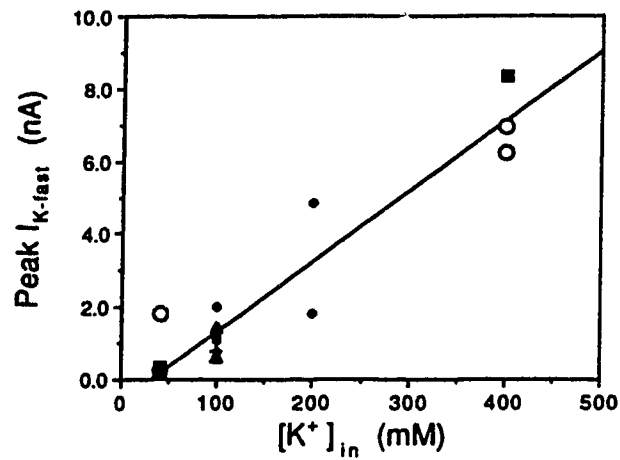
A

50 pA
600 pA
1 ms

I_{trans}

I_{Na}
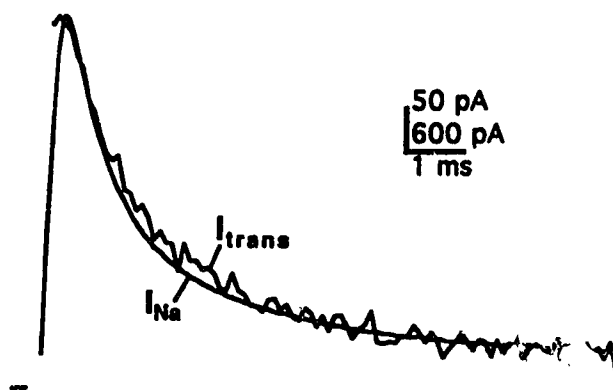
B
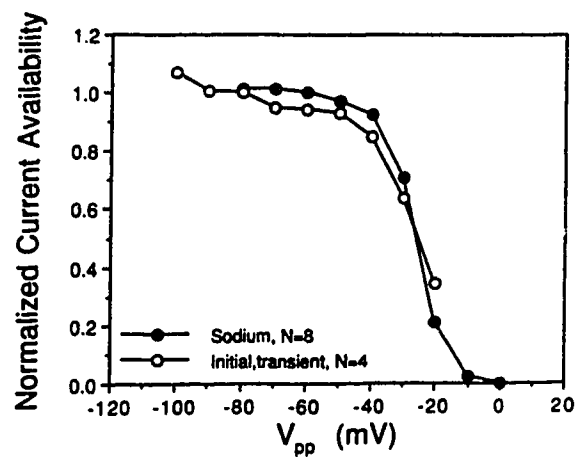
Figure 5.3 - The dependence of peak I_{K-fast} on the internal potassium concentration, $[K^+]_{in}$. The linear regression described in the Results is superimposed. The peak, total, outward current was assumed to represent I_{K-fast} because it arose ~10 times faster than did I_{K-slow}. Measurements were taken from 4, 11, 2 and 3 cells at each value of $[K^+]_{in}$, in ascending order. Data from separate animals are distinguished by their symbols. Each data point represents a measurement from one cell using only one value of $[K^+]_{in}$.
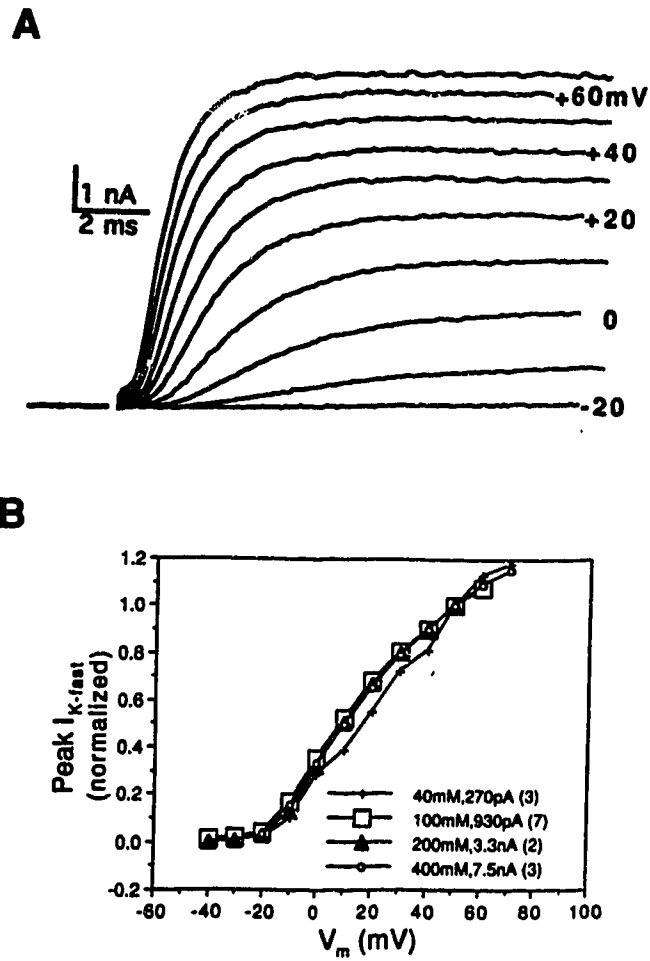
Figure 5.4 - *A.* The onset of I_{K-fast} accelerated with depolarization. Fast sweeps of I_{K-fast}, recorded from one cell, showing the voltage dependence of the onset phase. V_h = –80 mV, V_c = –20 mV to +70 mV (given beside some of the traces) in 10 mV increments. $[K^+]_{in}$ = 400 mM. The current peak was not as obvious as in Fig. 5.1 because of the fast sweep speed (sampling period was 100 μs). *B.* The voltage dependence of peak I_{K-fast} at different concentrations of internal potassium. The data at each concentration were normalized to the current amplitudes at +50 mV, which are given in the graph legend along with $[K^+]_{in}$ and the number of cells used for averaging. The equation and parameters fitted to the data at 100 mM are given in Table 5.2.
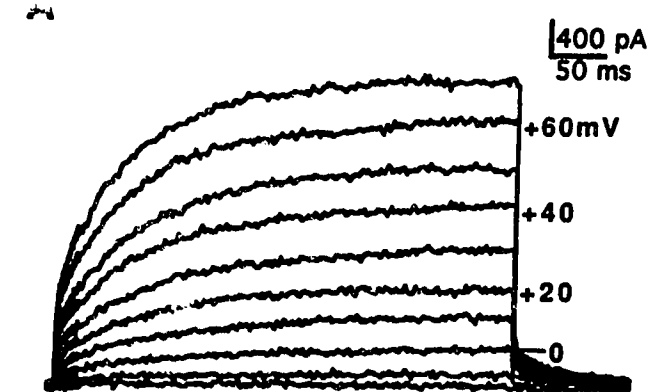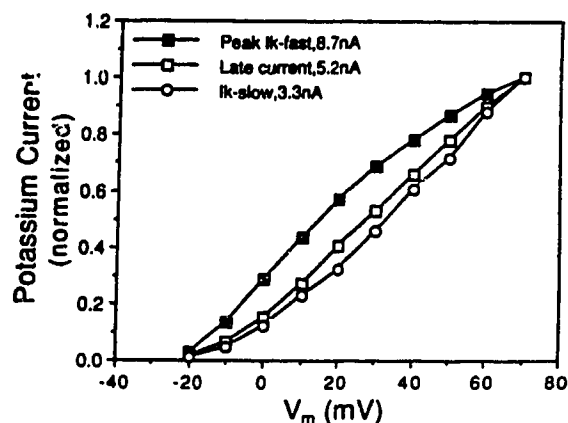
B

Figure 5.5 - *A.* I_{K-slow} responses to graded depolarizations, showing gradual acceleration of the onset. $V_h = -30$ mV, $V_c = -20$ mV to +70 mV (given beside some of the traces) in 10 mV increments. $[K^+]_{in} = 400$ mM. The sampling period was 100 μs for the first 25 ms of the episode and 1.9 ms for the rest of the trace. For this recording, R_{leak} was 0.3 GΩ and R_{ser} (5 MΩ) caused a V_{Rser} ranging from 0.5 to 14.2 mV. See text. Different cell from that in Figure 5.1A. *B.* The voltage dependencies of I_{K-slow} and the late current compared to that of I_{K-fast}. For comparison, all data were normalized to the current amplitudes at +70 mV, which are given in the graph legend. Averaged data for I_{K-fast} (*solid squares*; same as in Fig. 5.4B, 400 mM) and the late current (*open squares*) were taken from the same three cells, at peak and at 980 ms after the voltage step, respectively. I_{K-slow} (*open circles*) was measured 380 ms after the voltage step on the responses in Figure 5.5A. $[K^+]_{in} = 400$ mM in all cases. Parameters of functions fitted to I_{K-slow}-V are given in Table 5.2.
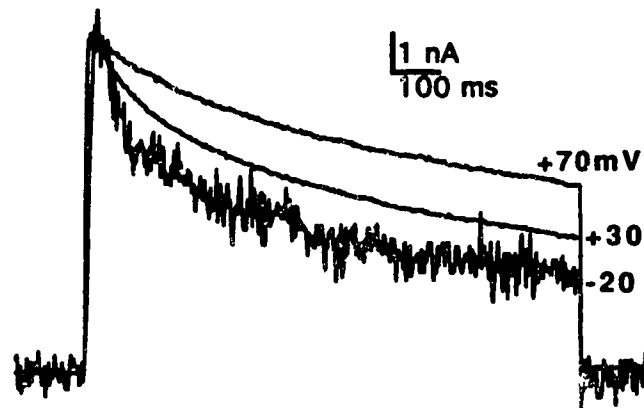
Figure 5.6 - The decay of the total, outward current was slowed with depolarization. One second, total outward currents at different command voltages (given beside traces) applied from a V_h of −80 mV. The traces were averaged from 2 cells, then scaled to match the peak currents. Data were extracted from an I–V series. $[K^+]_{in} = 400$ mM.
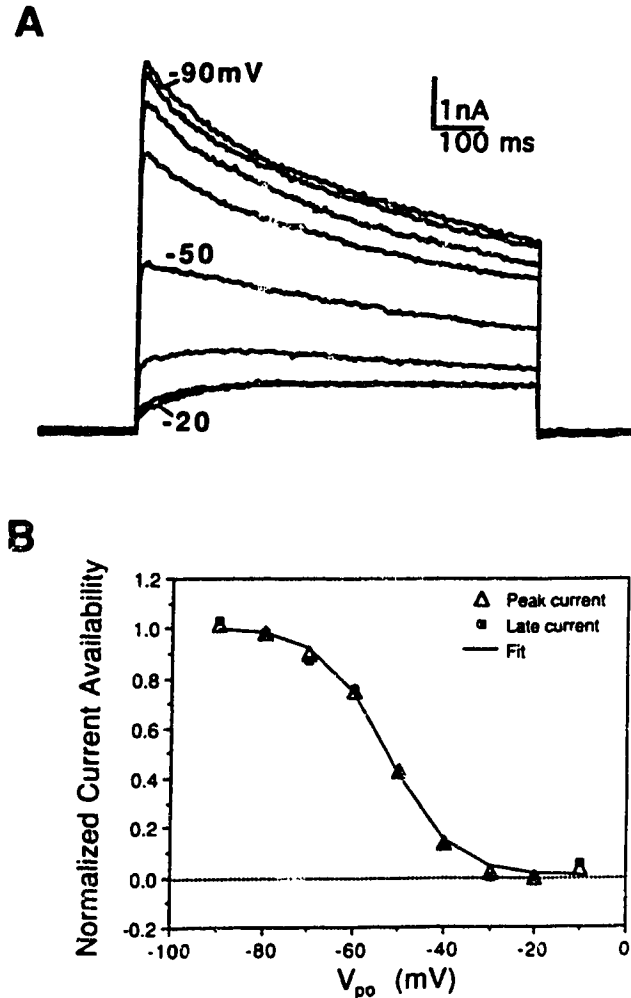
A

B

Figure 5.7 - The availabil₁ty ᴐ₁ ᴺtal, outward current following inactivating prepulses. **A.** Decrementing test respor.ᴐᴐs (V_c = +50 mV) recorded from one cell after 1 s prepulses to voltages incremented from –90 mV to –20 mV (shown beside some of the traces) in 10 mV steᵣ𝗌. The gradual unmasking of I_{K-slow} is apparent, as is the gradual disappearance of the inactivating current, I_{K-fast}. **B.** The voltage dependencies of the availability of peak (*triangles*) and late (*squares*) current in the same cell are identical. Data were normalized to the maximal current after the non-inactivating component was subtracted. Peak and late current measurements were taken from the traces in *A*, 12 ms and 780 ms after the voltage transition, respectively. Some increase of the test response was apparent when the prepulse began to activate outward current. This trace was omitted in *A*. The *solid curve* is a Boltzmann function fitted to the peak current with the parameters fitted in Table 5.3. The *broken line* represents zero availability.

8.0 ┬ ┌ 30

-32.2
b   20 mV
30 ms

Available I$_{K-fast}$ (nA)   6.0

-50.8   20

Slow Repolarization Rate (V/s)

4.0

a

2.0   b   10

Avail. Current
Repol.Rate

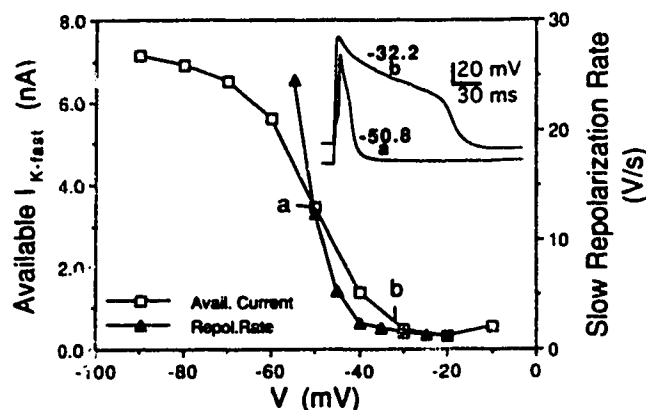0.0 ┴   0

-100   -80   -60   -40   -20   0

V (mV)

Figure 5.8 - The availability of I$_{K-fast}$ and the slow repolarization rate of SMN action potentials depend on the baseline membrane potential in similar voltage ranges. *Triangles:* Dependence of the spike plateau repolarization rate (S$_{repol}$; *right ordinate*) on the voltage preceding the action potential (*abscissa*). In 65 SMNs exposed to total-current conditions, 248 plateau action potentials were elicited with short (0.5–4 ms), depolarizing current injections (up to 1 nA), from different baseline potentials, maintained by DC current injection under manual control. The range of baseline voltages from which spikes could be elicited was limited to above –60 mV because below that value, the largest current pulses that could be applied by the digital-to-analog converter were sub-threshold. Slow repolarization rates were measured on the plateau phase of the action potentials, before the repolarization became rapid. The membrane voltages, were measured 5–10 ms before the action potential. These pre-spike voltages were grouped in bins of 5 mV, and the corresponding S$_{repol}$ values were averaged. Averages of 5, 11, 27, 75, 57, 44, 21 and 9 points are plotted from left to right. *Squares:* Availability of peak I$_{K-fast}$ (*left ordinate*) as a function of prepulse voltage (*abscissa*). The current amplitude was measured 7 ms after a voltage step to +50 mV, following 1 s prepulses to different voltages. Data were averaged from 2 cells. [K$^+$]$_{in}$ = 400 mM. *Inset* shows two stimulated spikes from one cell. The pre-spike voltages are given beside the corresponding traces, in mV. Stimulus was 900 pA for 2 ms.
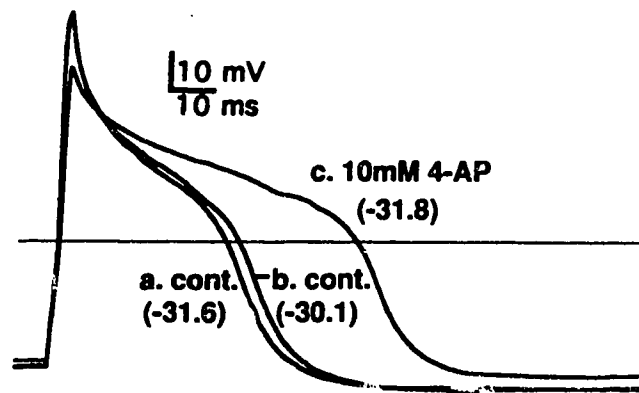
Figure 5.9 - Effect of 4–aminopyridine on SMN action potentials. Spikes were elicited with short, large depolarizing currents from baseline potentials that were maintained manually (given in figure). The drug was applied at 100 mM to a final bath concentration of 10 mM. The two control traces, taken 2 min (a) and 1 min (b) before 4–AP application, showed that slight changes in the baseline potential (given in mV beside the traces) did not alter the spike duration markedly. The experimental trace (c) was taken 4 min after drug application. The *straight line* represents 0 mV. Solutions used were SAL1 and ESA (see Table 5.1).
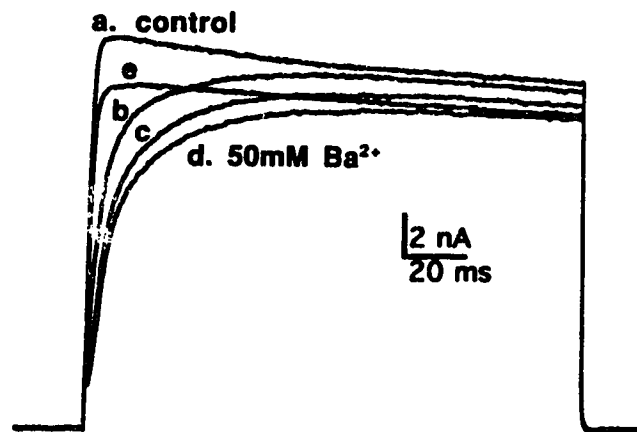
Figure 5.10 - Barium chloride slowed the onset of I_{K-fast}. The total, outward current was monitored every 30 s with pulses to +70 mV from a V_h of -80 mV, while 50 mM barium chloride was superfused into the bath. The traces, lettered in chronological order, were taken at the very beginning of superfusion and then 0.5, 1.5 and 3 min afterwards, respectively. Trace (e) was taken 10 min after trace (a), and 1 min after barium was washed out with ~5 bath volumes. Its lower amplitude relative to (a) probably reflected a change in R_{ser}. $[K^+]_{in}$ = 400 mM. Solutions were BSD2 and ESD.
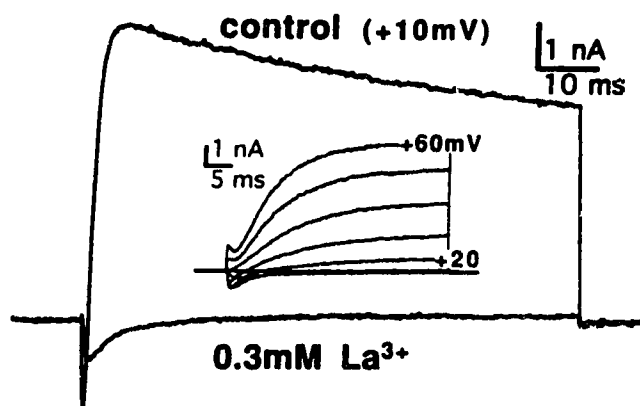
Figure 5.11 - Effect of lanthanum on the total current. *Main figure:* Test pulses to +10 mV from a V_h of −80 were applied every 30 s while 10 mM lanthanum nitrate was applied to a final bath concentration of 0.3 mM. The control trace was taken immediately before the application, while the experimental trace was taken 9 min after application. *Inset:* Total-current I–V series at −40 mV to +60 mV, in the presence of 0.3 mM lanthanum, showing the slowed outward current, which could only be elicited by pulses more positive than +20 mV. Solutions used in both figures were BS, ES.

REFERENCES

Anderson PAV, Mackie GO (1977) Electrically coupled, photosensitive neurons control swimming in a jellyfish. Science 197: 186-188.

Anderson PAV, McKay MC (1985) Evidence for a proton-activated chloride current in coelenterate neurons. Biol Bull 169: 652-660.

Anderson PAV, McKay MC (1987) The electrophysiology of cnidocytes. J Exp Biol 133: 215-230.

Anderson PAV (1989) Ionic currents of the Scyphozoa. In: Evolution of the first nervous systems (Anderson PAV, ed), pp 267-280. New York: Plenum.

Armstrong CM (1971) Interaction of tetraethylammonium ion derivatives with the potassium channels of giant axons. J Gen Physiol 58: 413-437.

Artalejo CR, Dahmer MK, Perlman RL, Fox AP (1991) Two types of Ca^{2+} currents are found in bovine chromaffin cells: facilitation is due to the recruitment of one type. J Physiol (Lond) 432: 681-707.

Barish ME (1983) A transient calcium-dependent chloride current in the immature *Xenopus* oocyte. J Physiol (Lond) 342: 309-325.

Bilbaut A, Hernandez-Nicaise M-L, Leech CA, Meech RW (1988) Membrane currents that govern smooth muscle contraction in a ctenophore. Nature 331: 533-535.

Connor JA, Stevens CF (1971a) Voltage-clamp studies of a transient outward current in gastropod neural somata. J Physiol (Lond) 213: 21-30.

Connor JA, Stevens CF (1971b) Prediction of repetitive firing behavior from voltage-clamp data on an isolated neuron soma. J Physiol (Lond) 213: 31-53.

o J, Simon B, Segal Y, Wehner F, Ramanujam VMS, Alcock N, Reuss (1991) Ba^{2+} release from soda glass modifies single maxi K^+ channel activity in patch clamp experiments. Biophys J 60: 931-941.

Coronado R, Rosenberg R, Miller C (1980) Ionic selectivity, saturation and block in a K^+-selective channel from sarcoplasmic reticulum. J Gen Physiol 76: 425-446.

Cota G, Armstrong CM (1988) Potassium channel "inactivation" induced by soft-glass patch pipettes. Biophys J 53: 107-109.

Dunlap K, Takeda K, Brehm P (1987) Activation of a calcium-dependent photoprotein by chemical signalling through gap junctions. Nature 325: 60-62.

Dubas F, Stein PG, Anderson PAV (1988) Ionic currents of smooth muscle cells isolated from the ctenophore Mnemiopsis. Proc R Soc Lond B 233: 99-121.

Duval A, Malécot CO, Pelhate M, Piek T (1992) Poneratoxin, a new toxin from an ant venom, reveals an interconversion between two gating modes of the Na channels in frog skeletal muscle fibers. Pflügers Arch 420: 239-247.

Furukawa Y, Kandel ER, Pfaffinger P (1992) Three types of early transient potassium currents in Aplysia neurons. J Neurosci 12: 989-1000.

Hagiwara S, Yoshida S, Yoshii M (1981) Transient and delayed potassium curents in the egg cell membrane of the coelenterate, Renilla koelikeri. J Physiol (Lond) 318: 123-141.

Hille B (1992) Ionic channels of excitable membranes. Sunderland, MA: Sinauer.

Hodgkin AL, Huxley AF (1952) A quantitative description of membrane current and its application to conduction and excitation in nerve. J Physiol (Lond) 116: 449-472.

Holman MA, Anderson PAV (1991) Voltage-activated ionic currents in myoepithelial cells isolated from the sea anemone Calliactis tricolor. J Exp Biol 161: 333-346.

Mackie GO, Meech RW (1989) Potassium channel family in axons of the jellyfish *Aglantha digitale*. J Physiol (Lond) 418: 14P.

Marty A, Neher E (1983) Tight-seal, whole-cell recording. In: Single-channel recording (Sakmann B and Neher E, eds), Chapter 7. New York: Plenum.

Meech RW (1989) The electrophysiology of swimming in the jellyfish *Aglantha digitale*. In: Evolution of the first nervous systems (Anderson PAV, ed), pp 281-298. New York: Plenum.

Meech RW, Arkett SA, Mackie GO, Maitland NJ (1989) Potassium channel family in the jellyfish, *Aglantha*. Soc Neurosci Abstr 15: 77.

Przysiezniak J, Spencer AN (1989a). Membrane ionic currents in identified neurons of a jellyfish. Soc Neurosci Abstr 15: 1145.

Przysiezniak J, Spencer AN (1989b) Primary culture of identified neurons from a cnidarian. J Exp Biol 142: 97-113.

Przysiezniak J, Spencer AN (1992). Voltage-activated calcium currents in identified neurons from a hydrozoan jellyfish, *Polyorchis penicillatus*. J Neurosci 12: 2065-2078.

Rudy B (1988) Diversity and ubiquity of K channels. Neuroscience 25: 729-749.

Spencer AN (1981) The parameters and properties of a group of electrically coupled neurons in the central nervous system of a hydrozoan jellyfish. J Exp Biol 93: 33-50.

Spencer AN (1982) The physiology of a coelenterate neuromuscular synapse. J Comp Physiol A 148: 353-363.

Spencer AN, Przysiezniak J, Acosta-Urquidi J, Basarsky TA (1989) Presynaptic spike broadening reduces junctional potential amplitude. Nature 340: 636-638.

Spires S, Begenisich T (1992) Chemical properties of the divalent cation binding site on potassium channels. J Gen Physiol 100: 181-193.

Stockbridge NL (1987) EGTA Comput Biol Med 17: 299-304.

Wei A, Covarrubias M, Butler A, Baker K, Pak M, Salkoff L (1990) K+ current diversity is produced by an extended gene family conserved in *Drosophila* and mouse. Science 248: 599-603.

Chapter 6

GENERAL DISCUSSION

SUMMARY

The currents

The studies constituting this thesis describe voltage-activated currents in the "swimming motor neurons" (SMNs) of the hydromedusa *Polyorchis penicillatus*, characterizing features such as ionic selectivity, voltage dependencies of activation and inactivation, time courses of onset and decay, and pharmacology. At least five currents were identified that were likely mediated by five separate channel populations. Their features are summarized in Table 6.1.

The calcium currents activated at relatively high voltages, with maxima around +10 mV, and could be separated into a high-voltage-activated, rapidly activating, transient component selective for calcium over barium, HVA-t, and a sustained component that activated at similar voltages to HVA-t but did not distinguish between calcium and barium, HVA-s.

The sodium current, I_{Na}, arose rapidly and decayed with a rapid, bi-exponential phase and a much slower, mono-exponential phase. The I–V curves and voltage dependencies of steady-state inactivation of the rapidly and slowly decaying components were overlapping, and may be identical if recording errors account for the differences. This may indicate that the two components of I_{Na} were mediated by the same channel population. However, it remains possible that the slowly decaying sodium current was mediated by calcium channels, because its voltage dependencies and time course resembled those of the slower component of the transient calcium current (HVA-t). Only the rapidly decaying sodium current will be discussed.

Two potassium currents could be identified. I_{K-fast} arose rapidly with a sigmoid time course that could be slowed by barium or lanthanum, and decayed relatively rapidly with two exponential phases. I_{K-slow} activated at more positive voltages than did I_{K-fast}, arose with a slow, mono-exponential time course and did not inactivate at any voltage.

Other ionic currents may be present in the SMNs but were not

systematically investigated. Closer analysis of responses to the very negative prepulses from steady-state inactivation experiments suggests that there may be a low-voltage-activated calcium current in SMNs (unpublished). Preliminary work (Basarsky, unpublished) on another type of cell isolated from *Polyorchis*, the "short-spike neurons", suggests that they may express a calcium-dependent potassium current, as well as a form of sodium current that runs down more easily than does that of SMNs.

Pharmacology

A limited pharmacological arsenal is now available to tease apart the roles of the voltage-activated currents in the physiological activity of the SMNs. Cadmium will be useful to distinguish the effects ʳ ˈ ward and outward currents. However, because its effectiveness on ˙ ˌ m and calcium currents differs by only about an order of magnit˟ ˌ roles of these currents may be difficult to separate in preparatioⁿ ˌre the ensheathing epithelium prevents the adequate control of the concentration of applied ions at the neuronal membrane. Nifedipine at high concentrations (~100 μM) shows a 23% greater block of the HVA–s calcium current than HVA–t (Table 6.1), but its effects on the sodium and potassium currents remain unknown (but see Nerbonne and Gurney, 1987). The drug 4–aminopyridine appears to be somewhat specific for I_{K-fast} over I_{K-slow}, while tetraethylammonium is not specific for either of the potassium currents. Barium and lanthanum slow the onset of I_{K-fast}, but affect the inward current similarly.

Recording errors

Recordings from SMNs using the tight-seal, whole-cell voltage-clamp technique may have suffered from errors due to inadequate spatial control of membrane voltage. However, most of the inconsistencies that could be interpreted as space-clamp artefacts, such as the very-high-voltage-activated calcium current and the positively shifted reversal potential for sodium current, occurred at very positive voltages, outside the physiologically relevant range. The decay of capacitive current through the series resistance prevented the close study of sodium and calcium current onset and of rapid tail current deactivation, although these were not crucial to these studies. Even with electronic compensation, the voltage error caused by large currents flowing through the series resistance may have been a significant problem in potassium and sodium current recordings. Mathematical correction was used to adjust the I–V data of the sodium current. However,

the I–V curves of large and small potassium currents, elicited with different intracellular potassium concentrations, did not differ visibly and were not corrected mathematically.

Taxonomy and evolution

The voltage-activated currents in SMNs generally resemble currents in other animals (see discussions in chapters 3 to 5), although they show certain peculiarities.

The transient sodium current exhibits a time course, selectivity, sensitivity to cadmium block and insensitivity to TTX block that make it similar to TTX-insensitive sodium currents in other animals (e.g. Visentin et al., 1990), but its voltage ranges of activation and steady-state inactivation are uncommonly positive.

The transient calcium current shares its time course and voltage dependence of activation with the N-type channels of vertebrates, its cadmium sensitivity with the L-type channels and its ionic selectivity with the T-type channels, but cannot be placed in any of those categories (McCleskey et al., 1986). However, the sustained calcium current, because of its time course and its potentially specific but relatively weak blockade by nifedipine, resembles the L-type channel.

The voltage dependence of I_{K-fast} inactivation covers a more negative range than that of other currents in the SMNs, so its role may be similar to that of the A current in other animals (Rudy, 1988). However, the absolute ranges of its voltage dependencies of activation and inactivation are more positive than those of the A current and tend to resemble those of the delayed rectifiers. Thus, it is classified as an atypical potassium current (Rudy, 1988).

Studies of other cnidarians (Hagiwara et al., 1981; Anderson, 1987; Dunlap et al., 1987; Holman and Anderson, 1991; Mackie and Meech, 1989) and of the Ctenophora (Bilbaut et al., 1988; Dubas et al., 1988) demonstrate that voltage-activated channels had alread evolved a variety of forms in these primitive animals. There is clear evidence of voltage-activated potassium (Hennessey, 1989) and calcium (Deitmer, 1984; Hennessey, 1989) currents in the Protozoa, but little sign of voltage-activated sodium currents (Febvre-Chevalier et al., 1986). The appearance of the latter and the radiation of calcium and potassium currents must have occurred sometime around the appearance of multicellular animals, so an examination of the sponges and Placozoa may offer a better glimpse of the diversification of voltage-sensitive ion channels.

FUNCTIONS OF THE VOLTAGE-DEPENDENT CURRENTS

Spike shape

The currents described play important roles in the generation and modulation of action potentials in the swimming motor neuron network. Anderson and Mackie (1977) and Anderson (1979) have shown that the action potential upstroke in these neurons is greatly dependent on the external sodium concentration. By its rapid onset and large amplitude, the transient component of the sodium current is most suitable for this role. Since low concentrations of cadmium, which inhibit I_{Ca} but not I_{Na}, remove the plateau phase of the action potential and some of its peak amplitude, I_{Ca} most likely underlies the plateau and plays some role in the spike upstroke. Furthermore, Spencer et al. (1989 or Appendix A) have demonstrated, using SMN action potentials as voltage-clamp waveforms, that I_{Ca} increases during the later part of the plateau, as the membrane potential repolarizes away from the calcium reversal potential. Because the HVA–t calcium current is larger than HVA–s, it probably has the most influence on the SMN spike shape. The voltage dependence of I_{K-fast} inactivation is more negative than that of any other current described in the SMNs, and overlaps with the dependence of the plateau repolarization rate on pre-spike voltage. Thus, this current likely regulates action potential duration as a function of pre-spike voltage (Spencer et al., 1989). The sustained potassium current, I_{K-slow}, probably contributes to the repolarization of long duration action potentials, during which most of the other currents are inactivated. The sustained calcium current is small and is probably overwhelmed by all the other currents during the action potential (Table 6.1); its role is unknown.

Since all of these currents activate at relatively depolarized voltages, they are unlikely to generate any subthreshold activity. Slow membrane potential oscillations can be recorded from SMNs in intact preparations (Anderson, 1979; Spencer and Satterlie, 1980; Spencer, 1981; Arkett and Spencer, 1986), but not from isolated SMNs. It is still unclear whether this subthreshold activity is endogenously or synaptically generated.

Synaptic physiology

The modulation of action potential duration by the pre-spike baseline level appears to serve in the synchronization of the swimming bell contractions. Spencer (1982) has proposed that the synchrony of contraction of all regions of the swimming bell is achieved because the SMN action

potential that has propagated the farthest from the spike initiation zone elicits a muscle contraction after the shortest synaptic delay, thus compensating for the increased delay in spike propagation. Spencer et al. (1989; appendix A) suggest that the voltage dependence of action potential duration, determined by I_{K-fast}, converts the SMN spike propagation delay to an appropriate level of neurotransmitter release, determined by I_{Ca} and calcium removal mechanisms. In the swimming epithelium, this produces a postsynaptic potential of a sufficient amplitude to elicit a muscle action potential and contraction after a delay that is appropriately shortened to compensate for propagation time.

Other aspects of this "delay-coupling" mechanism require more attention. First, the proportion of inward to outward current, and thus the spiking threshold, varies greatly among isolated SMNs (unpublished observations). If this variability exists in the intact preparation, then it is possible that only some of the neurons could initiate action potentials, so propagation would be saltatory between these spike-initiating cells, and active presynaptic sites would be clustered around these cells. Second, the spatial distribution of active postsynaptic sites and the electrotonic propagation and summation of postsynaptic potentials in the myoepithelial sheet are important in determining the coupling of the epsp to the muscle contraction, because the muscle spike-initiation zones are at some distance from the postsynaptic sites (Spencer, 1982). Third, the influx of calcium during pre- or postsynaptic action potentials may alter the conductance of gap junctions (Loewenstein, 1975) and the electrotonic properties of the SMN network or epithelial sheet. Finally, synaptic inputs to the SMNs may also affect action potential duration and the effectiveness of the delay coupling. For example, dopamine has been found in *Polyorchis* tissue (Chung et al., 1989) and was shown to decrease action potential duration (Chung and Spencer, 1991) by apparently enhancing a voltage-dependent potassium current that resembles I_{K-fast} (Chung, 1991). However, the cells releasing dopamine in *Polyorchis* remain unknown.

It is surprising that such a complex series of effects should translate spike propagation delay into the appropriate delay to muscle contraction. However, it seems that this delay-coupling mechanism can be labile (Spencer, 1982) yet still allow sufficiently synchronous and symmetric swimming contractions for the feeding, survival and reproduction of the species.

Other cells

The swimming motor neurons are only one of several types of neurons in *Polyorchis*, and the assortment of currents described here is tailored for the particular functions of this cell type. It will be important to describe the currents in other cell types with known functions. For example, the "B" neurons (Spencer and Arkett, 1984) produce short duration action potentials with no plateau and are expected to express little calcium current, but a rapidly-activating pota... m current that is available for spike repolarization at normal re...ing potentials, unlike I_{K-fast}. The "O" neurons (Spencer and Arkett, 1984), which do not spike but generate slow oscillations, probably do not exhibit a transient sodium current but may be equipped with a low-voltage-activated calcium current and a calcium-activated potassium current, which would produce the oscillations. The swimming myoepithelial cells produce large, long-lasting action potentials that are likely sustained by a calcium current. If this calcium current is small, then an inwardly-rectifying (potassium or chloride) current may be necessary during the spike plateau, to keep the membrane conductance minimal and the effect of the calcium current on membrane potential maximal. These kinds of analyses will allow a better understanding of how the electrophysiological phenotypes of different cells are determined from the assortment of ionic channels that such a primitive animal may express.

CONCLUSION

This work provides an extensive background of information for understanding the biophysical bases of excitability in the neurons of a primitive nervous system. Improvements to the speed of voltage clamping could make possible the collection of more data on the activation and deactivation kinetics of the sodium and calcium currents which can be incorporated into a mathematical model of SMN excitability. Additional pharmacological work could yield a greater variety of ager'' for the dissection of *in vivo* electrical activity. The work presented here can serve as a reference for future studies of single channel kinetics and for the molecular description of voltage-gated ion channels in this jellyfish.

Table 6.1

Summary of features of the voltage-activated currents in swimming motor neurons of *Polyorchis penicillatus*

	I_{Na}[a]	HVA-t[b]	HVA-s[c]	I_{K-fast}[d]	I_{K-slow}[e]
I_{max} (nA)	-7.2 (+10)	-0.22 (+10)	-0.025 (+10)	+7.5 (+50)	+2.3 (+50)
T_{peak} (ms)	0.84	4.0	----	6.7	~200
τ_{onset} (ms)	----	----	----	0.86, x=4	68.0, x=1
$V_{1/2\ act.}$ (mV)	≥-30	≥-40	~-20	~-30	≥-20
V_a (mV)	-2.5	+0.3	----	-10.1	+23.4
K_a (mV)	6.5	6.3	----	6.8	18.7
τ_{off} (ms)	1.1, 8.0	25.6, 187	sust.	~70, ~1000	sust.
V_i (mV)	-26.1	-23.5	----	-53.5	----
K_i (mV)	4.8	9.2	----	8.8	----
τ_{recov} (ms)	~100 (-80)	~50 (-80)	----	<1000 (-80)	----
Pharm.	Cd 1-10 mM TTX-insens.	Cd < 1 mM	Nifed.	Ba,La ↑T_{peak}, ↑V_a; 4-AP	----
Selectiv.	Na>K, Cs	Ca>Ba,Na?	Ca≈Ba	K>Cs	K>Cs

----: not relevant or not available

x : power of onset exponential

Values in parentheses are voltages at which measurements were taken. The same apply for I_{max}, T_{peak}, τ_{onset} and τ_{off}. All data recorded with a *holding potential* of -80 mV, except for I_{K-slow}, where it was -30 mV.

[a] Rapidly inactivating component only. Data taken from tables and figures in chapter 4. Values for V_a and K_a are from Table 4.2, corrected for series resistance error and rapid inactivation. Values for V_i and K_i are from Table 4.3, ascending series of prepulses.

[b] Data from tables, figures in chapter 3, using calcium as the permeant ion.

[c] I_{max} measured after 1 s.

[d] Data taken from tables, figures and text in chapter 5. For I_{max}, T_{peak}, τ_{onset} and τ_{off}, $[K^+]_{in}$ = 400 mM. For V_a and K_a, $[K^+]_{in}$ = 100 mM. V_i and K_i are averaged for 8 cells at different $[K^+]_{in}$. For τ_{recov}, $[K^+]_{in}$ = 140 mM.

[e] For all data in this column, $[K^+]_{in}$ = 400 mM.

REFERENCES

Anderson PAV (1979) Ionic basis of action potentials and bursting activity in the hydromedusan jellyfish *Polyorchis penicillatus*. J Exp Biol 78: 299-302.

Anderson PAV (1987) Properties and pharmacology of a TTX-insensitive Na^+ current in neurons of the jellyfish, *Cyanea capillata*. J Exp Biol 133: 231-248.

Anderson PAV, Mackie GO (1977) Electrically coupled, photosensitive neurons control swimming in a jellyfish. Science 197: 186-188.

Arkett SA, Spencer AN (1986) Neuronal mechanisms of a hydromedusan shadow reflex. I- Identified reflex components, and sequence of events. J Comp Physiol A 159: 201-213.

Bilbaut A, Hernandez-Nicaise M-L, Leech CA, Meech RW (1988) Membrane currents that govern smooth muscle contraction in a ctenophore. Nature 331: 533-535.

Chung J-M (1991) Dopamine as an inhibitory neurotransmitter candidate in the hydrozoan *Polyorchis penicillatus*. Doctoral thesis. University of Alberta.

Chung J-M, Spencer AN (1991) Dopamine as a neuroactive substance in the jellyfish *Polyorchis penicillatus*. J Exp Biol 156: 433-451.

Chung J-M, Spencer AN, Gahm KH (1989) Dopamine in tissues of the hydrozoan jellyfish *Polyorchis penicillatus* as revealed by HPLC and GC/MS. J Comp Physiol B 159: 173-181.

Deitmer JW (1984) Evidence for two voltage-dependent calcium currents in the membrane of the ciliate *Stylonychia*. J Physiol (Lond) 355: 137-159.

Dubas F, Stein PG, Anderson PAV (1988) Ionic currents of smooth muscle cells isolated from the ctenophore *Mnemiopsis*. Proc R Soc Lond B 233: 99-121.

Dunlap K, Takeda K, Brehm P (1987) Activation of a calcium-dependent photoprotein by chemical signalling through gap junctions. Nature 325: 60-62.

Febvre-Chevalier C, Bilbaut A, Bone Q, Febvre J (1986) Sodium-calcium action potential associated with contraction in the heliozoan *Actinocoryne contractilis*. J Exp Biol 122: 177-192.

Hagiwara S, Yoshida S, Yoshii M (1981) Transient and delayed potassium curents in the egg cell membrane of the coelenterate, *Renilla koelikeri*. J Physiol (Lond) 318: 123-141.

Hennessey TM (1989) Ion currents of *Paramecium*: Effects of mutations and drugs. In: Evolution of the first nervous systems (Anderson PAV, ed), pp 215-235. New York: Plenum.

Holman MA, Anderson PAV (1991) Voltage-activated ionic currents in myoepithelial cells isolated from the sea anemone *Calliactis tricolor*. J Exp Biol 161: 333-346.

Loewenstein WR (1975) Permeable junctions. Cold Spring Harbor Symp Quant Biol 40: 49-63.

Mackie GO, Meech RW (1989) Potassium channel family in axons of the jellyfish *Aglantha digitale*. J Physiol (Lond) 418: 14P.

McCleskey EW, Fox AP, Feldman D, Tsien RW (1986) Different types of calcium channels. J Exp Biol 124: 177-190.

Nerbonne JM, Gurney AM (1987) Blockade of Ca^{2+} and K^+ currents in bag cell neurons of *Aplysia californica* by dihydropyridine $Ca2^+$ antagonists. J Neurosci 7: 882-893.

Rudy B (1988) Diversity and ubiquity of K channels. Neuroscience 25: 729-749.

Spencer AN (1981) The parameters and properties of a group of electrically coupled neurons in the central nervous system of a hydrozoan jellyfish. J Exp Biol 93: 33-50.

Spencer AN (1982) The physiology of a coelenterate neuromuscular synapse. J Comp Physiol A 148: 353-363.

Spencer AN, Satterlie RA (1980) Electrical and dye coupling in an identified group of neurons in a coelenterate. J Neurobiol 11: 13-19.

Spencer AN, Przysiezniak J, Acosta-Urquidi J, Basarsky TA (1989) Presynaptic spike broadening reduces junctional potential amplitude. Nature 340: 636-638.

Visentin S, Zaza A, Ferroni A, Tromba C, DiFrancesco C (1990) Sodium current block caused by group IIb cations in calf Purkinje fibers and in guinea-pig ventricular myocytes. Pflügers Arch 417: 213-222.

Appendix A

PRESYNAPTIC SPIKE BROADENING REDUCES JUNCTIONAL POTENTIAL AMPLITUDE.[4]

ABSTRACT

Presynaptic modulation of action-potential duration may regulate synaptic transmission in both vertebrates (Lin and Faber, 1988) and invertebrates (Kusano et al., 1967; Fuchs et al., 1982; Hochner et al., 1986). Such synaptic plasticity is brought about by modifications to membrane currents at presynaptic release sites, which, in turn, lead to changes in the concentration of cytosolic calcium available for mediating transmitter release. The "primitive" neuromuscular junction of the jellyfish *Polyorchis penicillatus* is a useful model of presynaptic modulation. In this study, we show that the durations of action potentials in the motor neurons of this jellyfish are negatively correlated with the amplitude of excitatory junctional potentials. We present data from *in vitro* voltage-clamp experiments showing that short-duration voltage spikes, which elicit large excitatory junctional potentials *in vivo*, produce larger and briefer calcium currents than do long-duration action potentials, which elicit small excitatory junctional potentials.

RESULTS AND DISCUSSION

Synaptic modulation by changes in motor neuron action-potential duration serves to synchronize swimming contractions of the hydrozoan jellyfish *Polyorchis penicillatus*. Action potentials can arise in any depolarized part of the circular, electrically-coupled network of swimming motor neurons (Spencer, 1981, 1982). As action potentials propagate into progressively more polarized regions of the network, their duration progressively decreases, the excitatory junctional potentials (EJPs) elicited in

---

the swimming muscle become larger and the delay to generation of a muscle action potential is reduced (Fig. A.1; Spencer, 1982). This decreased delay automatically compensates for the conduction time of the motor spike through the network. These findings are paradoxical, since contemporary models (Augustine et al., 1987) of calcium-mediated release of transmitters predict that postynaptic-potential amplitude should be positively correlated with action-potential duration.

As *in vivo* study of membrane ionic currents in the motor neuron network of *Polyorchis* is problematic, because extensive electrical coupling makes voltage-clamp recording ineffective, to further investigate the above phenomena we have developed a method to isolate these cells in primary culture (Przysiezniak and Spencer, 1989). We have used the whole-cell recording technique to characterize the ionic currents regulating action-potential duration and the Ca^{2+} currents which probably mediate transmitter release in this jellyfish.

Current-clamp recordings from isolated motor neurons showed that the duration of stimulated action potentials increased with membrane baseline depolarization (unpublished). We presume this resulted from the steady-state depolarization-dependent inactivation of an "A-like", rapidly activating, transient potassium current (I_{K-fast}) that is responsible for action-potential repolarization. Voltage-clamp data showed that I_{K-fast} peaked within 2 to 15 ms, decayed with a time constant of about 200 ms (Fig. A.2A) and was half-inactivated at a prepulse potential of –47 mV (N = 4; Fig. A.2B). The normal *in vivo* range of resting membrane potentials (–25 mV to –50 mV) was within the steeper portion of the steady-state inactivation curve for this current, suggesting that I_{K-fast} was modulated at resting potentials where spike duration varied. A slower outward current, I_{K-slow}, was revealed at more depolarized holding potentials ($\geq$–30 mV; Fig. A.2A), where I_{K-fast} was almost completely inactivated. This slow current activated within 200 ms and decayed e–fold in 1–2 s. Tetraethylammonium at 100 mM in the electrode completely blocked both currents. Externally applied 4–aminopyridine at 5 to 10 mM reduced I_{K-fast} by about 40% after 30 min (N = 8), while I_{K-slow} was largely unaffected by this treatment (N = 3). Both these compounds applied externally caused spike prolongation in current-clamp recordings.

An inward calcium current (I_{Ca}) was recorded from voltage-clamped, cultured motor neurons, which could be eliminated by the replacement of external Ca^{2+} with Co^{2+} (Fig. A.3A) or by the addition of 0.1–0.5 mM $CdCl_2$. The I_{Ca} activated rapidly, reaching a peak of several hundred picoamperes within 4 ms, and inactivated with a time constant of 15 to 25 ms. In other

systems, calcium currents at presynaptic sites (Augustine et al., 1987) normally show slower activation and inactivation. A second time constant of decay (60–70 ms) could be measured suggesting the presence of an additional, smaller and more slowly inactivating component of I_{Ca}. Figures A.3B and C show the voltage dependence of peak I_{Ca}, peak G_{Ca} activation and peak I_{Ca} steady-state inactivation. It is important to note that these motor neurons have a compact morphology, lacking long or narrow processes (Przysiezniak and Spencer, 1989), and that the synapses they make onto myoepithelial cells are located throughout the neurons (Spencer, 1979). Thus, there is good electrical access to the synaptic sites. We have assumed that the large, transient Ca^{2+} current we observed mediates transmitter release in these motor neurons, although it is possible that a smaller I_{Ca} component may be involved.

To determine the dynamics of voltage-gated calcium influx when action potentials of varying duration invade a presynaptic release site, we stimulated motor neurons *in vitro* using voltage commands shaped like action potentials. Figure A.4A shows that a long-duration action potential elicited a small amplitude, slow calcium current which peaked during the slow repolarizing phase. The same potential *in vivo* had evoked a small amplitude EJP (Fig. A.1C). In contrast, a short-duration action potential produced a larger, more transient calcium current (Fig. A.4C) and, *in vivo*, had elicited a larger EJP (Fig. A.1C). Voltage-clamp stimuli of intermediate durations produced calcium currents of intermediate amplitude and time to peak (Fig. A.4B). Correspondingly, EJP amplitude has been recorded *in vivo* as varying continuously with AP duration (Fig. A.1A,B,C; Spencer, 1982).

The amplitudes and time courses of calcium currents seen using simulated action potentials can be explained in the following way. The holding potential preceding the spike determines the number of calcium channels available for activation and, in part, the peak calcium current elicited by the pulse. Thus, brief spikes arising from a more polarized baseline will be able to activate more calcium channels than prolonged spikes arising from a more depolarized baseline. The rising phase of the spike then activates all available calcium channels (Fig. A.4 top; Fig. A.3B,C) but little current flows until a large net inward driving force develops, during repolarization. The rapid repolarization of short-duration action potentials causes the driving force on Ca^{2+} to increase at a far greater rate than channels are closing and inactivating, resulting in a large, brief calcium current analogous to a "tail" current. In contrast, the slower rate of

178

repolarization of long-duration action potentials is associated with a slower development of the electrical driving force, thus resulting in a more slowly developing calcium current of smaller amplitude.

Measurements of the integrals of I_{Ca} responses reveal that despite the larger peak I_{Ca} elicited by short-duration action potentials, long-duration action potentials produced a larger total Ca^{2+} influx (Fig. A.4). How does a small but rapid entry of calcium release more transmitter, as judged by the amplitude of the EJP, than a larger but slower entry of calcium?

There is overwhelming evidence that fast transmitter release depends on the calcium concentration at cytosolic binding sites which regulate the rate of vesicle fusion to the plasma membrane (Augustine et al., 1987; Zucker and Lando, 1986). Calcium concentration at these sites, which are thought to be located just beneath the membrane, is in turn determined by the difference between the rate of calcium influx and the rate of Ca^{2+} removal by diffusion, active pumping, and sequestration (Augustine et al., 1987). It is possible that the Ca^{2+} sinks in *Polyorchis* motor neurons are very effective and that they counter the increase in submembranous $[Ca^{2+}]$ produced by slow Ca^{2+} influx (during long spikes), while allowing rapid influx to cause a large change in submembranous $[Ca^{2+}]$.

Since these experiments were carried out with 11 mM intracellular EGTA, however, it is possible that Ca^{2+}-dependent inactivation of I_{Ca}, if present, was reduced. Such inactivation would cause the long-duration spike to elicit a smaller total calcium influx than observed, which might be less than the influx produced by a short-duration spike in native conditions. In this case rapid removal of calcium from cytosolic binding sites would not be necessary to explain the effectiveness of short-duration spikes in releasing transmitter material.

This study shows that there can be considerable modulation of the time course of the presynaptic calcium transient by variations in the shape of the presynaptic action potential and that this can lead to differential efficacy of synaptic transmission.

179
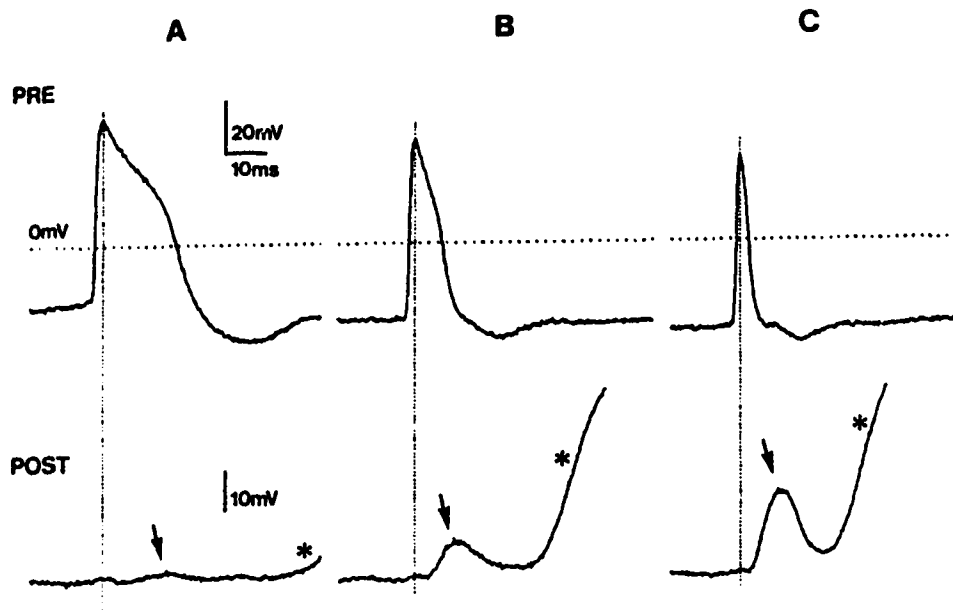
Figure A.1 - Motor neuron action-potential duration is negatively correlated with muscle EJP amplitude, *in vivo*. These simultaneous pre- and postsynaptic recordings were made across the swimming motor neuron-myoepithelial cell junction in a semi-dissected preparation of the bell margin from *Polyorchis penicillatus* (methods described in Spencer, 1982). Electrodes were positioned ~50 μm apart. Motor neuron action potentials were spontaneously initiated from random sites around the nerve-ring. *A.* When the initiation site was close to the recording electrodes, a broad action potential (*upper trace*) was seen to arise from a depolarized baseline and elicited a very small EJP (*bottom trace, arrow*) with a long delay to the muscle action potential (*bottom trace, asterisk*). *B.* When the initiation site was more distant from the electrodes, the recorded action potential propagated into a more polarized region of the electrically-coupled network, had a shorter duration and elicited a larger EJP (*arrow*) with a shorter delay to the muscle action potential (*asterisk*). *C.* An action potential that had propagated from the most distant initiation site to the recording electrodes was seen to arise from the most polarized baseline, had a very short duration and produced the largest EJP (*arrow*) with the shortest delay to the muscle action potential (*asterisk*). It is important to note that muscle action potentials occurred at a considerable delay after the EJP since the distance between the recording and muscle spike-initiation sites was large (Spencer, 1982). Electrodes were filled with 2 M potassium acetate. Bath solution was natural seawater at 20°C. Data were stored on FM tape, then digitized at 200 μs intervals for plotting.

Figure A.2 - Potassium currents in isolated motor neurons. *A.* I_{K-fast} and I_{K-slow} responses to 100 mV depolarizations applied for 2 s from holding potentials (V_h) of –80 mV and –30 mV, respectively. Current traces were digitized from chart recordings using a 45 ms sampling interval. Voltage protocols were redrawn. *B.* Plot of the voltage dependence of steady-state inactivation of I_{K-fast}. A "prepulse/pulse" protocol was applied from V_h = –80 mV. A 2 s prepulse was applied at command voltages incremented in 10 mV steps; a test pulse to +10 mV then followed. Early peak outward currents elicited by the test pulses were measured, leak-subtracted, and normalized to the largest current obtained; these ratios were plotted against prepulse potential. This current was active and modulated at *in vivo* resting potentials (shown by stipled bar above plot). Average maximal peak current, elicited after a prepulse potential of –90 mV, was 2.99 nA. Voltage of half-inactivation (–47 mV) is shown by the *arrowhead*. N = 4 except for the last 3 points on the right which are N = 3, 3 and 2, left to right. Contamination by I_{K-slow} was assumed to be minimal during the early (<20 ms) phase of the response where measurements were taken, since I_{K-slow} was only weakly activated at the test potential and arose ten times more slowly than did I_{K-fast}. Sodium-free bath solution was used that contained (in mM) choline–Cl, 437; $MgSO_4$, 5.7; $MgCl_2$, 23.3; $CaCl_2$, 9.5; KCl, 7.8; HEPES, 10; KOH, 5.6. Calcium current was blocked with 0.1–0.5 mM $CdCl_2$ in the bath. Whole-cell recording internal solution contained (in mM) dextrose, 740; KCl, 105; $MgCl_2$, 2; $CaCl_2$,1; EGTA, 11; HEPES, 10; KOH, 35. Experiments were carried out at 20–25°C. Dissociation and culture techniques are explained (Przysiezniak and Spencer, 1989). The culture medium in the present experiments had been modified and contained (in mM) NaCl, 378; $MgCl_2$, 29; $CaCl_2$, 9.5; Na_2SO_4, 5.7; KCl, 13.4; choline–Cl, 42; HEPES, 10; NaOH, 5; 50 mg/l gentamycin sulfate was added. The pH for all solutions was adjusted to 7.5.
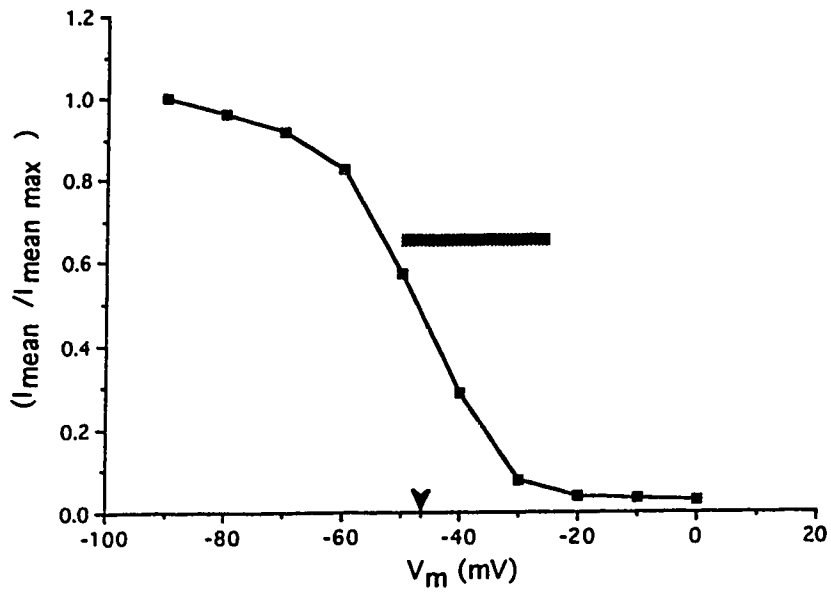
A

1nA
500ms

+70
+20
-30
-80
50mV

B

182
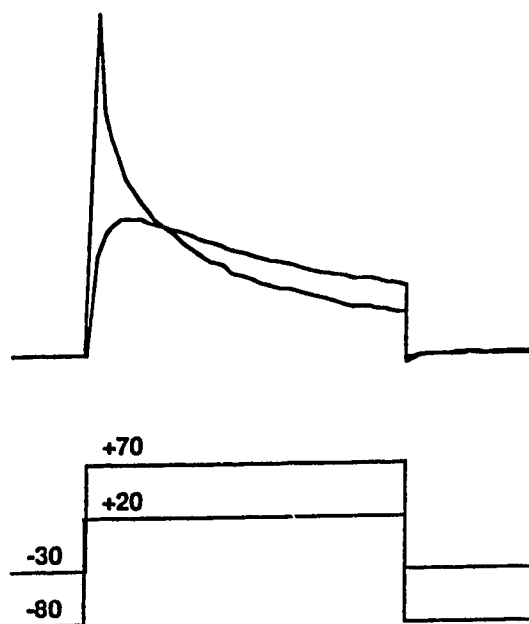
Figure A.3 - Calcium current from isolated motor neurons. *A.* I_{Ca} elicited by a 200 ms voltage step from V_h –50 mV to +10 mV. This current was blocked after 5 min in a bathing medium in which Ca^{2+} was replaced by Co^{2+}. *B.* Current/voltage (I–V) plot for peak I_{Ca}. Depolarizing test pulses lasting 80 ms were applied from V_h –40 mV to the voltages shown on the *abscissa*. Leak-corrected responses from 10 cells were averaged for each voltage point, and the peak inward current was plotted. The reversal at +66 mV suggests contamination of I_{Ca} by some residual outward current, evident at more positive V_c. *C.* Steady-state inactivation (*solid squares*, $N = 5$) and peak activation (*open squares*, $N = 10$) of I_{Ca} as a function of V_c Voltages of half-activation (*clear arrowhead*, +3 mV) and half-inactivation (*solid arrowhead*, –26 mV) are indicated. Average maximal peak I_{Ca} for inactivation data was –434 pA; average maximal peak Ca^{2+} conductance for activation data was 7.9 nS. The inactivation data was obtained using a prepulse/pulse protocol where V_h was –40 mV, the prepulse lasted 1 or 2 ms and the test pulse went to +10 mV; peak responses were averaged and plotted as a function of prepulse potential. The activation curve was drawn from data for *B*; the driving force and conductances were calculated assuming a reversal potential of +66 mV. The range of normal resting potentials is indicated as a stippled bar. Bath solution was the same as in Fig. A.2. Internal solution used in *A* and for inactivation data in *C* contained (in mM) CsCl, 140; TEA–Cl, 100; dextrose, 477; $MgCl_2$, 2; $CaCl_2$, 1; EGTA, 11; HEPES, 10; NaOH, 28. The IV data in *B*, and activation data in *C* were collected using the following, sodium-free electrode solution (in mM) CsCl, 109; TEA–Cl, 100; dextrose, 536; $MgCl_2$, 2; $CaCl_2$, 1; EGTA, 11; HEPES, 10; CsOH, 31.

A

no Ca⁺⁺,9.5mM Co⁺⁺

100pA
50mV
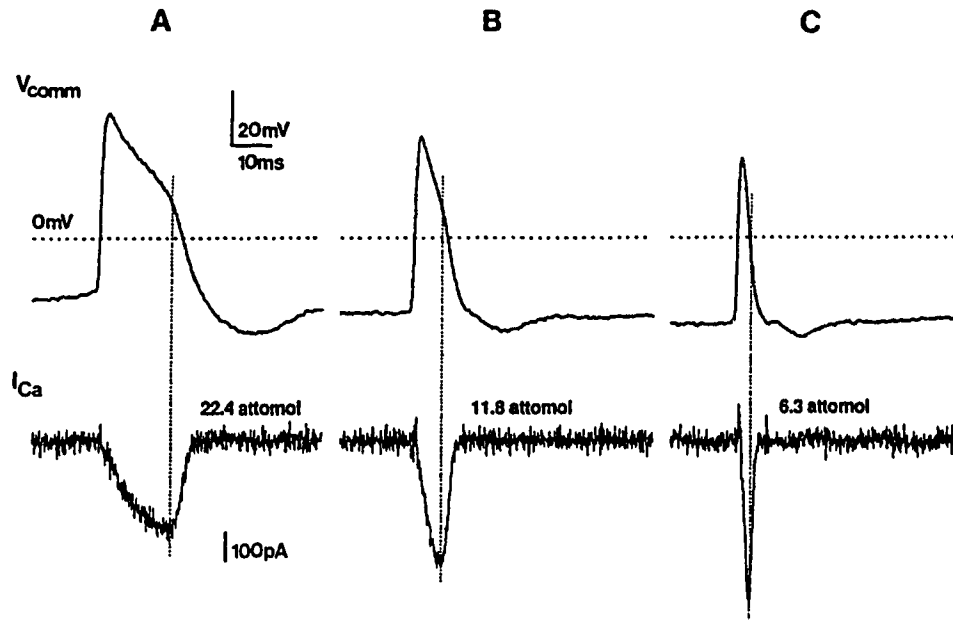10ms

9.5mM Ca⁺⁺

+10

-50

B

Peak I$_{ca}$
(pA)

C

184
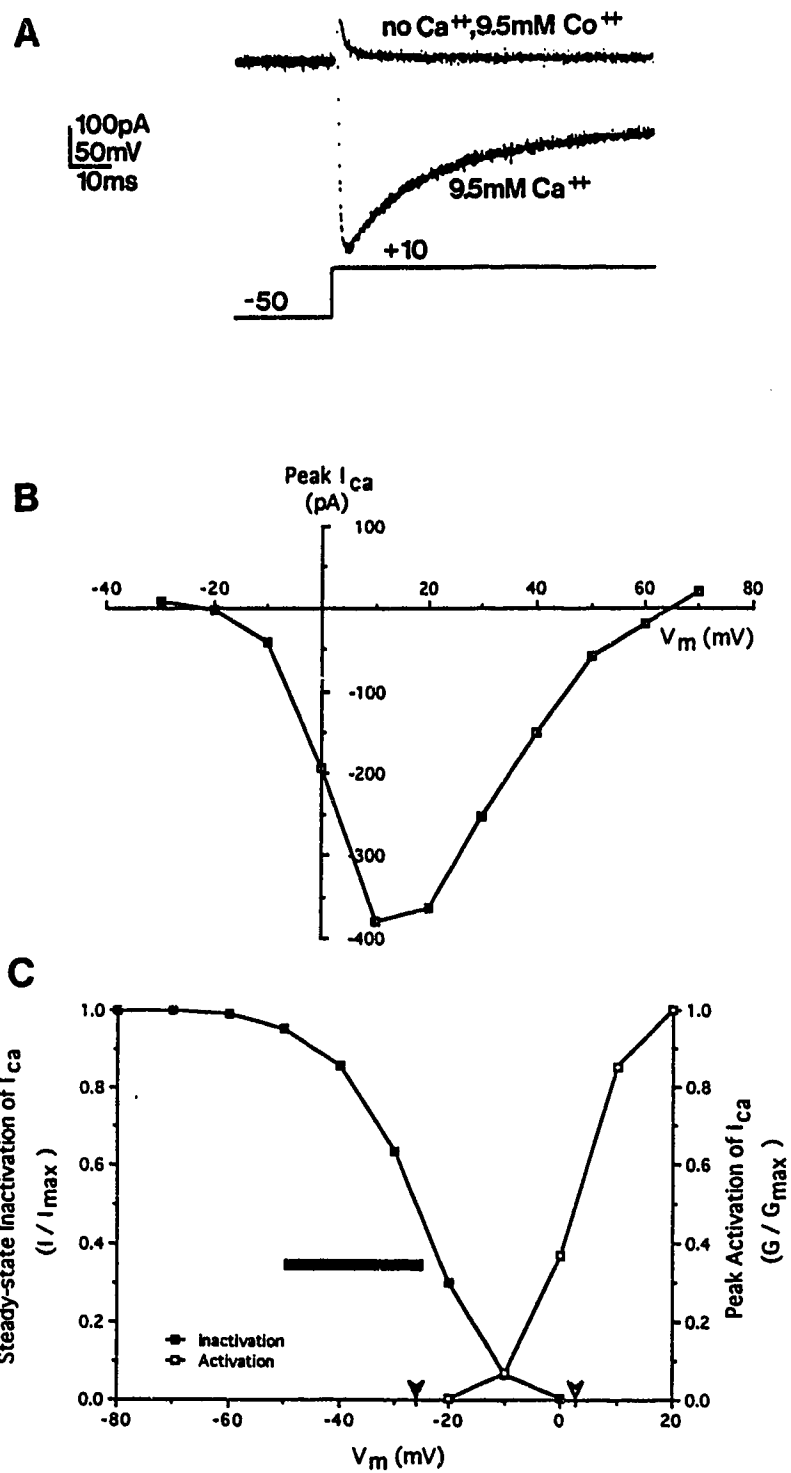
Figure A.4 - Calcium currents elicited from *in vitro* motor neurons by spike-shaped command pulses. *A.* A long-duration spike command elicited a slowly developing, small amplitude I_{Ca}. Progressively shorter spike commands (*B* and *C*) elicited a progressively more transient and larger amplitude I_{Ca}. Integrals of these currents are indicated, in attomoles (10^{-18} mole) of Ca^{2+}, above the current traces. Voltage commands were digitized in 200 µs samples from the FM-recorded action potentials shown in Fig. A.1, filtered at 600 Hz to reduce capacitative noise, and applied with 70% series-resistance compensation (final R_{ser} = 1–3 MΩ), through the command input of a List Medical EPC-7 voltage-clamp amplifier. Current responses were digitally recorded on videotape at 44 kHz, then transferred to pCLAMP files at 100 µs per sample for data processing. Capacitance artifacts and leakage were subtracted using responses to inverted, scaled-down (20%) versions of the spikes, applied at the same holding potential as their full-scale counterparts; similar results were obtained if subtraction pulses were applied at more polarized values for V_h. Contaminating, Ca^{2+}-independent currents were subtracted using leakage- and capacitance-corrected responses obtained from the same cell in Ca^{2+}-free, Co^{2+}-substituted saline. All solutions as for Fig. A.3*B*. Experiments done at 20°C.

185

REFERENCES

Augustine GJ, Charlton MP, Smith SJ (1987) Calcium action in synaptic transmitter release. Ann Rev Neurosci 10: 633-693.

Fuchs PA, Henderson LP, Nicholls JG (1982) Chemical transmission between individual Retzius and sensory neurons of the leech in culture. J Physiol (Lond) 323: 195-240.

Hochner B, Klein M, Schacher S, Kandel ER (1986) Action-potential duration and the modulation of transmitter release from the sensory neurons of *Aplysia* in presynaptic facilitation and behavioral sensitization. Proc Natl Acad Sci USA 83: 8410-8414.

Kusano K, Livengood DR, Werman R (1967) Tetraethylammonium ions: effect of presynaptic injection on synaptic transmission. Science 155: 1257-1259.

Lin J-W, Faber DS (1988) Synaptic transmission mediated by single club endings on the goldfish Mauthner cell. II. Plasticity of excitatory postsynaptic potentials. J Neurosci 8: 1313-1325.

Przysiezniak J, Spencer AN (1989) Primary culture of identified neurones from a cnidarian. J Exp Biol 142: 97-113.

Spencer AN (1979) Neurobiology of Polyorchis. II. Structure of effector systems. J Neurobiol 10: 95-117.

Spencer AN (1981) The parameters and properties of a group of electrically coupled neurones in the central nervous system of a hydrozoan jellyfish. J Exp Biol 93: 33-50.

Spencer AN (1982) The physiology of a coelenterate neuromuscular synapse. J Comp Physiol A 148: 353-363.

Zucker RS, Lando L (1986) Mechanism of transmitter release: voltage hypothesis and calcium hypothesis. Science 231: 574-578.